On the application of detached eddy simulation turbulence modelling to hydrocyclonic separators for shipboard ballast water treatment

McCluskey, Daniel Keppie

Award date:
2009

Awarding institution:
Coventry University

On the Application of Detached Eddy Simulation Turbulence Modelling to Hydrocyclonic Separators for Shipboard Ballast Water Treatment

Daniel Keppie McCluskey

A Thesis Submitted in Partial Fulfilment of the Requirements of Coventry University for the Degree of Doctor of Philosophy

The programme of research was carried out at the Energy & Environmental Technology Applied Research Group, Faculty of Engineering and Computing, Coventry University, UK.

October 2009

ACKNOWLEDGEMENTS

I would firstly like to thank my friends and family for all their guidance and unwavering support throughout my PhD studies. Without their encouragement and good humour I doubt I would have kept my sunny disposition along the way. Furthermore I would like to truly acknowledge the support and guidance of my supervisor, Professor Arne Holdø. Throughout my PhD he has been a source of wisdom and a friend. I would also like to thank my fellow students, as both friends and technical sound boards you have been invaluable in helping me get my thoughts on paper.

I would also like to thank the Institute for Marine Engineering, Science and Technology (for awarding me with the Stanley Grey fellowship), the EU FP6 Project SHIPMATES (for funding the initial phase of my studies), and to Coventry University (for funding the later stages of my work).

I would also like to take the opportunity to say a special thank you to Tara, your unfaltering love, support and understanding has been invaluable along the way.

To all of you, thank you and happy reading!

Daniel Keppie McCluskey 2009

ABSTRACT

There is significant worldwide environmental concern related to the transportation of Invasive Aquatic Species (IAS) by ships ballast water into non-native environments. This has given rise to the development of a vast array of technological ballast water treatment systems. The complex environmental challenges and tight operational characteristics of marine vessels limits the scope of the technologies used for Ballast Water Treatment (BWT). As a result few technologies have progressed beyond the research and development stage; however one of the most promising technologies for ship board use is the cyclonic separator, or hydrocyclone. Despite the use of hydrocyclones in a wide variety of engineering applications they have yet to be successfully adapted towards the removal of suspended sediment and marine organisms from large volumes of ballast water.

The following primary objectives of this study have been met:

- Via critical review identify the technological solutions for treating ballast water best suited to onboard use.
- Define the critical flow regimes evident within hydrocyclonic separators.
- Establish a series of Computational Fluid Dynamics (CFD) simulations, evaluating standard turbulence models in order to determine the capacity for commercial CFD to model hydrocyclonic flow.

This study has detailed the operational characteristics of ballast water hydrocyclones with the aim of enabling hydrocyclones to be optimised for individual ship configurations. Flow simulations have been conducted using CFD, and in particular the Detached Eddy Simulation (DES) turbulence model. Finally the DES model is shown to be a legitimate turbulence model for hydrocyclonic flow regimes, validated against empirical and experimental data.

TABLE OF CONTENTS

List of Figures

List of Figures continued

PAGE

List of Figures continued

PAGE

List of Tables

List of Charts

List of Charts continued

PAGE

Nomenclature

I_x	Ultraviolet radiation energy (mW/cm^2)
Q_{UV}	Capacity of ultraviolet chamber (m^3/h)
$Ð_{UV}$	Ultraviolet dose (µWs/cm^2)
D_H	Hydraulic Diameter (m)
CSA	Cross Sectional Area (m^2)
Q	Volumetric Flow Rate (m^3/h)
Re_{PIPE}	Pipe Reynolds Number
t	Time
ℓ	Length scale
k	Turbulence kinetic energy
$E(k)$	Energy Spectral Density
Ri	Richardson Number
F_D	Froude Number
u	Relative velocity between a particle and fluid (m/s)
g	Acceleration due to gravity
h	Representative vertical length scale
U	Fluid velocity
p	Pressure
F_D	Drag force
C_D	Coefficient of drag
A	Frontal area of a particle
x	Particle diameter (characteristic length)
$Re_{particle}$	Particle Reynolds Number
Stk	Stokes Number
D	Cyclone Diameter
Eu	Euler Number
S_{ij}	Stress tensor
C_1 - C_2	Constant (K-Epsilon model)
C_k	Kolmogorov constant
C_s	Smagorinsky constant
C_μ	eddy viscosity constant (K-Epsilon model)
Re	Reynolds Number

Nomenclature Continued

A_R	Complete internal surface area of cyclone (m^2)
G	Cyclone wall friction factor
a	Cyclone inlet width
b	Cyclone inlet length
CS	Control Surface (Cyclone cone to Vortex finder)
H_{CS}	Height of control surface
Eu_{in}	Inlet Euler number
Δp	Total pressure difference (loss)
Δp_{body}	Pressure loss due to cyclone wall losses
Δp_x	Pressure losses due to cyclone main core and vortex finder
Δp_{acc}	Pressure losses due to acceleration of particulate slurry
x_{50}	50% cut size
Rw	Flow ratio
Dc	Dimensionless cut size
Rf	Recovery of water to underflow
Rv	Volumetric recovery of debris to underflow
R_w	Water flow ratio
C_v	Volumetric feed concentration
Stk50Eu	Product of Stokes number and Euler number
W_B	Inlet bulk velocity (m/s)
T	Temperature
m	Mass
c	Specific heat capacity
t_1	Initial temperature
t_2	Final temperature
Q	Heat energy (J)

Greek Symbols

ψ	Ultraviolet Radiation output
υ	Kinematic viscosity
ρ	Fluid density
μ	Dynamic viscosity
β	Coefficient of volumetric expansion
η	Kolmogorov length scale
τ_{μ}	Kolmogorov time-scale
ε	Rate of dissipation of turbulence kinetic energy
τ_{ij}	Reynolds stress tensor
Γ_{false}	False (numerical) diffusion
τ	Particle relaxation time
μ_t	Turbulent viscosity
σ	Prandtl number
δ_{ij}	Kronecker delta

Abbreviations & Acronyms

DES	Detached Eddy Simulation
BWT	Ballast Water Treatment
EU	European Union
SHIPMATES	SHIPrepair to MAintain Transport which is Environmentally Sustainable
FP6	Framework Programme 6
IAS	Invasive Aquatic Species
CFD	Computational Fluid Dynamics
IMO	International Maritime Organization
CAD	Computer Aided Design
CFU	Colony forming units
ANS	Aquatic Non-Indigenous Species
GISD	Global Invasive Species Database
ISSG	Invasive Species Specialist Group
MEPC	Marine Environment Protection Committee
UV	Ultraviolet
MV	Merchant Vessel
GBT	Gas Bubble Trauma
BWE	Ballast Water Exchange
DNS	Direct Numerical Simulation
LES	Large Eddy Simulation
KE	K-Epsilon
RANS	Reynolds-Averaged Navier Stokes
RSM	Reynolds Stress Model
RNG	Re-Normalised Group
SGS	Subgrid Scale
RINA	Royal Institute of Naval Architects
RFH	Reverse Flow Hydrocyclone
MARTOB	On Board Treatment of Ballast Water (Technologies Development and Applications) and Application of Low-sulphur Marine Fuel
CS	Control surface
SPD	Square Profile Duct
ERCOFTAC	European Research Community On Flow, Turbulence and Combustion
CM3D	Choi Mesh in 3 Dimensions
HDM	High Density Mesh
MS	Mesh Sensitivity
ROI	Region of Interest
QUICK	Quadratic Upstream Interpolation Convective Kinetics
MUSCL	Monotone Upwind Scheme for Conservation Laws

Abbreviations continued

PISO	Pressure Implicit with Splitting of Operators
SIMPLE	Semi-Implicit Method for Pressure-Linked Equations
SIMPLEC	Semi-Implicit Method for Pressure-Linked Equations Corrected
LDV	Laser Doppler Velocimetry
3D PTV	3 Dimensional Particle Tracking Velocimetry
ROH	Rietema Optimised hydrocyclone

CHAPTER 1: GENERAL INTRODUCTION

CHAPTER CONTENTS

1.1 Introduction

A significant worldwide problem plagues our oceans, lakes and waterways. The focus of the problem is the introduction of non-native organisms into aquatic eco-systems where they would otherwise not be present. The resulting organisms can establish themselves in these waters, damaging the local eco-systems and environment. Their impact significantly affects the economics of the target areas and can cause significant harm to indigenous organisms and human health. The problem is of such a scale that it has been identified as one of the top four threats to the world's oceans and waterways. Marine vessel ballast water has been identified as a key factor responsible for the transfer and introduction of these harmful organisms.

The significance of ballast water transferral of species has led to diverse research and development into Ballast Water Treatment (BWT) methods. Despite these research programmes, the vast majority of the worlds 85,000 vessels are limited to employing ballast water management techniques as the treatment technologies are either not at an advanced stage or they are currently operationally prohibitive. The result is that between 3000 and 5000 billion litres of untreated water continues to be transported by marine vessels annually. This transfer of water around the world has an enormous biological effect on coastal and freshwater ecosystems, due in part, to the significant quantity of organisms and organic matter suspended in ballast water. These organisms are deposited freely in coastal waters upon deballasting. The ready transport of debris and micro-organisms, coupled with the complex design of ballast tanks can also result in large quantities of sediment being deposited within ballast tanks create a breeding ground in which certain organisms may flourish. These healthy organisms can then be deposited at ports around the world and, providing the environment is suitable, take hold.

The need for BWT techniques has arisen due to the significant quantity of organisms present within sea water. These organisms vary in type and consequently are present in a range of sizes and quantities, from microscopic bacteria and Viruses

through to larger organisms including fish and crustaceans. In the past these organisms have been known to invade ecosystems in waters to which they are not indigenous as a direct result of their transportation within ballast water. It is the primary focus of this research to take a positive step towards prevention of alien species invasion via transportation within ships ballast water. To this end a thorough literature review of the current treatment techniques in development has been conducted. This incorporates a review of the current legislation surrounding ballast water on board vessels and also includes a critical analysis of the potential biological effectiveness for the treatment techniques currently being developed. From the underlying literature review it has become apparent that no single method will be capable of meeting the standards imposed by the International Maritime Organisation (IMO). The intention of this research is to determine whether the effectiveness of a generic cyclonic separator, either coupled with or without a secondary treatment mechanism, can meet the proposed IMO legislation. In the case of the cyclonic separator this secondary system is likely to target smaller micro-organisms including bacteria and similar sized pathogens.

An additional problem, highlighted by the BWT investigation, is the sheer quantity of sediment transported within ballast tanks (see figure 1.1). The potential to minimise this issue in conjunction with the ballast water issue significantly improve the economic survival of a viable BWT.

Figure 1.1 An indication of the accumulated sediment within ballast tanks. (Source:[1]).

The problem is a complex one, and the task of meeting the requirements laid down by the IMO regulations is demanding. As stated previously the cyclonic separator or hydrocyclone is one of the most promising treatment mechanisms in production. The basic design of the hydrocyclone is almost 100 years old, but their use onboard marine vessel as a ballast water treatment mechanism is less than a decade old. Hydrocyclones lend themselves well to shipboard use, the lack of moving components makes them both reliable and simple to use. Coupled with their relative low cost and the ease with which they can be implemented on older vessels it would appear they are the ultimate solution to the problem. Unfortunately hydrocyclones are not currently optimised to remove the organisms present in sea water.

1.2 Aims

The main aim of this work is to contribute to the successful developments within Ballast Water Treatment technology. In order to achieve this aim a thorough critique of BWT technologies has been presented. All available technologies have been reviewed against the requirements of the IMO. The outcome of the critique has identified that the focus of the study, which centres on is on one of the most promising and practicable technologies.

This study is presented as a thesis consisting of seven main chapters. The narrative proceeds through the Introduction (Chapter 1) into the literature review (Chapter 2). Chapters 3 and 4 are concerned primarily with the theoretical background and the CFD modelling of the flow regimes with hydrocyclonic separators. Chapter 5 is a detailed discussion of the findings, while chapters 6 and 7 conclude the findings and present recommendations for future work. The appendices incorporate supporting information results and publications from the PhD study.

CHAPTER 2: LITERATURE REVIEW

CHAPTER CONTENTS

2.1 Introduction

There are two aspects to this review, a detailed synopsis of the current problem regarding transport of non-indigenous organisms via the uptake of ballast water by the shipping industry [2-5] and the analysis of a suitable technology to use on board ships in order to minimise the environmental impact from ballast water uptake [6-8]. A review of the specific CFD aspects of this study, domain setup, turbulence modelling etc, will be discussed in Chapters 3 and 4 as relevant.

2.2 Why Ballast water?

Marine vessel ballast water has been identified as a key factor responsible for the transfer and introduction of harmful organisms into non-indigenous environments. This has been identified as one of the four greatest threats to the world's oceans. The significance of ballast water transferral of species has led to diverse research and development into Ballast Water Treatment methods. Despite the number of ballast water management techniques in development, at present ballast water exchange is the only technique widely used. This literature review summarises the Ballast Water Treatment techniques currently at a research or development stage. An assessment of the potential effectiveness of each method, its corrosion implications and economic cost are all presented together with preliminary recommendations.

Approximately 80% of world trade is transported by shipping. Currently there is a world shipping fleet of approximately 85,000 vessels and many of these ships use sea water as ballast. The use of water as ballast is currently essential to ensure the safe operation of vessels, and equates to approximately 3 to 5 billion tonnes of water transported by marine vessels annually. This transfer of water around the world has an enormous biological effect on coastal and freshwater ecosystems, due in part, to the significant quantity of organisms and organic matter suspended in ballast water. These organisms are deposited freely in coastal waters upon deballasting. The

ready transport of debris and micro-organisms, coupled with the complex design of ballast tanks can also result in large quantities of sediment being deposited within ballast tanks (see figure 2.1). This can create a breeding ground in which certain organisms may flourish. These healthy organisms can then be deposited at ports around the world and, providing the environment is suitable, take hold.

Figure 2.1. Photographs' showing accumulated sediment within ballast tanks (Source: [1]).

The use of water as ballast on board ships, instead of solids such as rocks, sand or metal, has led to a number of high profile invasions by aquatic non-indigenous species (ANS) worldwide. The sheer scale of the biological introductions prevent a detailed analysis to be presented here. Instead a focussed description based principally on the ten most significant invasions as identified by IMO is presented, along with a brief outline of the scales of the invasion.

2.2.1 Organisms

The organisms listed in table 2.1 consist of the IMOs top 10 invasive species in recent history.

	Organism	Scientific name
1		
2		
3		
4		
5		
6		
7		
8		
9		
10		

Table 2.1. The 'Ten Most Unwanted'. A list of organisms identified by the IMO as the most invasive in recent history [9].

The nature of these organisms, along with their respective biological impacts has been derived from an online database (The Global Invasive Species Database (GISD)) constructed by the Invasive Species Specialist Group (ISSG) [10].

Cholera, *Vibrio Cholerae*

This straight (or curved) rod bacteria is native to the aquatic environment, primarily residing in the normal flora of brackish, and estuarine waters. The bacteria, Vibrio Cholerae is responsible for Cholera, a potentially epidemic and life threatening secretory diarrhoea. It has been introduced to the Gulf of Mexico and South America

as well as a number of other locations. A number of Cholera epidemics have been directly associated with Ballast Water transferral. In 1991 three ports in Peru where affected by a strain of Cholera previously only reported in Bangladesh. The introduction of Cholera to the Peruvian ports resulted in an epidemic that swept across South America affecting in excess of 1 million people and killing over 10,000 people by 1994.

Cladoceran Water Flea, *Cercopagis pengoi*

Cercopagis pengoi is an euryhaline and eurythermic species, resulting in its ability to withstand a wide variety of salinities and temperatures. It occurs naturally in brackish and fresh waters. It is native to the Black and Caspian seas, however it has recently been introduced to the Baltic sea. It is capable of reproducing to form very large populations affecting zooplankton communities by selective predation. Resulting in decreases grazing pressures on phytoplankton and resulting in increased algal blooms. The organisms also clog fishing nets and trawls, resulting in significant economic losses for fishing industries.

Mitten Crab, *Eriocheir sinensis*

Eriocheir sinensis is capable of tolerating a wide variety of abiotic conditions. It has also exhibited significant tolerance to temperature variation and is highly adaptable to modified aquatic environments, including an ability to survive in polluted waters. It is a migrating crab that contributes to the extinction of native invertebrates, and can decimate local fisheries. It has also been found to cause severe erosion due to its burrowing activities. The crab is primarily native to northern Asia it has been introduced to Western Europe, the Baltic Sea and the West Coast of North America. Recently it has been discovered that the crab may carry a lung fluke parasite that infects humans.

Toxic Algae, *Various Species*

There are a vast array of toxic algae species associated with the development of Red, Brown and Green Tides. In many instances these species are capable of forming large algae blooms. These blooms are capable of killing significant quantities of marine life due to oxygen depletion and the release of toxins or mucus. The algal blooms can travel on the tides resulting in potential beach fouling. This can have an obvious effect on tourism and recreation. Furthermore some species of algae can contaminate filter feeding shellfish stocks with an economic impact on fisheries. The consumption of contaminated shellfish may result in severe illness or death in humans.

Round Goby, *Neogobius melanostromus*

Neogobius melanostromus is a bottom dwelling fish found in the near shore regions of lakes and rivers. It is native to the Black, Asov and Caspian seas although it has recently been found in the Baltic Sea and across North America. It preys on small fish as well as the egg and larvae stages of larger fish. They are also known for their aggressive protection of spawning areas, pushing native species away from the more protected habitats. It is also capable of out competing native fish for food due to its ability to feed in darkness. The fish also consumes numerous bi-valve species providing a direct line of transfer of disease from bivalve to larger game fish or humans.

European Green Crab, *Carcinus maenas*

Carcinus maenas is a crab species native to Europe and North Africa renowned for its voracious and diverse variety of prey which includes more than 100 families and 158 genera in 5 plant and 14 animal groups. It has been introduced to Northern America, Australia and South Africa resulting in the decimation of native crab and bi-valve species. It is a known to reproduce in vast quantities with the female capable of spawning up to 185,000 eggs at a time.

Asian Kelp, *Undaria pinnatifida*

This marine plant species is native to Northern Asia but has been subsequently introduced to Southern Australia, New Zealand, Europe, Argentina and the west coast of Northern America. It is a rapidly growing plant that spreads vegetatively as well as through the release of spores. Its rapid growth stages result in the displacement of native algae and marine life. It has the ability to affect commercial shellfish stock due to habitat alteration and space competition.

Zebra Mussel, *Dreissena polymorpha*

Perhaps one of the most publicised invasion is that of the Zebra mussel into the Great Lakes of North America. This species is native to Caspian and Black seas, though it has been introduced into the UK, Western Europe, Canada and the USA. The Zebra Mussel is a small bi-valve mollusc capable of filtering all particles between 7 and 400µm, putting it in direct competition with native planktivores. it such an efficient filter feeder that it can increase water clarity significantly, resulting in increased algal growth. Their small size, between 7mm and 30mm long, results in them propagating up into pipes and similar water outlets, the cost of which in the USA alone is estimated at $500 million per year.

North Pacific Seastar, *Asteria amurensis*

Originally native to North Pacific waters including areas around Japan, Russia, North China and Korea, the Northern Pacific seastar can now be found along the southern coast of Australia. It is capable of reproducing in large numbers reaching 'plague' proportions , with estimates from Port Philips Bay indicate a population increase of 12 million individual seastars in 2 years. The seastar consumes a wide range of prey, resulting in economic and ecological damage particularly to commercially valuable scallop, oyster and clam species..

North American Comb Jelly, *Mnemiopsis leidyi*

The north American Comb Jelly is a carnivorous predator of edible zooplankton, pelargic fish eggs and larvae. It is responsible for the destruction of numerous fisheries in its native waters of the Atlantic coast of North and South America. Its introduction into black sea has had a catastrophic effect on the entire ecosystem and supported fisheries, an introduction directly attributed to ballast water transferral. It has subsequently been introduced into the Azov, Marmara, Aegean and Caspian sea, all which are considered to be as a result of Ballast water transferral.

Within this list of ten invader alone there is a size distribution ranging from 0.2-2µm for organisms such as *Vibrio Cholerae* and *algae* through to the 100mm size ranges of the Chinese Mitten Crab, European Green Crab and North American Comb Jelly and the >0.5m size ranges of the North pacific seastar and Asian Kelp (fully developed Asian Kelp can have a central pinnatifid blade*, pinnae,* in excess of 0.8m long) . This size range distribution further highlights the complex nature of organism removal from ballast water, especially when the developmental stages of each of the organisms are taken into consideration.

2.2.2 Scale of Invasive Introductions

Due to the ecological and economical impact of invasive species a significant amount of research has been conducted in a bid to establish the target location for invasion. Figure 2.2 below indicates the potential hot spots and the expected scale of the invasion. Initial indications suggest that the primary invasion hot spots are directly linked to the major trade routes of large shipping vessels, with the most significant invasions predicted within European and Asian Pacific waters.

Figure 2.2. (a) Global hot spots for biological invasion from ballast water. Expected invasion rates range from 0 (blue) to 2.94 × 10^{-4} species km^{-2} yr^{-1} (red). (Source: [11])

Additional research studies have been able to deduce the pathways and mechanisms of specific organisms transfer. Figure 2.3 graphically surmises the primary organism transfer routes via ballast water, highlighting the scale of organism transfers into each region.

Figure 2.3. Major pathways and origins of invasive species infestations in the marine environment. (Source: [12])

Many organisations are conducting research into potential treatment techniques for ballast water; however design of ballast tanks, complex operational characteristic, and huge costs involved currently limit the advance of the individual technologies. The intention of this review is to highlight the current situation with respect to ballast water treatment techniques in development. It aims to draw attention to significant issues which surround many of the treatments, with respect to the criteria laid down by the IMO.

2.3 Performance of Ballast Water Treatment Methods

The IMO in particular have recognised the significance of BWT and consequently set-up GloBallast in parallel to their introduction of the Ballast water and Sediments Convention (2004). Criteria for new BWT technologies laid down by the IMO subdivision GloBallast at the1st International Ballast Water Treatment Standards Workshop [13] are as follows:

- The technique must be safe (in terms of the ship and its crew).
- It must be environmentally acceptable (not causing more or greater environmental impacts than it solves).
- It must be practicable (compatible with ship design and operations).
- It must be cost effective (economical).
- It must be biologically effective (in terms of removing, killing or otherwise rendering inactive aquatic organisms and pathogens found in ballast water).

From the criteria listed biological effectiveness was deemed to be the most significant and hence the focus of most BWT mechanisms. The standard states that organism mortality/deactivation should be at least 95%. An additional category for organisms >100 microns specifies 100% mortality/deactivation.

These additional requirements are such that the survival of particular organisms, regardless of what stage of development they are at (see figure 2.4), is drastically

minimised. The use of treatments which greatly reduce the numbers of organisms entering the ballast tanks during uptake of ballast will have a knock on effect with the quality of surviving organisms upon deballasting.

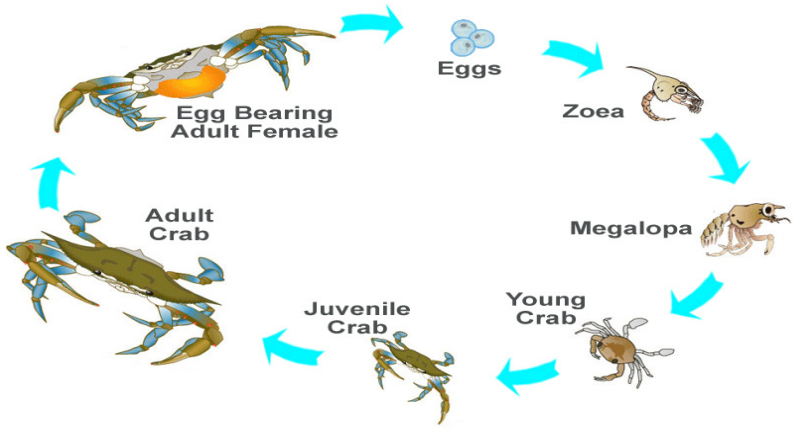

Figure 2.4. Example of the various life stages of organism development, Blue Crab shown. (Source: [14] modified)

Further legislation is being developed by the US coastguard similar to the IMO convention. This will place further restrictions on ballast water and could potentially be more stringent than the current requirements.

Although ballast water systems are being developed it is unlikely that a single system will be applicable to all vessels. The installation and operating costs of some systems may be prohibitive to large vessels, while the need to store consumables may not be suitable for smaller vessels. It is thus necessary to highlight the manner in which a treatment system achieves the IMO convention requirements in conjunction with its suitability for vessels of varying types. To this end an in-depth description of each treatment is presented along with an approximate operating cost breakdown. However, due to the design differences between vessels it near impossible to have a definitive summary of applicability of treatments.

Other methods of ballast water management may also be accepted as alternatives to the ballast water exchange standard and ballast water performance standard, provided that such methods ensure at least the same level of protection to the environment, human health, property or resources, and are approved in principle by IMO's Marine Environment Protection Committee (MEPC).

Based on regulation B-3 it is apparent that ballast water treatment standard D-2 should be regarded as the highest priority and all vessels which shall be operating beyond 2014 shall be considered for the fitting of treatment capable of meeting regulation D-2 as follows:

- Regulation D-2: Ballast Water performance standard

Ships conducting Ballast Water Management in accordance with this regulation shall discharge less than 10 viable organisms per cubic metre greater than or equal to 50 micrometers in minimum dimension and less than 10 viable organisms per millilitre less than 50 micrometers in minimum dimension and greater than or equal to 10 micrometers in minimum dimension; and discharge of the indicator microbes shall not exceed the specified concentrations described in paragraph 2.

- Indicator microbes, as a human health standard, shall include:
  - Toxicogenic Vibrio Cholerae (O1 and O139) with less than 1 colony-forming unit (cfu) per 100 millilitres or less than 1 cfu per 1 gram (wet weight) zooplankton samples;
    - Escherichia coli less than 250 cfu per 100 millilitres
    - Intestinal Enterococci less than 100 cfu per millilitre.

The convention will enter into force twelve months after the date on which not less than thirty States have signed and accepted the convention, provided that the thirty states constitute a combined merchant fleet constituting not less than thirty-five percent (35%) of the gross tonnage of the world's merchant shipping. At present (31st December 2005) there are 6 ratifying states representing 0.62% of the world tonnage including Argentina, Australia, Brazil, Finland, Maldives, The Netherlands, Spain and Syrian Arab Republic [15].

2.4 Available Technologies for Treatment

Ballast Water Treatments can be categorized into one of three broad areas. These are mechanical, physical and chemical treatment methods. A number of treatment techniques are currently undergoing development. The treatment methods often form part of a multi stage system which can be constructed as a modular unit and designed to retro fit older ships as well as new build vessels. Screens and filters are essential part of ballast water exchange system as well as any other treatment system. Hydrocyclone is very effective as primary treatment system whereas all other methods are secondary methods, many of which are still in early development or prototype stages (see table 2.2).

A thorough description of each treatment system has been presented in order to fully understand the implications and concerns for installing each system type on board an ocean going vessel.

1	Screen filtration
2	UV radiation
3	Sonic methods
4	Heat treatment
5	Chemical biocides
6	Ozone introduction
7	De-oxygenation
8	Gas super-saturation
9	Ballast Water Exchange
10	Hydrocyclonic Separation

Table 2.2. Current BWT techniques in use or development (Source: Author).

2.4.1 Screen filtration

Screen filtration has been in use for many years in a large variety of applications. Screen filtration in its current form has been around for many years. This has led to significant research and development conducted into filtration systems. The

technology has been developed continually over the years to a point where screens are capable of filtration down to 10µm. Large scale tests have seen screens shown to be 74-94% effective at removing debris (Using 25µm filters) [16] however tests have shown that 50µm is the practical limit for ship board use [17]. The major advantages of mechanical filtration include the lack of harmful by-products, and the return of debris to the initial ballasting site. Filtration units could easily be incorporated into existing plumbing and pump systems. Filtration in its current form could provide adequate primary particle removal, however bacteria and virus removal would be far too costly when compared to other systems such as UV radiation .

Clogging with waste is a common drawback of traditional screen filters during heavy use. In order to overcome this, a differential pressure sensor allows for a brief “backwash” cycle in order to clean the screens. This backwashing can delay the ballast water intake and output rates, and although the exact water loss achieved can be as low as 1%.

2.4.2 UV radiation

Micro organisms absorbed Ultra Violet (UV) radiation with the effect of rendering the organism inactive, preventing reproduction, or even potentially killing the organism. The relatively compact nature of UV systems makes them ideal for use on marine vessels. UV induced mortality can be influenced by a number of variables including water clarity, temperature, flow rate and organism type.

UV radiation is particularly useful as a secondary stage in a treatment setup, targeting micro-organisms specifically. The method can achieve IMO standards when used in conjunction with a first stage system to induce desirable conditions for UV dosing [5]. Water clarity problems are resolved through the use of a primary system. Significantly UV can be used for both incoming and outgoing ballast water, reducing the effects of bacteria growth within ballast tanks [18]. This can all be

controlled electronically ensuring the correct dose of UV radiation to deactivate organisms [19].

Case study: a typical UV reactor:

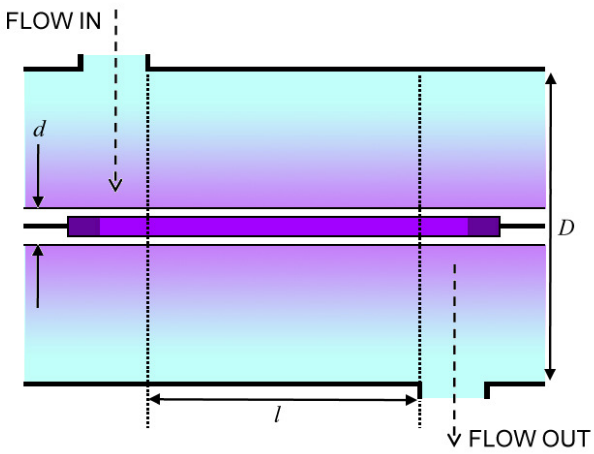

Figure 2.5. Cross section of a typical UV reaction chamber (Source: Author).

From the Beer-Lambert law we can determine the maximum UV dose a typical BWT UV reactor [dimensioned as per *OptiMar Microkill UV Reactor [20] (*see figure 2.5) will provide:

$$I_x = \left(\frac{\psi \times 1000}{2\pi (D/2) l} \right) \cdot 10^{-AX} \qquad [2.1]$$

Hence:

$$Ix \approx 2100 \text{ mW/cm2}$$

Assuming a maximum loss of 40% due to shielding by suspended particulate:

$$Ix \approx 1260 \text{ mW/cm2}$$

The dose ($Ð_{UV}$) received will therefore be the UV intensity multiplied by the length of time that the organisms are within the UV reactor:

$$Ð_{UV} = I_x \cdot t \qquad [2.2]$$

Therefore: Dose ≈ 3500 μWs/cm2

The capacity (Q_{UV}) of the typical UV chamber analysed is thus,

$$Q_{UV} = \frac{\left(\left(\pi D^2\right) - \left(\pi d^2\right)\right) \cdot l}{t} \qquad [2.3]$$

Resulting in:

Q_{UV} ≈ 94.5 m3/h

Thus UV can achieve IMO standards when used in conjunction with a first stage system to induce desirable conditions for UV dosing (See Appendix C for UV induced mortality rates of key organisms).

2.4.3 Sonic methods

The technique relies on a transducer to generate ultrasound (20 kHz – 10 MHz) energy within the ballast tank. As the sound energy passes through the ballast water it energises local particles resulting in the formation of cavities (bubbles). As these cavities collapse there is an intense energy output which causes both physical and chemical effects within the ballast water. These conditions can cause the cells of the organisms local to the collapsing bubble to rupture [21]. The temperature surrounding the collapsed bubble can reach in excess of 2000° C and attain pressures of up to 1800 atmospheres; these factors ensure that organism mortality is achieved. The frequency and power density of the ultrasound system can be controlled to alter the cavitation effects due to ballast water density differences.

Ultrasound as a feasible treatment technique still requires further development as current laboratory tests have been unable to achieve organism mortality greater than 40% (University of Newcastle, UK). This may, in part, be due to the inability to induce cavitation accurately. In tests carried out the water used was flowing under laminar conditions into a static tank, however turbulent flow has been seen to increase the efficiency of ultrasound treatment. Due to the flow rates of water entering ballast tanks it is highly likely that turbulent conditions will arise.

Many organisations are looking to minimise the amount of sound generated by marine applications and an increase in ocean noise levels would be another limiting factor of any sound or cavitation induced ballast water treatment use. This has come about due to evidence that high use of sonar and other general marine noise can disturb and potentially harm many marine species, particularly mammals. It has been suggested that marine mammals such as whales or dolphins communicate using sound in the frequency range of 1000 to 100,000 HZ. While the specific sonic frequencies used in treatment research are out of the immediately harmful range, the significant increase in sonar as a result of mandating treatment could prove hazardous to marine mammals, ongoing research is attempting to identify to what extent [22].

Treatment of Ballast Water by sonic methods on the world fleet of about 85,000 vessels each year could increase ocean noise tenfold. With the prospect of legislation being introduced to minimise ocean noise, and in particular the use of sonar, it would appear prudent to avoid the implementation of sonic methods as a standard treatment on ocean going vessels. To use sonar with the aim of conserving ocean biodiversity in light of current backlash from conservation organisations could potentially be costly.

2.4.4 Heat treatment

The increase of water temperatures has long been used as a form of disinfection and results in the breakdown of organisms. The use of heat for ballast water has the same effect of either destroying or deactivating unwanted organisms. Most current heat treatment systems in development employ the use of a heat exchanger, linked to the vessels exhaust system. System using this arrangement would be ideally suited to longer voyages in the region of 10 or more days as the time taken to increase the temperature within the ballast tanks is significant. Other systems heat small quantities of water either on entering or leaving a vessel, achieved using heat circulation methods, ideally be suited to passenger or container ships which tend to have frequent stops with only minor changes in ballast volume made. Two key temperature ranges tend to be targeted, low temperature systems (< 40℃) and high temperature systems (40 – 80 ℃). Low temperature trials onboard *Merchant Vessel (MV) Iron Whyalla* have shown that most phytoplankton are killed at temperatures as low as 35℃ with treatment times ranging between 30 minutes and several hours.

The diverse nature of ship design leads to a minimum of 4,000 tonnes (general cargo vessel [23]) of ballast needs to be treated and can increase up to 80,000 tonnes. The heat energy required to achieve this can be immense, additionally while some trials have shown total mortality of specific species at temperatures as low as 35℃ as previously stated, this may be too low to destroy all hazardous organisms including dormant cysts.

Significantly high temperature systems may be required to ensure that temperatures in excess of 70℃ are achieved and these are still at early development stages [24]. Early indications based on a study [5] is that the power required to heat the ballast water, even for smaller vessels, is greater than the excess currently available from engines. The majority of ships engines generate no more than 20 MW of excess energy, and the actual requirement could be as high as 90 MW [25]. As such initial cost effectiveness of heat based treatments may not be applicable to high

temperature techniques and sustained heating may be unachievable on shorter journeys.

Heat treatment trials onboard *MV Iron Whyalla* [26] suggest that short term local heating would be insufficient to ensure mortality and may not be practical for many commercial ventures. On a commercial vessel the time to temperature would need to be in the region of five hours. Power required to achieve this rapid heating for a large scale bulk carrier is also given and equates to 106 MW more than currently available engine excess, again assuming tank heating. This form of heating would also have significant thermal stress implications on the vessel. Cost implications related to the power requirement may render heat treatment unviable as a treatment mechanism. Ship design and layout may prevent appropriate piping or heating capabilities. Heat treatment trials so far have relied heavily on the initial temperature of the water taken onboard. Operationally it seems highly likely that heat treatment will not be able to guarantee the 95% mortality rate required by the IMO.

2.4.5 Chemical biocides

There is a limit to the types of chemical treatment available for treatment. This is due to the diverse nature of the organism targeted. Despite the availability of many commercial chemicals capable of rendering inactive all ballast water transported species, the chemicals used would have to have a short lifespan in order to prevent damage to indigenous coastal species on ballast deployment. As a result of the marine cross section encapsulated in ballast water most current chemical biocides are organic based, resulting in complete degradation during the course of the voyage [27]. The use of chemicals as treatment will require regular handling by crew and as such treatments will need to be safe for repeated handling. Advantages of chemical treatments include low purchase cost and no requirement to modify existing vessels. Many existing chemicals are being tested for ballast water use. As a result chemical treatments should be ready for ship deployment much sooner that mechanical or physical treatments. Due to the nature of ballast water requirements it may be that

chemical treatments are used as an interim treatment while other methods continue being developed [28].

However as with all chemical agents the long term implications are unknown and the potential environmental impacts could be severe. Additionally large quantities of decaying organic matter would be pumped into coastal waters; this could become a significant food source to indigenous species eventually causing an imbalance in current species biodiversity.

2.4.6 Ozone introduction

The use of ozone as a disinfectant for water has occurred since the late 1800's, since when it has been implemented in many marine applications. Ozone is an oxidising agent which destroys hazardous organism within minutes. The short half life of ozone (5.3 seconds) makes it an environmentally safe chemical treatment [29]. This short half life requires the ozone to be generated on site, thus necessitating an ozone generator. This works by passing a high frequency electrical discharge through air. Despite the safe environmental impact of ozone the gas itself is highly toxic and is difficult to detect. This would require a high number of safety measures to be adopted by the crew. In addition to these factors ozone treatment is not suitable for water with a high turbidity, thus requiring a primary treatment method to remove larger organisms and debris [5].

Ozone introduction is a chemical process and as such it suffers from similar issues to chemical biocides. The potential long term environmental impact of chemical use is unknown hence Chemicals and biocides should be avoided.

2.4.7 De-oxygenation

By removing saturated oxygen from the ballast water effectively the micro-organisms in existence are oxygen starved. De-oxygenation can be achieved by a number of different methods including nitrogen introduction, vacuum generation and biological introduction. This system works on any oxygen dependent organism, however it

does not affect certain organisms adapted to low oxygen environments such as bacteria, fungi and viruses. A number of hazardous organisms also have an oxygen resistant phase of development such as a cyst or pore. However in conjunction with a secondary mechanism such as UV or ozone treatment de-oxygenation can ensure almost total fatality of organisms. The benefits of each method include at least a 10% reduction in corrosive effects of ballast water on tank walls [30]. Nitrogen introduction purges the oxygen from the ballast water creating hypoxic ballast water. An alternative system works by creating a vacuum within the ballast tanks and maintaining a low oxygen level for up to 10 days. The de-oxygenation of the water also reduces the corrosive effects of both sea water and organism pollutants on the vessels structure. As a mechanical system crew would have full control over the system if required, however the device used could be automated. The benefits of such a system include long service life and the ability to “plug and play” with relative ease of introduction to current systems. Biological de-oxygenation requires the addition of nutrients to encourage growth of oxygen dependent organisms. These organisms rapidly use up the oxygen during growth which results in anoxic ballast water within 3 days, if this state is maintained for up to six days complete mortality of oxygen dependent organism can be achieved [31]. De-oxygenation could easily be incorporated into a multi stage treatment system. Oxygen depleted water would mix readily with coastal waters ensuring re-oxygenation on ballast water emptying [32]. Vacuum induced de-oxygenation would be favourable as there is no addition to the ballast water. The increase in nitrogen generated from nitrogen purging and the potential for high levels of H_2S generated by biological methods could be deemed undesirable.

Structurally the vessel may not be suitable for de-oxygenation. The generation of a vacuum within a ballast tank is likely to be outside the original design parameters of the tank. As such the unknown stresses may put vessel owners off the idea of vacuum induced de-oxygenation.

2.4.8 Gas super-saturation

Gas supersaturation is a mechanism which induces gas bubble trauma (GBT) within organisms. GBT is known to affect a number of the organisms present in ballast water; however the vulnerability to gas supersaturation varies between organism types. GBT affects multi-cellular marine organisms resulting in embolism and haemorrhages [33]. The process works best when hydrostatic pressures are lowered. The procedure involves over saturation of the ballast water with a gas, usually air or nitrogen. The equipment required consists of a gas generator connected to the existing ballast plumbing. This technique does not require the storing or use of harmful chemicals ensuring no detrimental effect to the crew or the outgoing ballast water and no handling of chemicals [34]. The main disadvantage of the technique lies in its inability to destroy micro organisms requiring a treatment targeted specifically at micro organisms, such as UV radiation.

Cavitation based techniques such as Ultra-sound or Gas Super-saturation can lead to significant erosion problems on the walls within a ballast tank. The problems arising from cavitation around a ships propeller are well documented and have been seen to cause rapid damage sometimes requiring replacement of a ships propeller after a single voyage [35]. While Propellers are not manufactured from the same material as tank walls the corrosion effects could significantly reduce the life of the vessel.

2.4.9 Ballast Water Exchange

At present the existing IMO guidelines recommend Ballast Water Exchange (BWE) at sea as the method used to minimise the transfer of invasive species. The problem with BWE is that it is a management process rather than a treatment and as such has certain limitations. The technique involves changing the ballast in deep water locations where there is no harmful sediment or potentially invasive organisms. This is based on an assumption that coastal organisms do not survive in deep water

locations and vice versa. There are a number of variations on the BWE method including re-ballasting, continuous flushing and dilution [36].

A large proportion of the ballast water carried by ships (2.7 billion tonnes per year, [37]) will require a treatment other than ballast water exchange, this is confirmed by the fact that BWE has not led to eradication of organism transferral via ballast water, with an estimated 100 million tonnes of untreated ballast water transferred into the North Atlantic annually.

As well as the environmental risk associated with ballast water there is also an important consideration in the use of Ballast water exchange with regards to the level of potential exposure of crew members to harmful contaminants. There are variants on BWE that minimise this risk such as continuous flushing or Brazilian dilution [38]. The Brazilian dilution method involves the loading of ballast water through the top of the ballast tank at the same flow rate as ballast water is unloaded through the bottom of the tank. A significant advantage of Brazilian dilution is that crew interaction is no longer an issue. This method requires at least three complete cycles of exchange to be completed to ensure <95% effectiveness.

Case Study: A worked example of Ballast Water Exchange using the Iron Whyalla Bulk Carrier demonstrates the limitations of the technique:

With a ballast capacity of 57,000 tonnes and capable of pumping up to 2000 tonnes/hour per tank, a total ballast/deballast rate of 10,000-20,000 tonnes/hour can be achieved [39]. With an average pump rate of 15,000 tonnes/hour, ballast exchange would complete in 3 $^{3}/_{4}$ hrs. Therefore 11 $^{1}/_{4}$ hrs would be required to achieve 3 complete ballast cycles, within this time (average cruise speed of 16 Knots) the vessel would have travelled 180 Nautical Miles (333 Km)

Hence organisms may be transported beyond any natural boundaries in their current environments into neighbouring waters. While this is the intention of BWE this transportation could lead to a "local" invasion particularly when a number of stoppages are made in quick succession such as tourist routes around the Caribbean and other ship operations within coastal waters. In this instance the ballast water may only be transported within a relatively small geographical area but due to the extreme diversity of the organisms present it could still result in the introduction of organisms which would otherwise have a very small geographical environment.

Furthermore the current ballast tank design can also give rise to areas of stagnant ballast within the tanks, resulting in reduced "biological exchange" despite a high "volumetric exchange". This scenario is highly dependent on the exact design of individual ballast tanks and while it may not be applicable to all vessels it could be seen as a significant downside to any method of ballast water exchange. Even if the regulations required additional "volumetric exchange" this may not reduce the transfer of organisms. Even in cases where vessels are declared as NOBOB (No Ballast On Board) there has been evidence of tank sedimentation and remaining ballast in the region of 50 metric tonnes or more still on board [40]. In fact the experiments of *Forsberg et al* on board the *Berge Nord* Bulk Carrier showed signs of bio-particles remaining within the ballast tanks one year after being seeded into the tank. This was after the tank had been exchanged over 80 times with a volumetric flow through in excess of 10,000m^3 on each occasion, equating to over a million fold dilution over the given period.

Significantly the bio-particles used in the experiments by *Forsberg et al* were inert fluorescent beads. The findings may have been even higher if a specific biological entity was assessed due to the potential rate of growth of resident organisms within the ballast tanks. This is entirely feasible as there is the potential for an increased food source in the form of nutrients within the sediment. For this reason treatment systems which remove organisms and biological matter at the sources are likely to have the least affect on coastal waters. The proposed mechanical and physical BWT

devices are the most likely options for this scenario. Furthermore ship based operation, observation and maintenance of these forms of BWT would be simpler to maintain over their chemical based counterparts.

2.4.10 Hydrocyclonic separation

In terms of viable technologies to use on board a ship, the Hydrocyclone ranks amongst the most useful. By design Hydrocyclones have no moving parts and do not require back flushing. This lack of moving parts, minimal maintenance and additional benefits appear to suit the demanding environment of ocean going vessels. The operation of a hydrocyclone is relatively straightforward, the fluid enters tangentially and a conical section induces spiral flow. This rotational flow causes dense solid particles to be forced towards the walls of the separator where they are discharged back into ocean waters, this discharge makes up for less than 5% of the total ballast water intake [41]. However some organisms have a similar density to water and as such are not affected by the separating action of the hydrocyclone, instead passing through the vortex finder with the main uptake water.

Presently dual stage hydrocyclone/UV systems are the only BWT systems fitted to commercial vessels. Currently commercial use will increase the rate of development of BWT hydrocyclones as existing BWT hydrocyclones do not resemble separators from other engineering fields. Further development of separators using research conducted in other sectors, such as water processing and waste removal industries, may achieve the efficiency required for BWT. In particular this study will concentrate on hydrocyclones of the design proposed by K. Rietema, often referred to simply as Rietema cyclones. Whilst other well known industrial cyclone designs exist (e.g. Stairmand, Bradley, Mozley etc.) [42] the Rietema cyclone is considered to be a high capacity design [43], critical for handling the quantities of ballast water taken onboard vessels (typically between 5000-200,000 tonnes [44]).

In the majority of modern hydrocyclones the fluid flow and particle motions are similar regardless of the purpose of the hydrocyclone. The schematic (see figure 2.6) highlights the inlet, outlet and purge line of a conventional hydrocyclone, including that of the Rietema cyclone design used for this study..

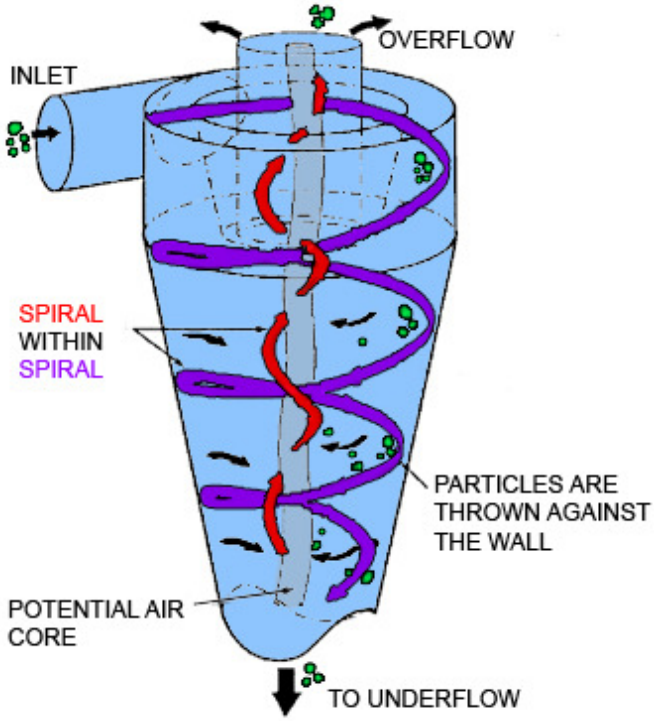

Figure 2.6 Schematic of the flow within a conventional reverse flow hydrocyclone (Source: [45] modified)

The separation of particles relies on the particle size and/or density. The vortex within the cyclone is generated by an inlet tangential to the circular chamber of the separator is maintained by the geometry characteristics of the cyclone. The particles to be separated are forced to the walls of the cyclone where they move down the wall and exit the cyclone at the purge (also known as the underflow). The remaining body of water reverses its vertical direction as it nears the purge and exits via the outflow. A critical aspect of most industrial hydrocyclones is the presence of an air core. The air core is a column of air which is generated due to the low pressure present at the centre of the vortex. Where the outlets are not open to the atmosphere it is still possible for an air core to be present as a result of any dissolved gasses in the fluid separating and forming an air core. The absence of a gas core generally

results in an increase in the total pressure drop at the same throughput while lowering the efficiency [46].

Current hydrocyclones used onboard marine vessels are not usually open to the atmosphere and as such any air cores that are generated are unlikely to be stable. Initial BWT hydrocyclone designs retained some geometrical similarities with the conventional hydrocyclones but in most cases they did not utilise the reverse flow mechanism. Recent installations and developments have moved towards the reverse flow separator and in other studies have suggested that a battery of smaller reverse flow separators may be the ideal solution. This would be in keeping with the suggestions by Rietema [46-49] and Svarovsky [43, 50]. Figures 2.7 and 2.8 illustrate how the required cyclone diameter and resultant pressure drop would alter with an increase in cyclones within a battery arrangement.

Figure 2.7 Effect on cyclone diameter with increasing No. off cyclones in a battery. (Source: [43]).

Figure 2.8 Effect on cyclone pressure loss with increasing No. off cyclones in a battery. (Source:[43]).

There are a number of factors which may prevent a particle from being separated from a body of fluid. If the radial velocity of the liquid is sufficiently high it will cause the liquid and suspended particles to become entrained towards the centre of the cyclone, away from the wall, and ultimately the particles will enter the reverse flow field exiting the cyclone via the outlet, figure 2.9 shows the expected velocity profiles within reverse flow hydrocyclone (RFH). This can also occur if the inlet is positioned in such a way as to allow the particle to enter the cyclone at too great a distance from the wall, once again causing the particles to be entrained into the reverse flow. If the residence time of a particle (the time it spends within the cyclone) is too small the particle may not fully reach the wall and therefore will not exit via the purge. Additionally turbulence within the flow field can also cause eddy diffusion of the particles which would interrupt the separation.

A) B) C)

Figure 2.9 (A) Radial, (B) tangential and (C) axial velocity profiles within a reverse flow hydrocyclone. (Source:[43]).

Dimensionless Parameters affecting Hydrocyclone Design

The use of 'scaling rules' and subsequent associated dimensionless parameters is intrinsically linked to the effective design of hydrocyclones. Whilst it is possible to model an untested cyclone design, the ability to predetermine approximate geometry and flow regimes is a fundamental step in the process of good cyclone design. The design rules developed my hydrocyclone researchers are primarily based on three key dimensionless groups. while this study does not replicate the design theory of hydrocylones, these dimensionless groups are embedded within the analytical models (see Chapter 4) and are a fundamental basis for the development of the these models.

Stokes Law

Stokes law is the theoretical solution to C_D based on the Navier-Stokes equations for low Reynolds number flows, where viscous forces prevail.

This is given as:

$$F_D = 3\pi \cdot \mu \cdot u \cdot x \qquad [4.3]$$

However this approximation is only valid for low particle Reynolds number (Re_p). These conditions are not usually found in the hydrocyclones used for shipboard ballast water treatment. Figure 2.10 highlights the relationship between Drag coefficient and particle Reynolds number for spherical particles.

Figure 2.10 Drag coefficient versus particle Reynolds number for spherical particles (Source:[43]).

Stokes Number

Stokes number, *Stk*, relates the inertial forces to the hydrodynamic forces and is given by:

$$Stk = \frac{\tau \cdot v}{D} \qquad [4.4]$$

The resistance coefficient, defined in the Euler number (Eu), is defined as the static pressure drop across the inlet and outlet of the cyclone, divided by the dynamic pressure. Figure 2.11 indicates the relationship between Eu and Re for Spherical particles.

$$Eu = \frac{\Delta p}{\left(\frac{\rho v^2}{2}\right)} \qquad [4.5]$$

Figure 2.11 Relationship between Eu and Re for Spherical particles (Source:[43]).

Froude Number

The final dimensionless group, relating the gravity and inertia forces, is given by:

$$Fr = \frac{g \cdot D}{v^2} \qquad [4.6]$$

This is known as the Froude number and shows the effect of gravity on separation efficiency using large separators, where the larger coarse particles are affected by gravity.

Summary of the effects caused by modification to hydrocyclone geometry

On the basis of the resultant effects of the individual variables contained with the Stokes and Froude numbers the following generalisations have been suggested as a guideline to the effects geometrical changes have on the functionality of cyclonic separators by Svarovsky [43, 50]), and incorporate comments by Rietema [46-49] and Hoffman [51].

For the purpose of shipboard cyclones there are three fundamental aspects to be addresses, these are:

- Overall Capacity of the cyclone
- Pressure Drop
- Cut size (Collection Efficiency)

The overall capacity of the cyclone is a function of geometrical design entirely. in this respect an increase in any the following dimensions, provided cyclone design rules are adhered to, would result in a cyclone with a higher capacity;

- Cyclone Overall Diameter
- Inlet Diameter
- Outlet Diameter
- Overall Cyclone Body Length

Alternatively a reduction in the length of the vortex finder will also result in an increase in the capacity of the cyclone, however this will also affect the elementary flow regime within the separator. An increase in the cyclone capacity will also reduce the overall pressure drop across the cyclone, for a given volumetric flow rate at the inlet.

In order to reduce the cut size of the separator, and hence increase the collection (or removal) efficiency the inverse of the capacity rules are generally true (with one addition). The following geometrical dimensions could be reduced:

- Cyclone Overall Diameter
- Inlet Diameter
- Outlet Diameter
- Overall Cyclone Body Length
- Angle of the Conical Section

Whilst it is true that an increase in the overall cyclone body length will increase the residence time and thus also increase efficiency, the body length will have an

adverse effect on other geometrical parameters when cyclone design rules are adhered to. Regardless of the primary intention of the cyclone in all cases the most significant design variable is the overall cyclone diameter hence all geometry parameters are usually referenced with respect to the cyclone diameter.

With the knowledge of the hydrocyclone separation capabilities and the variety of end user definable characteristics it is clear to see why the hydrocyclone is used in a wide variety of industrial applications and is considered to be the ideal separation tool for these applications. Cyclone separators have thus successfully spread i into industry which includes mining, paper manufacture, metal processing, petrochemical and farming industries amongst others, where the hydrocyclones are used to separate particles based on density and size. It is with this in mind that the hydrocyclone has been selected as an initial stage separator for ballast water particle removal. However the empirical approaches currently used to design hydrocyclones for ballast water separation have yet to achieve the efficiencies required to meet the IMO legislation. While it is unlikely that Hydrocyclones on their own will be able to achieve the required biological effectiveness it is possible with further optimisation that cyclones can form a fundamental component of shipboard piping

The visual difference between current industrially used *Rietema* based hydrocyclones and a typical commercial BWT Hydrocyclone is shown in figure 2.6.

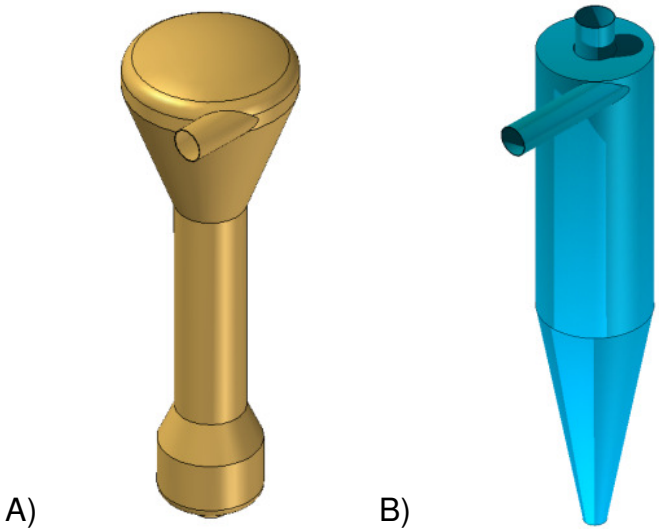

Figure 2.12. A) Current commercial BWT Hydrocyclone Design. B) Rietema optimum designed Reverse flow Hydrocyclone. (Source: Author).

There is an urgent environmental need for a valid treatment system on board marine vessels. It is with this knowledge in mind that the IMO has put a 2009 deadline on the mandatory inclusion of a ballast water treatment mechanism onboard all necessary vessels. To this end the flexibility provided by computational fluid dynamics as a design and evaluation tool will allow for an accelerated research and development program in the verification process of applicable systems. However unlike other forms of computer aided design, CFD software is not a point and click answer. The software is only capable of accurate simulations provided the input data is correct. In order to ensure that this is the case it is necessary to understand the CFD process, and validate the results wherever possible.

Due to the design of current BWT separators it is difficult to apply the geometry and scaling rules of other separators. One of the most widely used hydrocyclone designs follow the parameters set by *Rietema*. The *Rietema* empirical data relating to geometry ratios etc. can potentially be applied to redesign BWT hydrocyclones therefore allowing verification of multiple hydrocyclone designs and their corresponding efficiencies through the use of Computational Fluid Dynamics (CFD). Experimental work in conjunction with numerical calculation will provide the support required to verify future BWT hydrocyclones using CFD.

2.5 The Aim of the Research

The project is centred on the need for an effective technology for the prevention of transportation of non-indigenous marine organisms with ballast water. The focus in the project is the evaluation of the flow conditions which establish the separation capabilities of liquid cyclonic separators, also known as hydrocyclones. In particular the research will identify the potential benefit of utilising numerical simulations in order to validate successive design iterations of shipboard hydrocyclones. It is intended that the research will cover the following:

- Investigate Ballast Water Treatment (BWT) technologies for ship board use.
- Investigate the suitability of the hydrocyclone with respect to the other BWT technologies
- Establish the use of Computational Fluid Dynamics (CFD) as a prototype design evaluation and flow simulation tool.
- Present a computational simulation modelling the flow in an optimised BWT hydrocyclone.

The scientific and engineered approach documented for the development of a BWT mechanism will be in stark contrast to the empirical trial and error methods used previously and should ensure the optimum biological security required when using ballast water onboard ships.

2.6 Objectives

The intention of this thesis is to contribute to the successful development of future practicable shipboard BWT technology and to the knowledge required to progress beyond the state-of-the-art. To achieve this it is clear that a deeper understanding of the problems associated with the limitations of BWT implementation on board ship is required. Furthermore a realistic, commercially viable tool is required in order to

successfully develop suitable technology for the myriad of ocean going vessels requiring Ballast Water Treatment.

Whilst it is acknowledged that the shear variety of approaches to the BWT issue prevents a single technology from emerging as a clear frontrunner, from the critical review the use of hydrocyclonic separation has been identified as a potential leading technology. The objective of this study therefore, is to show that CFD has the capability to be utilised as a development tool for hydrocyclonic separation, and that it can be used to design a technological system that meets both the needs of the shipping industry and the legislative requirements.

This will be achieved by evaluating the turbulence modelling approaches of the CFD simulation on an industrial test case. This test case is based on geometry that replicates the inlet section of a reverse flow hydrocyclone, crucially it is a simplified geometry that isolates a number of flow regimes that are likely to be present within a hydrocyclone.

2.7 Chapter Summary

The objectives of this study are clearly defined based on the outcomes of the initial literature review, the impending legislation and the environmental concerns of the maritime industry. With respect to the primary aim of this study, that is to contribute to the successful developments within Ballast Water Treatment technology, the critical literature review has identified the focus of the study, centring on one of the most promising and practicable technologies, hydrocyclonic separation. Further evidence in support of hydrocyclonic separation can be found in the authors publications (see Appendix A).

It is highly likely that most viable BWT systems will consist of two stages; a large matter removal system, in this case hydrocyclonic separation, in conjunction with a secondary system targeting micro-organism mortality, such as UV radiation.

For the purpose of this study the secondary technologies shall be neglected, instead the focal point for the PhD will centre on the analysis and simulation of flow regime within a hydrocyclone in order to develop a more comprehensive understanding of the separation efficiency.

CHAPTER 3: THEORETICAL BACKGROUND

CHAPTER CONTENTS

3.1 Introduction

In a bid to establish the fundamental properties of the motion of fluids in relation to the uptake of ballast water and the associated removal of suspended particulate. It is necessary to define the operating characteristics of the ballast water system. According to the Royal Institute of Naval Architects (RINA) shipboard ballast configurations enable fully loading of ballast tank arrays at a volumetric flow rate of between 500 m^3/h and 1500 m^3/h. Furthermore RINA indicate that the piping used for Bilge, Ballast and all Seawater transport is of 5mm thickness, 210mm external diameter. Assuming a simplified, best case scenario of a ballast water pumping configuration consisting of twins pump delivering a combined volumetric flow rate of 500 m^3/h the following can be determined:

For Seawater at 4℃:

υ = 1.17 x10^{-6} m^2/s
ρ = 1.030 x10^3 kg/m^3
μ = 1.2051 x10^{-3} Ns/m^2

With an piping system configuration thus:

D_H = 0.2 m
CSA = 0.1257m
Q = 500 m^3/h

The fluid velocity within the pipe can be calculated using:

$$Q = A \times V \qquad [3.1]$$

Therefore the velocity of the fluid delivered by each of the two pumps is calculated to be 2.2101m/s per pump. The pipe Reynolds number, Re_{pipe}, can now be calculated by [3.2].

$$Re_{pipe} = \frac{\rho v D}{\mu} \quad [3.2]$$

This results in a pipe Reynolds number of 3.8 x10^5. It should be noted that the Reynolds number indicates the state of the flow, such that for Reynolds numbers (including Re_{pipe}) greater than 4000 the flow can be considered to be fully turbulent, with the onset of turbulence occurring at an Re of 10^4.

The outflow from the ballast pumps will then undergo treatment by the selected BWT technology, in this case a hydrocyclone. The principles of the hydrocyclone design have been in existence for over 100 years having been originally patented in 1891 by E. Bretney. Their fundamental operational is founded on the separation of particulate of the dispersed phase from the continuous phase. This separation is based primarily on the density difference between the phases, however separation depends heavily on particle size as well. In order to establish the viability of hydrocyclones for BWT it is necessary to understand the theory of particulate separation from a turbulent continuous phase liquid. Depending on the treatment technology under review the ballast tanks themselves may become the focal point of the BWT technology. In this instance the high Reynolds number turbulent flows do not resolve to become laminar flows, in fact as illustrated in figure 3.1 it can be seen that the large volume of the ballast tanks (upwards of 1000 tonnes per tank), coupled with the complex internal geometry of the supporting structure, will result in a fluid path that requires complex analysis in order to establish the best treatment mechanisms.

Figure 3.1. Cross section of a Containership. Red Outline shows Lower and 'J' Ballast tanks. (Source: [52])

The prediction of the motion of fluids and gases has long been a focus of scientific and engineering research. The ability to accurately simulate fluids, and thus to accurately predict the effects of these fluids has given rise to the development of a number of approaches including mathematical modelling, numerical techniques and computational solvers. Computational Fluid Dynamics is a tool combining numerical methods and mathematical algorithms to enable the simulation of fluidic problems. However at present CFD is only capable of provide approximate solutions to most fluidic problems and a careful understanding of the limitations of this tool is a prerequisite for successful use of CFD.

3.1.1 Navier Stokes: The Governing Equations

The fundamental laws that govern the dynamics of fluid flow concern the relationship between the inherent convective, viscous and pressure forces within a given flow. This relationship is the basis of the Navier Stokes equations. These governing equations detail the fundamental physical principles of mechanics, these being the conservation of mass, momentum and energy.

Conservation of mass

Restating these laws with respect to the motion of a fluid over time gives rise to the Continuity Equation: Conservation of rate of change of mass with respect to time (*wrt*) such that for incompressible flow:

$$\frac{\partial u}{\partial x}+\frac{\partial v}{\partial y}+\frac{\partial w}{\partial z}=0 \qquad [3.3]$$

Thus for a given closed volume the mass is a constant, regardless of any re-arrangement of its constituent parts, i.e within a closed system mass cannot be created nor destroyed, though it may be rearranged.

Conservation of momentum

Newton's Second Law, the conservation of rate of change of momentum *wrt* time, when applied to a fluid gives rise to the Navier-Stokes equations. The conservation form of the Eulerian 3 dimensional equations for incompressible flow are given thus:

$$\frac{\partial u}{\partial t}+u\frac{\partial u}{\partial x}+v\frac{\partial u}{\partial y}+w\frac{\partial u}{\partial z}=-\frac{1}{\rho}\frac{\partial p}{\partial x}+\frac{\mu}{\rho}\left(\frac{\partial^2 u}{\partial x^2}+\frac{\partial^2 u}{\partial y^2}+\frac{\partial^2 u}{\partial z^2}\right) \qquad [3.4]$$

$$\frac{\partial v}{\partial t}+u\frac{\partial v}{\partial x}+v\frac{\partial v}{\partial y}+w\frac{\partial v}{\partial z}=-\frac{1}{\rho}\frac{\partial p}{\partial y}+\frac{\mu}{\rho}\left(\frac{\partial^2 v}{\partial x^2}+\frac{\partial^2 v}{\partial y^2}+\frac{\partial^2 v}{\partial z^2}\right) \qquad [3.5]$$

$$\frac{\partial w}{\partial t}+u\frac{\partial w}{\partial x}+v\frac{\partial w}{\partial y}+w\frac{\partial w}{\partial z}=-\frac{1}{\rho}\frac{\partial p}{\partial z}+\frac{\mu}{\rho}\left(\frac{\partial^2 w}{\partial x^2}+\frac{\partial^2 w}{\partial y^2}+\frac{\partial^2 w}{\partial z^2}\right) \qquad [3.6]$$

Conservation of energy

The last of the three laws of conservation, when applied to a controlled volume of fluid, is also known as the First law of Thermodynamics, that is, the conservation of rate of change of energy *wrt* time.

$$\frac{\partial(\mathrm{e})}{\partial t}+\frac{\partial(\mathrm{ve})}{\partial x}=\frac{1}{\rho}\frac{\partial}{\partial y}\left(k\frac{\partial T}{\partial x}\right) \qquad [3.7]$$

In effect the first law of thermodynamics states that the heat added to a system minus the work done by the system gives rise to the change in internal energy of that system.

3.1.2 The Scales of Turbulence

One of the critical aspects of CFD use is the selection of the appropriate Turbulence Model for the problem. The direct use of the three conservation equations to study the turbulent flow within a domain is termed Direct Numerical Simulation (DNS). The difficulties surrounding the use of DNS to model flow comes from the wide scope for variety in the various turbulent time and length scales (the duration of existence and the size of the turbulent eddies). The smallest scales of motion (both time and length) encountered within turbulent flows are known as the Kolmogorov scales [53]:

$$\eta = \left(\frac{v^3}{\varepsilon} \right)^{1/4} \qquad [3.8]$$

$$\tau_\mu = \sqrt{\frac{v}{\varepsilon}} \qquad [3.9]$$

At the opposite end of the turbulent eddy spectrum reside the integral scales (ℓ). We can assume the separation of the scales within turbulent flows such that the integral scales are much larger than the Kolmogorov;

$$\ell >> \eta$$

Additionally within all turbulent flows there is an energy cascade process present which is created by the transfer of turbulent kinetic energy (*k*) from the larger integral scale eddies to the smaller Kolmogorov scale eddies. This process starts with the largest eddies generating turbulent kinetic energy. At the Kolmogorov scales, the most dominant forces are the viscous forces (the right hand side of the Navier

Stokes equations) resulting in the dissipation of this kinetic energy as heat through the action of molecular viscosity. Thus the Kolmogorov length and time scales dissipate naturally within turbulent flows. Although this energy is dissipated by viscosity in the smallest Kolmogorov wavelengths, the rate of dissipation is determined by the longer wavelengths at the start of the energy cascade.

Additionally the turbulence Reynolds number (Re_T) is based on the characteristics of the turbulent motion of the parameters $\sqrt{k}$, ℓ and *v.* Thus for very high Reynolds numbers (such as Re_{pipe} applied to hydrocyclone inlets) Kolmogorov hypothesised that there are a number of wave numbers at which the inertial forces dominate the transfer of energy. This is known as Kolmogorov's -5/3 power law and thus the energy spectral density, *E(k)*, under these conditions is defined [54]:

$$E(k) \sim \varepsilon^{2/3} k^{-5/3} \qquad [3.10]$$

This law is particularly significant for both Direct Numerical Simulation and Large Eddy Simulation, which will be discussed later. The range of wave numbers this applies to lies between the Integral and Kolmogorov length scales and is termed the *Inertial sub-range* (see figure 3.2). It is worth noting at this point that although there are specific terms applied to the length scales, the scales themselves are a continuous spectrum rather than a discrete set.

Figure 3.2. Energy Spectrum for a turbulent flow. (Source: [55]).

The Kolmogorov scale can be linked to the Reynolds number of the flow in another way such that:

$$\eta = (\mathrm{Re})^{-3/4} l \qquad [3.11]$$

where Re in this instance is given as:

$$Re = \frac{\rho v l}{\mu} \qquad [3.12]$$

In effect the size of the smallest length scale present within a flow is determined by the Reynolds number. The Reynolds number also indicates the range of the scales within the flow. This is due to high Reynolds number indicating that the viscous forces have only a local impact on the characteristics of the flow. Therefore without significant viscosity the smaller scales are left undamped, conversely the lower the

Reynolds number the greater impact viscosity has on the flow, thereby damping only the smaller scales and leaving the larger scales undamped. A flow is usually considered fully laminar at Reynolds numbers below 400 and fully turbulent at Reynolds numbers in the region of 10^4. It is assumed that the flows within the hydrocyclone would have a Reynolds above 10^4 and would be considered to be turbulent.

As well as the Reynolds and turbulence Reynolds numbers there are additional important scaling parameters when dealing with the Navier-Stokes equations. These are of particular use when dealing with experimental models.

The Richardson number expresses the ratio of potential to kinetic energy.

$$Ri = \frac{gh}{u^2} \qquad [3.13]$$

The reciprocal to the square route of the Richardson number is the Froude Number. The Froude number compares inertial and gravitational forces. Froude is used to quantify the resistance of an object moving through a fluid and as such objects of varying sizes can be compared by their respective Froude numbers.

$$F_D = \frac{U}{\sqrt{gd}} \qquad [3.14]$$

3.2 Modelling Turbulent Flows

One of the key issues surrounding the accurate modelling of the hydrocyclone within the CFD environment is appropriate selection of turbulence models. Turbulence occurs in a wide range of applications, broadly speaking a Reynolds number in excess of 10,000 indicate that the flow will be turbulent. This is characterised by the presence of a diverse and chaotic range of fluid 'packets' of differing scales of motion from Kolmogorov through to larger eddies. This range of scales can result in

considerable mixing and transport behaviour. The nature of turbulent flow varies significantly from application to application and the fluctuations in the velocity field can have a major impact on the transport of momentum, energy, and species concentration, the latter of which is of particular importance for the removal of particles in ballast water hydrocyclones. CFD software provides a number of different turbulence models which can be employed to model different turbulence characteristics within the domain. The requirement for a model for turbulence arises due to the need to simplify the otherwise complex governing equations. This is often achieved through either time averaging or equation manipulation in order to remove smaller scales, which would otherwise require a significant amount of computing time to solve. However these modified equations contain a number of additional unknown variables, hence turbulence models are used to determine these unknowns. It is worth noting that there is no single universal turbulence model, and the selection of an appropriate turbulence model is critical in order to achieve appropriate results. The selection of the most suitable model is determined by analysing the known characteristics of the flow to be simulated, taking into account such issues as the physics of the flow, the level of accuracy required, and the intended purpose of the results. Furthermore in order to utilise turbulence models to predict flow, it is necessary to understand the limitations of each turbulence model.

The aforementioned study of turbulent flows using the DNS method requires significant computer processing capabilities in order to achieve an accurate simulation for all but the smallest and simplest of domains because all scales of motion from ℓ to η have to be simulated. As a result DNS is regarded as unsuitable for the vast majority of research. As previously discussed the wide ranges of length scales present within turbulent flows gives rise to the requirement for a particularly dense mesh, that is the grid used to represent the flow domain. To resolve all spatial and temporal scales, the spatial and temporal grids would need to be extremely small in order to pick up the flow characteristics accurately. Hence the use of DNS is, for the most part, unrealistic due to the financial implications. This has led to the further development of turbulence models which can be applied to specific cases.

The selection and manner of use of the correct turbulence model is critical in order to achieve appropriate results from CFD simulations.

The primary focus of this study is to determine whether the Detached Eddy Simulation (DES) model can be utilised effectively for hydrocyclone modelling, however it is necessary to fully appreciate the advantages and the limitations of the alternatives. A summary of the alternatives follows and includes:

1. Reynolds-Averaged Navier-Stokes equations (RANS)
2. K-Epsilon model (KE) [Standard configuration]
3. Renormalisation Group K-Epsilon model (KE-RNG)
4. Large Eddy Simulation (LES)
5. Reynolds Stress model (RSM)
6. Detached Eddy Simulation (DES)

3.2.1 Reynolds-Averaged Navier-Stokes Equation

The Reynolds-Averaged Navier-Stokes equations (RANS) are a basis for a number of turbulence models. The RANS equations govern the transport of the averaged flow quantities, with the whole range of the scales of turbulence being modeled rather than solved. This approach leads to RANS based models requiring significantly less computational effort and resources than solution based approaches (such as DNS). In particular RANS based approaches are often adopted for practical engineering applications where the computational and time resources are commercially driven. In Reynolds averaging, the solution variables in the instantaneous Navier-Stokes equations are decomposed into the mean (either ensemble-averaged or time-averaged) and fluctuating components [56]. For incompressible constant flow the Reynolds averaged equations of motion written in conservation form [55] results in:

$$\rho \frac{\partial U_i}{\partial t} + \rho U_j \frac{\partial U_i}{\partial x_j} = -\frac{\partial P}{\partial x_i} + \frac{\partial}{\partial x_j}\left(2\mu S_{ji} - \rho \overline{u'_j u'_i}\right) \qquad [3.15]$$

The quantity $-\rho\overline{u_j' u_i'}$ is known as the Reynolds-stress tensor. One negative aspect of Reynolds averaging lies in the generation of additional unknown quantities. It is the intention of all turbulence models utilising RANS as a basis to approximate values for these unknowns and "close" the system.

3.2.2 The Standard K – Epsilon Turbulence model [57] [58]

Launder and Spalding's K-Epsilon model is the most widely used two equation turbulence model it includes two extra transport equations to represent the turbulent properties of the flow. This allows a two equation model to account for transient, historical flow effects such as convection and diffusion of turbulent energy. This version of the K-Epsilon model is often referred to as the Standard K-Epsilon model. The model provides two transport equations for both the turbulent kinetic energy, k, as well as the dissipation per unit mass, ε , the latter of which determines the scale of the turbulence. It is built using the aforementioned RANS equations as a backbone and closes the resultant Reynolds stress tensor using an assumption which relates the Reynolds stress tensor to the velocity gradients and an eddy viscosity. The latter is obtained from the two transported scalars. At high Reynolds numbers the rate of dissipation of kinetic energy ε is equal to the viscosity multiplied by the fluctuating vorticity. An exact transport equation for the fluctuating vorticity, and thus the dissipation rate, can be derived from the Navier Stokes equation. The k - epsilon model consists of the turbulent kinetic energy equation and the dissipation rate equation together with an equation for the eddy diffusivity [FLUENT]:

$$\mu_t = C_\mu \rho k^{1/2} l = \rho C_\mu \frac{k^2}{\varepsilon} \qquad [3.16]$$

The original development of the K-Epsilon model was instigated in order to improve the mixing-length model, as well as to find an alternative method to the algebraically set turbulent length scales in moderate to high complexity flows. The K-Epsilon

model attempts to model turbulence by performing time averaging, and under certain conditions this method can be very accurate. However the model is best suited to free-shear layer flows with small pressure gradients. Where large pressure gradients are present in transient flows the averaging process numerically diffuses most of the important characteristics of these time-dependent flows. Similarly, for wall-bounded and internal flows, the model gives good results only in cases where mean pressure gradients are small; accuracy has been shown experimentally to be reduced for flows containing large adverse pressure gradients. As such the K-Epsilon model could be considered to be inappropriate for flow analysis problems such as inlets and compressors.:

3.2.3 The RNG K – Epsilon Turbulence model

The RNG, or *Renormalisation Group* theory, model is a recent rework of the Standard K-Epsilon model. The RNG model employs the same eddy viscosity, *k* and ε equations given in the previous section. The differences lie in the use of a modification of the coefficient $C_{\varepsilon 2}$ [55] given as:

$$C_{\varepsilon 2} \equiv \tilde{C}_{\varepsilon 2} + \frac{C_\mu \lambda^3 (1 - \lambda / \lambda_0)}{1 + \beta \lambda^3} \qquad [3.17]$$

Where:

$$\lambda \equiv \frac{k}{\varepsilon} \sqrt{2 S_{ij} S_{ji}} \qquad [3.18]$$

The closure coefficients are:

$$C_{\varepsilon 1} = 1.42 \qquad \tilde{C}_{\varepsilon 2} = 1.68 \qquad C_\mu = 0.085 \qquad \sigma_k = 0.72$$
$$\sigma_\varepsilon = 0.72 \qquad \beta = 0.012 \qquad \lambda_0 = 4.38 \qquad [3.19]$$

This model is designed to predict better flow for systems with a high degree of swirl or system rotation. However, the model is comparable to the standard K-E model for

flow regimes that do not exhibit any swirl, examples of which include the flow over a flat plate, or cases involving flow impingement and axisymmetric jets.

3.2.4 Large Eddy Simulation (LES)

Large Eddy Simulation is an approach to turbulence modelling in which the larger eddies are computed in a time dependent simulation utilising a set of filtered equations rather than basing the solution on the RANS equations. The requirement for these filtered equations comes about as a result of the space or volume averaging process used to reduce computational time. LES, like DNS, solves large scale turbulent eddies explicitly. In order to pick up the smaller scales they are modelled as an effect on the flow field using a sub-grid scale. The basis for this is two-part. First, the larger scales are responsible for energy production and are usually anisotropic, therefore they cannot be modelled accurately. Second, the smaller scales have been found to be more universal i.e. isotropic, and hence are more easily modelled. The end result is a process which combines numerical solution with modelling approximations. This is achieved by filtering the Navier-Stokes equations in order to separate scales which will be modelled from those which will be solved numerically (see figure 3.3). Hence LES is generally considered to be a compromise between DNS and K-Epsilon variants.

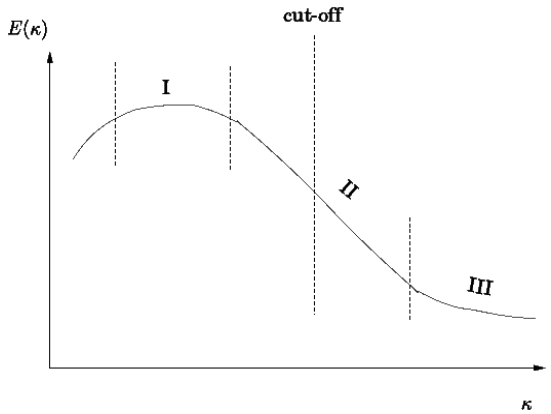

Figure 3.3. The limit between numerically solved large scales and modelled small scales in Large Eddy Simulations. Key-: I: Large, energy-containing scales, II: inertial subrange (Kolmogorov -5/3 range), III: dissipation subrange (Source: [55, 59]).

The filtered equations have the same form as the Navier-Stokes equations thus:

$$\frac{\partial \overline{u}_i}{\partial t} + \frac{\partial}{\partial x_j}\left(\overline{u}_i \overline{u}_j\right) = -\frac{1}{\rho}\frac{\partial \overline{p}}{\partial x_i} + \nu \frac{\partial^2 \overline{u}_i}{\partial x_j \partial x_j} - \frac{\partial \tau_{ij}}{\partial x_j} \qquad [3.20]$$

Whereby the Reynolds Stress tensor for LES is defined:

$$\tau_{ij} = \overline{u_i u_j} - \overline{u}_i \overline{u}_j \qquad [3.21]$$

This method is well suited for detailed time dependent calculations such as flow and mixing in large tanks. However, although not nearly as computationally intense as DNS, LES modelling is still a significantly costly computer process compared to the use of other turbulence models such as a two equation turbulence models or the Reynolds Stress Model.

3.2.5 The Reynolds Stress Model (RSM)

The Reynolds Stress Model discards the isotropic eddy-viscosity hypothesis in favour of closing the Reynolds-averaged Navier-Stokes equations by solving the Reynolds stress transport equations in conjunction with a dissipation rate equation. This effectively adds a further five transport equations for two dimensional flows and seven additional transport equations in three dimensions. RSM takes into account the effects of streamline curvature, swirl, rotation, and rapid changes in strain rate [60]. Significantly the RSM has the potential to give accurate predictions for complex flows; however the level of accuracy is dependent on the assumptions used to close the model with respect to the various terms in the transport equations in the Reynolds Stresses. The exact transport equations, as defined by FLUENT V6.3.26, for the transport of the Reynolds stresses, $\rho\overline{u_i' u_j'}$, is written [60]:

$$\underbrace{\frac{\partial}{\partial t}\left(\rho\overline{u_i'u_j'}\right)}_{\text{Local Time Derivative}} + \underbrace{\frac{\partial}{\partial x_k}\left(\rho u_k\overline{u_i'u_j'}\right)}_{C_{ij}\equiv\text{Convection}} = \underbrace{-\frac{\partial}{\partial x_k}\left(\rho\overline{u_i'u_j'u_k'} + \overline{p\left(\delta_{kj}u_i' + \delta_{ik}u_j'\right)}\right)}_{D_{T,ij}\equiv\text{Turbulent Diffusion}}$$

$$+ \underbrace{\frac{\partial}{\partial x_k}\left[\mu\frac{\partial}{\partial x_k}\left(\overline{u_i'u_j'}\right)\right]}_{D_{L,ij}\equiv\text{Molecular Diffusion}} \underbrace{-\rho\left(\overline{u_i'u_k'}\frac{\partial u_j}{\partial x_k} + \overline{u_j'u_k'}\frac{\partial u_i}{\partial x_k}\right)}_{P_{ij}\equiv\text{Stress Production}} \underbrace{-\rho\beta\left(g_i\overline{u_j'\theta} + g_j\overline{u_i'\theta}\right)}_{G_{ij}\equiv\text{Bouyancy Production}}$$

$$+ \underbrace{\overline{p\left(\frac{\partial u_i'}{\partial x_j} + \frac{\partial u_j'}{\partial x_i}\right)}}_{\phi_{ij}\equiv\text{Pressure Strain}} \underbrace{-2\mu\overline{\frac{\partial u_i'}{\partial x_k}\frac{\partial u_j'}{\partial x_k}}}_{\varepsilon_{ij}\equiv\text{Dissipatio n}}$$

$$\underbrace{-2\rho\Omega_k\left(\overline{u_j'u_m'}\varepsilon_{ikm} + \overline{u_i'u_m'}\varepsilon_{jkm}\right)}_{F_{ij}\equiv\text{Production by System Rotation}} + \underbrace{S_{\text{user}}}_{\text{User - Defined Source Term}} \qquad [3.22]$$

Whereas the differential equations governing transport of the kinematic Reynolds stresses $-\overline{u_iu_j}$ are given as [59]:

$$\frac{D\overline{u_iu_j}}{Dt} = -\left[\overline{u_ju_k}\frac{\partial U_i}{\partial x_k} + \overline{u_iu_k}\frac{\partial U_j}{\partial x_k}\right] - 2v\overline{\frac{\partial u_i}{\partial x_k}\frac{\partial u_j}{\partial x_k}} + \overline{\frac{p}{\rho}\left(\frac{\partial u_i}{\partial x_j} + \frac{\partial uj}{\partial xi}\right)}$$

$$-\frac{\partial}{\partial x_k}\left[\overline{u_iu_ju_k} - v\frac{\partial\overline{u_iu_j}}{\partial x_k} + \overline{\frac{p}{\rho}\left(\delta_{jk}u_i + \delta_{ik}u_j\right)}\right] \qquad [3.23]$$

The use of RSM is highly regarded when the flow features of interest are the result of anisotropy in the Reynolds Stresses. However the RSM requires significantly more computational time, especially when compared to the more simple K-ε RNG model. In addition due to the strong coupling of the Reynolds stresses there is a reduction in computational stability.

3.2.6 Detached Eddy Simulation (DES)

The DES model is considered to be a viable option for this study due to the fact that the near wall regions are modelled with an unsteady Reynolds Averaged Navier Stokes (RANS) model, while filtered versions of the same models are used away from the near-wall. The hydrocyclone central core region often generates an 'air-core', numerical reproduction of this flow characteristic is of particular interest.

In the DES model the central core of the domain is generally treated with LES as this is the region where the large turbulence scales have most significance [4], with the DES model utilised for the respective subgrid models in this region. Additionally the respective RANS models are used in the near-wall region.

In terms of computational cost it is generally considered that the use of a DES model is a suitable compromise in situations where a full LES model may result in unnecessarily high computational expenditure but where a standard RANS model may not provide suitable accuracy [5].

In effect the Detached Eddy Simulation (DES) turbulence model is a combination of LES and RANS methods. When the DES model is employed the domain is treated such that the boundary layer is modelled with a RANS approach whereas the detached eddies in the domain are captured with the LES turbulence model. The RANS model used is the one equation model proposed by [61].

$$\frac{\partial \rho \tilde{\nu}_t}{\partial t} + \frac{\partial \rho \overline{u}_j \tilde{\nu}_t}{\partial x_j} = \frac{\partial}{\partial x_j}\left(\frac{\mu + \mu_t}{\sigma_{\tilde{\nu}_t}} \frac{\partial \tilde{\nu}_t}{\partial x_j} \right) + \frac{C_{b2}\rho}{\sigma_{\tilde{\nu}_t}} \frac{\partial \tilde{\nu}_t}{\partial x_j} \frac{\partial \tilde{\nu}_t}{\partial x_j} + P + Y \qquad [3.24]$$

$$\nu_t = \rho \tilde{\nu}_t f_1$$

Additionally the production term *P* and the destruction term *Y* have the form:

$$P = C_{b1}\rho\left(\Omega + \frac{\tilde{\nu}_t}{\kappa^2 d^2} f_2\right)\tilde{\nu}_t$$

$$\Omega = \left(\overline{\Omega}_{ij}\overline{\Omega}_{ij}\right)^{1/2}, \quad \overline{\Omega}_{ij} = \frac{\partial \overline{U}_i}{\partial x_j} - \frac{\partial \overline{U}_j}{\partial x_i} \qquad [3.25]$$

$$Y = C_{\omega 1}\rho f_\omega \left(\frac{\tilde{\nu}_t}{d}\right)^2$$

Whereby *d* is ascertained by the distance to the nearest wall.

However *Shur et al* [62] proposed the DES model in which *d* is the minimum of the RANS turbulent length scale *d* and the cell length $\Delta = \max(\Delta x_\xi, \Delta x_\eta, \Delta x_\varsigma)$ as shown:

$$\tilde{d} = \min(d, C_{des}\Delta) \qquad [3.26]$$

Where Δ is based on the largest grid spacing in the three grid directions Δx_ξ, Δx_η. Additionally C_{des} is a constant and is usually set to 0.65.

In the boundary layer $d > C_{des}\Delta$, and so the model utilises the RANS approach. Where $C_{des}\Delta > d$ the LES model is employed. In this situation the modelled length scale is reduced and thus *Y* increases, thus reducing the turbulent viscosity $\tilde{\nu}_t$. The reduction in turbulent viscosity has a subsequent effect giving rise to a smaller production term *P* thereby reducing the turbulent viscosity even further.

The production term P given by equation [3.24] would increase as a result of the reduction in *d* during the transition from RANS to LES, however this has a negligible effect as the term is viscous and is only active close to the wall.

This study utilises the standard FLUENT DES turbulence model, this uses the Spalart-Allmaras model with the modification as prescribed by Shur et al in equation [3.27].

3.2.7 Outline of Turbulence models

We have already established that throughout the fluid path of a ships ballast system the fluid flow is turbulent. Turbulence is merely the catch-all terminology used to describe an irregular fluid motion whereby the velocity, pressure, concentration and temperatures (amongst other quantities) all exhibit an apparent random variation, with respect to the time within the flow field. However Hinze [63] discerned that these random variations can be statistically deduced.

It should be noted that turbulent motion is always rotational, and as such it is possible to define turbulence as an eddying motion, whereby a turbulent flow field consists of an array of eddies of varying size from low frequency to high frequency.

There are a number of fundamental characteristics observed in natural turbulent flow conditions [64].

Irregularity	This defines the fact that the flow is of a complex nature, it cannot be clearly predicted nor can it be easily described
Three Dimensional	There is always a three dimensional element to the flow regime. Even in the presence of an apparently strong directional flow, there is always secondary flow mechanisms in place.
Diffusivity	There is usually a rapid mixing of momentum, heat and mass.
Dissipation	Kinetic energy of the associated turbulent eddies are readily dissipated into heat under the influence of fluid viscosity. The energy required to maintain the turbulence itself therefore comes from the mean flow via the interaction of shear stresses and velocity gradients
Other	The fluid remains as a continuum. Turbulence is a flow feature and not a property of the fluid itself.

Understanding the physical aspects of turbulence and applying this knowledge to the defined operation of ship board ballast treatment enables greater understanding of the reported flow regimes exhibited by ship ballasting and deballasting. In this regard the turbulence models for computational fluid dynamics can be surmised with respect to the hydrocyclone.

KE

As the hydrocyclone exhibits strong three dimensional non-axisymmetric flows the use of the Standard K-epsilon model would yield insufficient detail as the time averaging process numerically diffuses most of the important characteristics of time-dependent flows. Thus the Standard K-epsilon turbulence model is not viable as a design validation tool for the highly turbulent, time dependent nature of the complex three dimensional flows of hydrocyclone separation.

KE-RNG

The Ke-RNG model is considered to be a successful reworking of the standard K-epsilon model, primarily focusing on the modelling of smaller scale eddies exhibited by systems with a high degree of swirl or system rotation. Despite the reworking the use of the KE-RNG model has shown mixed results for swirling flows in the literature, showing limited improvements over the Standard KE model with regards to the prediction of vortex evolution. Furthermore the use of this model is often limited to steady state analysis. Thus, as with the Standard KE model, the Ke-RNG model cannot be used as a detailed design tool for hydrocyclone evolution.

LES

Large Eddy Simulation is a popular technique for modelling turbulent flows, it shows good compromise between the highly computationally complex (and expensive) Direct Numerical Simulation techniques and the more simplistic modelling approaches of the K-Epsilon variants. It is particularly suited to detailed time dependent calculations such as flow and mixing in large tanks, and in this regard it may be considered for BWT techniques that are conducted within the ballast tanks themselves. However, although not nearly as computationally intense as DNS, LES modelling is still a significantly costly computer process compared to the use of other turbulence models such as a two equation turbulence models or the Reynolds Stress Model. As a design evaluation tool it is also more complex in its setup, as a result it is better suited to the research stage of fluid mechanics analysis.

RSM

The Reynolds Stress Model discards the isotropic eddy-viscosity hypothesis in favour of closing the Reynolds-averaged Navier-Stokes equations by solving the Reynolds stress transport equations in conjunction with a dissipation rate equation. The RSM has the potential to give accurate predictions for complex flows; however the level of accuracy is dependent on the assumptions used to close the model with respect to the various terms in the transport equations in the Reynolds Stresses. In this regard the RSM is a viable turbulence modelling approach for hydrocyclone

analysis, and could be well suited to BWT applications. However the momentum and turbulence equations are tightly coupled in the RSM, this requires a more robust setting of the boundary conditions, as well as possible convergence issues.

DES

As the primary focus of the study is on the hydrocyclone main flow, the fact that in the DES model the near wall regions are modelled with an unsteady Reynolds Averaged Navier Stokes (RANS) model speeding up the unnecessary computational time devoted to this region is beneficial. In contrast filtered versions of the same models are used away from the near-wall, in effect the Detached Eddy Simulation (DES) turbulence model is a combination of LES and RANS methods. The DES model is primarily in competition with the RSM model in terms of computational robustness, however from the point of view of the hydrocyclone designer the DES model primarily needs to show improved results over the less computationally costly models

Which turbulence model?

With regards to the turbulence models summarised here the DES model is potentially on a par with the RSM model in terms of computational prediction. However while the RSM model has been shown to outperform the KE and KE-RNG models when applied to cyclonic flows [65], the DES model has been shown to have improvements over the RSM for similar cyclonic flows [66]. In this regard the DES model will be assessed to identify its capabilities with respect to the flows exhibited by BWT hydrocyclones.

3.2.8 On the Detached Eddy Simulation: working with DES

The detached eddy simulation has already been identified as one of the most suitable turbulence models for the accurate simulation of the flow regimes expected within the BWT hydrocyclone. However as with all CFD modelling the application of

a specific turbulence model is not merely a matter of 'point and click'. The turbulence models themselves have been constructed with the view to enable them to be applied to a wide range of engineering applications. This results in a diverse range of setup parameters that, if incorrectly utilised, can result in simulations that not only inaccurately represent the real life flow domain, but in some cases artificially exaggerate modelling inconsistencies resulting in unrealistic flow domains. An example of this is that when using DES it is possible to degrade predictions by the improper use of grid density, whereby it is possible that the grid is too fine for the RANS region and too coarse for the LES region.

Another significant issues of hybrid RANS-LES models, of which the DES model is one type, is that there exists a “grey area” in which a shear layer, after separation, must generate LES content, such as random eddies, which were not present in the boundary layer upstream [67]. A sharp edge within the domain geometry provides a better shear layer for the LES content. As such the quality of the prediction achieved through the application of the DES turbulence model is dependent on the geometry and the subsequent flow regime exhibited.

Furthermore the destruction term contained within the Spalart-Allmaras model for eddy viscosity $\tilde{\nu}$ is proportional to ($\tilde{\nu}$ /d)^2. When balanced with the production term the eddy viscosity term adjusts to scale with the local deformation rate *S* and *d*: $\tilde{\nu} \propto Sd^2$. Additionally Subgrid-scale (SGS) eddy viscosities scale with *S* and the grid spacing Δ, i.e. $\nu_{SGS} \propto S\Delta^2$ [68]. The result of which is that the improper design and scaling of mesh size can greatly affect the 'handshaking' between the RANS and LES components of the model.

In order to minimise the effects of badly selected algorithm coefficients the DES model used in this study will consist of the standard FLUENT 6.3.26 Spalart-Allmaras Detached Eddy Simulation model. Instead a detailed mesh sensitivity study will be conducted in order to mitigate the adverse effects detailed above.

3.3 Sources of Error

As with any scientific work there is always the potential for error to occur. In the case of CFD there are two primary sources for error. These are generally split into domain modelling and simulation errors.

3.3.1 Domain modelling

These errors can occur for a number of different reasons, the modelled domain may be characterised by a more simplistic geometry than its real world counterpart, and the assumptions of which features to be neglected, such as fine details or simplifications to complex geometry may have adverse effects on the final results. Furthermore the application of incorrect physics parameters, such as fluid viscosity, or the absence of specific parameters, such as neglecting to account for gravitation, may also be a factor. Whilst it is widely acknowledged that simplifications are required in order to successfully model an engineering problem these simplifications, if incorrect, can have a profound effect on the final outcome of the simulation.

3.3.2 Simulation errors

The term Simulation Errors covers an array of different error sources. The numerical code itself may have coding errors that affect the simulation. For the work presented in this study the use of an industry leading commercial code significantly minimises this particular error source. However there are other potential error sources including numerical diffusion, discretization and iterative errors.

The presence of false diffusion (numerical diffusion) within the modelled domain can heavily influence the result of a simulation. Patankar [69] stated that:

"*False diffusion occurs when the flow is oblique to the grid lines and when there is a non zero gradient of the dependent variable in the direction normal to the flow."*

He goes on to demonstrate mathematically how numerical diffusion is not present if the flow is along a grid line, coincidently the equation also highlights that the resultant effect of numerical diffusion is at its most sever when the flow is at 45° to the grid. Equation 3.27 highlights this analysis;

$$\Gamma_{\text{false}} = \frac{\rho U \, \Delta x \, \Delta y \sin 2\theta}{4(\Delta y \sin^3\theta + \Delta x \cos^3\theta)} \qquad [3.27]$$

Where u is the resultant velocity and θ is the angle between 0-90° made by the velocity vector with the x direction.

This is an important point to note when using tetrahedral grids. However the use of small Δx and Δy, coupled with correctly flow aligned grids minimises the effect. In particular as real diffusion occurs in most flow problems it is possible to make the numerical diffusion significantly smaller that the real diffusion. To account for this effect all tetrahedral meshes used within this study utilise meshes with a small Δx and Δy.

In order to achieve a numerical solution to an engineering flow problem without incurring undue computation cost the equation series, which tend to be infinite, are discretized in order to provide a fixed set of data values. However the net effect of discretization is that the complete series is not utilised, consequently the solution is an approximate and not an absolute result. Depending on the purpose of the simulation and the required accuracy of the results, higher order terms can be included at the expense of computational cost.

Finally the iterative process involved in solving an approximation to the Navier Stokes equation requires a series of predetermined values to be prescribed in order to constitute convergence. An incorrect set of convergence criteria can result in a numerical solution which does not fully converge, furthermore the iterative process itself can enable errors to cascade with subsequent iterations.

3.4 Objectives - Review

Relating back to the objectives of the study; having identified the use of hydrocyclonic separation as a viable, and potentially leading, technology for the treatment of ballast water, the study will ascertain the ability of the Detached Eddy Turbulence model to out-predict both the KE RNG and the RSM models for non-isotropic situations where secondary flows are a significant feature, this will be achieved through the careful selection of a suitable test case of known experimental and prior numerical analysis.

CHAPTER 4: MODELLING THE FLOW IN A HYDROCYCLONE

CHAPTER CONTENTS

4.1 Particle fluid interaction and the theory of separation

4.1.1 Introduction

Computational simulations are an incredibly valuable tool to validate and assess the impact of geometry modification on the flow within hydrocyclones. To this end simulated flow conditions should replicate the real flow within the hydrocyclone as accurately as possible. In order to achieve accurate simulation it is crucial to understand the separation characteristics of a cyclone, determined by the particle-fluid interactions.

In order to build an accurate computational model it is necessary to understand the interactions between the fluid and the suspended particles. In the case of ballast water the main area of concern with regards to separation efficiency is the removal of the finest particles, such as bacteria and sediments. The prevention of large particle (>20mm) uptake is usually achieved upstream of the hydrocyclone through the use of a coarse mesh steel screen at the ballast water inlet. Additionally by targeting the smallest particles the assumption is that the larger objects will also be separated. Sea water naturally has a vast array of organisms present, with the greatest diversity in the micro-organism range. The removal of particles in this micro-organism range, such as bacteria, is an immensely difficult task, and may not be achievable at the scale required for onboard use. Therefore it is necessary to remove a sufficient percentage of fine and coarse particles, in order to allow any secondary treatment stages such as UV exposure to adequately deactivate harmful particles and pathogens (See Appendix C for UV calculations). In order to fine tune the geometry of the hydrocyclone through refined computational simulations it is necessary to determine the dimensionless groups which affect particle separation within hydrocyclones.

A beneficial aspect of sea water is that, while it contains a vast array of organisms, it is considered to be a fluid with a low concentration of solids. That is, the particles are sufficiently far apart that they can be assumed to act as if each is on its own. For the

purpose of initial simulation this assumption will be deemed to hold true for larger mobile organisms including fish.

4.1.2 Forces acting on a particle within a Cyclonic Separator

There are a number of factors designed into a hydrocyclone which contribute to the removal of particles from a fluid. The most fundamental separation action comes due to the separator exerting a force on the particle causing it to move towards the wall. In order to evaluate the effectiveness of the hydrocyclone design it is necessary to know the force exerted on the particle. The drag force on a particle is expressed as follows [43]:

$$F_D = C_D \cdot A \frac{\rho u^2}{2} \qquad [4.1]$$

For fast moving, coarse particles, the majority of the drag force is due to the inertia of the suspending fluid itself, therefore C_D is assumed to be constant. For fine particles, which tend to move much slower, it is the fluid viscous forces which affect the particle transport most significantly. This results in the drag coefficient being dependent on the particle Reynolds number, $Re_{p,}$ which determines the characteristics of the flow around the particle:

$$\mathrm{Re}_{particle} = \frac{u \cdot x \cdot \rho}{\mu} \qquad [4.2]$$

In the case of ballast water hydrocyclones the Reynolds number at the inlet is significantly high enough to ignore the effects of low Reynolds number laminar conditions. At the inlet the pipe Reynolds number (Re_{pipe}) is greater than 1000 (Newton's Region) the flow is considered fully turbulent and inertial forces are dominant with C_D being constant (C_D equates to approximately 0.44 in this scenario).

The difficulties associated with cyclonic separators used for BWT arise from the knowledge that in ideal situations a cyclonic separator, used to remove fine particles

from a fluid, will run flow rates with low Reynolds numbers and therefore fully laminar flow conditions. Ballast water uptake on vessels can require significant flow rates in order to fully ballast/deballast within the required time frame. As such it would be expected that the flow within a ballast water hydrocyclone is turbulent.

4.1.3 Biological Complexity of Sea Water

Whilst this study is composed of numerical simulation rather than experimental evaluation, it is worthwhile briefly discussing the complexities of the particulate composition of ballast water. Sea water is by definition a diverse fluid, incorporating estuaries, coastal region and open water. The biological composition varies significantly by location and timescales, from hours through seasons. Furthermore the diverse arrangements of biological target particles can differ, for example there are eight arrangements of the target bacteria alone (see figure 4.1).

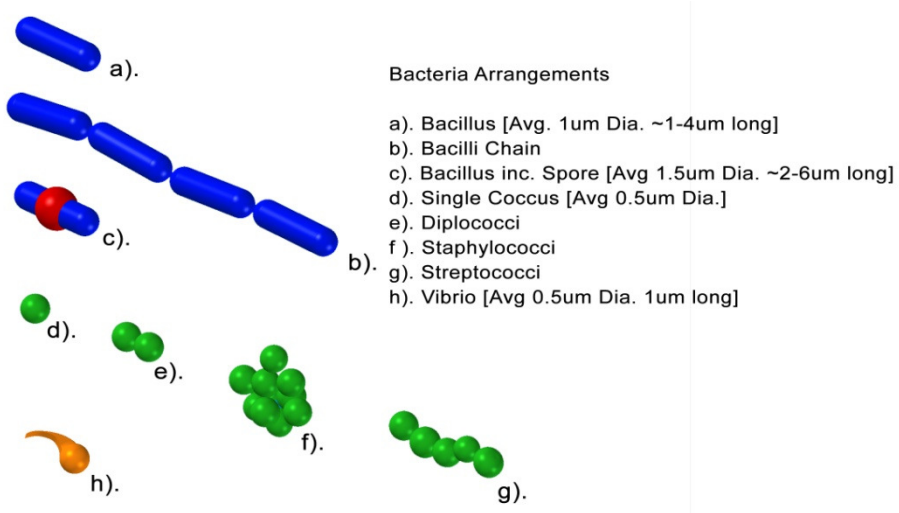

Figure 4.1. Diagram showing the array of bacterial arrangements possible within sea water. (Source: Author).

The combinations across each of these variables is so vast that it is not possible to define a standard natural sea water, to this end the European Union funded project "*On Board Treatment of Ballast Water (Technologies Development and Application and Application of low-Sulphur Marine Fue*l" (MARTOB) developed a biological test

solution that could be used for ballast water trials, this water was termed the MARTOB SOUP and its composition is given in table 4.1. It should be noted that even this solution is significantly different to any real sea water, concentrating on biological particulate only without incorporating any inorganic particulate. However in open water the composition of sea water is dominated by bacteria growth which tends to be an order of magnitude greater than inorganic particulates [70].

Species	Image	Size	Maximum field densities (in div.s m^{-3})	Standard mix composition (in div.s m^{-3})

Table 4.1. MARTOB SOUP: A Proposed 'standard' sea water for biological removal in Ballast Water Treatment experimentation [76].(data removed for copyright reasons)

The information on the MARTOB soup has been included to provide an insight into the size range, and quantities of particulate that the BWT will have to target. Furthermore this solution is only intended to establish effectiveness against these specific biological. The added complexities of larger macro organisms and general detritus within the sea water has been neglected.

4.2 Cyclone Analytical Models

One of the fundamental benefits to CFD as a tool for cyclone design becomes evident when you assess the analytical models available for cyclone design. The sheer complexity and scope for variation in design parameters has resulted in a number of different analytical models being made available. The majority of these analytical models have either been tailored for a specific cyclone configuration, or are necessarily simplistic in their approach and as such can only be used to determine approximate flow regimes for cyclones which fall outside of these ideal configurations.

A significant amount of comparative work has been conducted by other researchers in a bid to establish the suitability and subsequent limitations of the various analytical models. However the discrepancies between models are best highlighted by a direct back to back comparison. In our case five separate models will be used to determine the pressure drop across a cyclone designed according to the cyclone parameters identified by Rietema. The models under scrutiny are those from Barth, Stairmand, Shepherd & Lapple, Casal & Martinez and Muschelknautz. The complexity of these models varies significantly and provides a cross section of analytical models from the literature.

Each of the models will be used to calculate the pressure drop for a cyclone with the following design parameters, additional required flow characteristics are also provided (see figure 4.2):

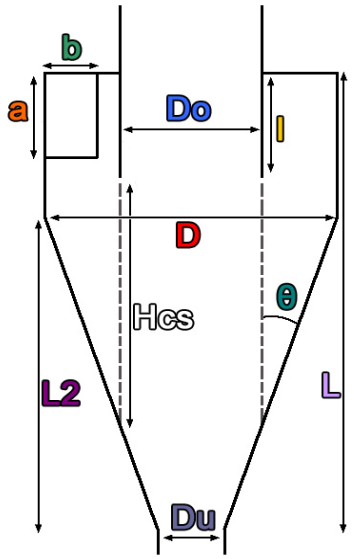

Component	Description	Dimension	Units
D	Cyclone Diameter	0.026	m
Do	VF Internal Diameter	0.0088	m
Du	Underflow Diameter	0.0017	m
L	Cyclone Length	0.13	m
L	VF Length	0.064	m
L2	Conical Length	0.0689	m
A	Slot Width	0.041	m
B	Slot Length	0.008	m
Θ		10	°
Hcs		0.066	m
Vin	Bulk Inlet Velocity	13.07	m/s
Vx	Axial Velocity	70.5	m/s
Solids Density		0.001	kg/m^3
Fluid Density		1.2041	kg/m^3
Flow Rate	Q	0.0043	m^3/s

Figure 4.2. Cyclone schematic and associated parameters conforming to Rietema design rules. Inlet flow characteristics based on experimental setup (see Appendix D). (Source: Author).

The first model to be assessed is that of Stairmand [77, 78]. His approach was to estimate the pressure drop as entrance and exit losses in conjunction with losses due to swirl within the cyclone body, this was primarily based on his calculations of the velocity distributions within the cyclone. A concise form of Stairmands model is provided by Iozia and Leith [79]:

$$\frac{\Delta p}{\frac{1}{2}\rho v_{in}^2} = Eu_{in} = 1 + 2q^2\left(\frac{2(D-b)}{D_x} - 1\right) + 2\left(\frac{4ab}{\pi D_x^2}\right)^2 \quad [4.7]$$

Where:

$$q = \frac{-\left(\frac{D_x}{2(D-b)}\right)^{0.5} + \left(\frac{D_x}{2(D-b)} + \frac{4A_R G}{ab}\right)^{0.5}}{\left(\frac{2A_R G}{ab}\right)} \quad [4.8]$$

In this case A_R is considered to be the complete internal surface area of the cyclone including the outer wall of the Vortex finder. The parameter *G* is a friction factor for the walls and is set at 0.005 in the Stairmand model.

By comparison the model proposed by Barth [80] {*via* [51]} focused on determining the wall velocities based on the inlet velocity to the cyclone. This was then used to establish the tangential velocity at a region within the cyclone referred to as the "Control Surface" or "CS". This control surface is an imaginary surface that projects from the tip of the vortex finder to the surface of the conical section of the cyclone (see figure 4.8). The fundamental principle of the Barth pressure loss model, like the Stairmand model, is to estimate the dissipative losses, in this case as individual components which arise from the inlet, cyclone body and vortex finder respectively. Where the loss in the inlet can be negated by good design and the loss in the cyclone body can be calculated by:

$$\frac{\Delta p_{body}}{\frac{1}{2}\rho v_x^2} = \frac{D_x}{D}\left(\frac{1}{\left(\frac{v_x}{v_{\theta CS}} - \frac{(H-S)}{0.5D_x}f\right)^2} - \left(\frac{v_{\theta CS}}{v_x}\right)^2\right) \quad [4.9]$$

Of significance is the fact that this model accounts for the effect of solids loading within the sample fluid where:

$$f = 0.005(1 + \sqrt[3]{c_o}) \quad [4.10]$$

The final equation used establishes the pressure loss within the Vortex Finder and is calculated as follows:

$$\frac{\Delta p_x}{\frac{1}{2}\rho v_x^2} = \left(\frac{v_{\theta CS}}{v_x}\right)^2 + k\left(\frac{v_{\theta CS}}{v_x}\right)^{\frac{4}{3}} \quad [4.11]$$

The value of K was determined empirically as either 3.41 or 4.4 for round or sharp edged vortex finders.

By contrast the research of Shepperd & Lapple [81, 82] and Casal & Martinez [83] resulted in proposals for empirical models based purely on the Inlet Euler (Eu_{in}) number of their respective cyclone designs.

The model proposed by Shepperd & Lapple, which is only valid for slot inlets, is as follows:

$$Eu_{in} = \frac{16ab}{D_x^2} \quad [4.12]$$

While the model proposed by Casal & Martinez is as follows:

$$Eu_{in} = 3.33 + 11.3 \left(\frac{ab}{D_x^2}\right)^2 \quad [4.13]$$

In both instances the models are simplistic in their approach and only provide inlet to outlet area ratios, whilst making the assumption that the Euler number is independent of the Reynolds number. In particular this assumption is valid for cyclones that posses similar geometry. Typically for two flows to be considered similar they require the same geometry, with equal Reynolds and Euler numbers, such that a direct comparison between a model and full scale fluid behaviour can be determined at specific locations. In this instance the use of the ratio of the cross sectional areas of the inlet to outlet ensure pressure loss similarity irrespective of whether Reynolds number similarity is maintained. In each case the resultant pressure loss can be determined by:

$$\Delta p = Eu_{in} \rho v_{in}^2 \quad [4.14]$$

The final model presented is that of Muschelknautz [84]. Based on the early work of Barth the Muschelknautz model is considered to be one of the more advanced models currently available and it has been developed significantly by research groups around the world. As a result of the sheer complexity of the model it will not be presented in full. It forms part of this analysis due to the fact that, unlike the

previous simpler model, the Muschelknautz model attempts to account for such factors as wall roughness and roughness due to particle deposition, inlet mass loading effects and changes in particle size distributions within the inlet stream.

The overall cyclone pressure loss is calculated by determining the losses associated with the cyclone walls (Δp body), the main core and vortex finder losses (Δp x) and finally any losses associated with the energy required to accelerate the particulate slurry (Δp acc).

$$\Delta p_{body} = \frac{f\ A_R \rho (v_{\theta\omega} v_{\theta CS})^{1.5}}{2x0.9Q} \quad [4.15]$$

$$\Delta p_x = \left(2 + \left(\frac{v_{\theta CS}}{v_x}\right) + 3\left(\frac{v_{\theta CS}}{v_x}\right)^{\frac{4}{3}}\right)\left(\frac{1}{2}\rho v_x^2\right) \quad [4.16]$$

$$\Delta p_{acc} = (1 + c_o)\left(\frac{\rho(v_2^2 - v_1^2)}{2}\right) \quad [4.17]$$

$$\Delta P = \Delta p_{body} + \Delta p_x + \Delta p_{acc} \quad [4.18]$$

Applying each of the models to a cyclone of known design, detailed previously, results in the following values for Pressure drop (see table 4.2):

Model: Pressure Loss, ΔP (Pa)	
Stairmand	7.34E+03
Barth	5.21E+03
Shepherd & Lapple	1.39E+04
Casal & Martinez	4.24E+04
Muschelknautz	1.12E+04
EXPERIMENTAL	1.71E+04

Table 4.2 Resultant Pressure loss (ΔP) for Rietema based cyclone design across the five Analytical models with reference to the experimental measurement. (Source: Author).

The reported analytical pressure drop vary from a low of 5.21E+03Pa to a high of 4.24E+04Pa, a range of 3.72E+03 Pa or -30% to +147% of the calculated experimental data for the design. Of significance here is the fact that the Muschelknautz and Shepherd & Lapple models most closely fit the experimental data despite the variation in model complexity between the two approaches.

This difference across models is not unique to pressure drop analysis. A somewhat condensed analysis of predicted cut size for the same cyclone design yields similar discrepancies across a number of analytical models further highlighting the requirement for accurate design data for bespoke cyclones (see table 4.3).

Model: Separation Efficiency, x50 (M)	
Barth	1.53113E-06
Time of Flight	3.02722E-06
Rietema	9.02273E-05
EXPERIMENTAL	n/a

Table 4.3 Resultant Separation Efficiencies (based on 50% cut size, x50) for a Rietema based cyclone design across the three Analytical model approaches. (Source: Author)

The complex array of analytical models is testament to the industry requirements for accurate cyclone design. Significant analytical research has been conducted in a bid to establish a simplified cyclone design process but, due in part to the endless permutations of the physical design parameters, the application of analytical models can result in significantly differing results. Whilst the literature points to a number of well matched analytical models the case in point highlights the fact that analytical models do not present an “off-the-shelf” solution to cyclone design. To this end the ability to simulate the flow regime within a cyclone via CFD can yield a better understanding of both the required design information as well as the physical flow phenomenon within the system, furthermore the use of CFD does not negate the application of analytical models but can be used to validate or preselect a known model to further enhance the design process.

4.3 Establishing a protocol: The use of a test case

Whilst the primary aim is to conduct a full CFD simulation of a known hydrocyclone geometry by far the simplest method of establishing the correct model setup is via the use of a test case. A Test case, in this instance, is a known problem. It is supplied with all the necessary required input criteria and has a corresponding known result. Selecting a suitable test case is critical in order to accurately apply the identified model domain criteria to the final problem. The fundamental principle of a test case is that it is a simplified model with respect to the final problem. In order to successfully identify the appropriate test case it is crucial that the geometry and physical flow of the final model is understood. In this instance the inlet section of the hydrocyclone is identified as one of the most fundamental regions within the cyclone domain. The presence of the vortex finder directly downstream of the inlet provides a curved physical obstruction which can give rise to flow separation. Furthermore as the flow approaches 360° revolution it impinges on the inlet flow.

4.3.1 Test Case: Square Profile Duct with 180° Bend

The test case has been used in this instance to identify the effects of a number of standard turbulence models. The test case geometry is clearly defined as a square profile duct (SPD) with a 180° bend, the inlet is an opening at the start of the straight section, located upstream of the bend. The outlet is at the 180° plane of the bend section. The SPD has been chosen as it has similar flow properties (as a result of geometry) to many commercially available cyclone inlets including the Rietema cyclone design used in this study. An outline of this SPD can be seen in association with a hydrocyclone, the image shown in figure 4.3 draws comparisons between three dimensional isometric images of the SPD and a cropped image of the uppermost section of a hydrocyclone, in this instance the hydrocyclone has been rotated through 90° and as such is effectively shown resting on its side. The inner curved wall of the duct suitably replicates the outer wall of the cyclone vortex finder, ensuring separation occurs as the flow rounds the bends. The initial data for the test case was made available by the European Research Community On Flow, Turbulence And Combustion (ERCOFTAC) [85]. Alongside the experimental setup of

the ERCOFTAC test case there has been further research conducted on the square profile duct with 180° bend, including additional experimental work alongside numerical modelling. This work was conducted by Choi et al [86, 87] including CFD work by Johnson (1984) [referenced via Choi et al].

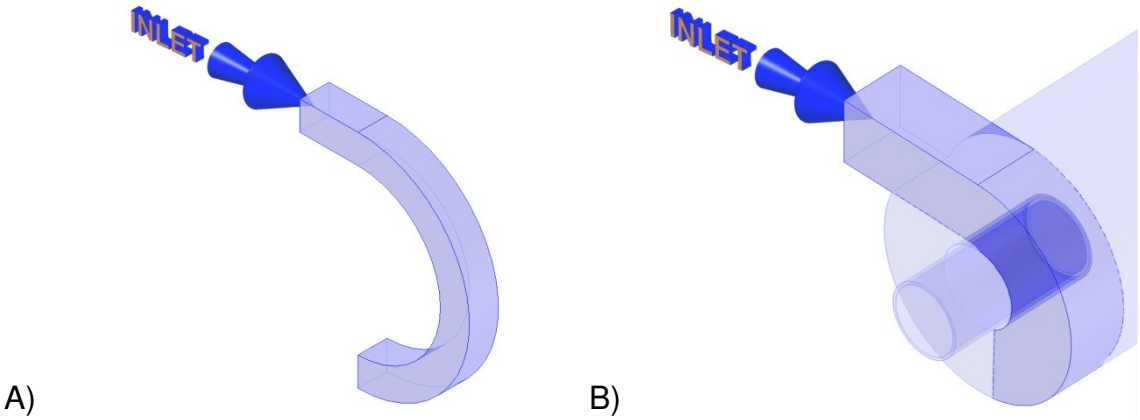

Figure 4.3 A) Diagram showing the geometry of the square profile duct test case, B) Diagram to show the area within a Rietema cyclone that the square profile duct test case will be approximating. (Source: Author).

The test case domain is of square section with a characteristic dimension of 1D. The profile consists of a straight inlet section of length 30D connected to a section that bends through 180°. The centreline curvature of the bent section has a radius of R = 3.375D. For the purpose of this study the characteristic dimension, D, is equal to 0.0899m, the metric equivalent of a 3.5" standard profile duct. The exact dimensions of the comparative work differs between sources and will be discussed further on. A schematic of the profile used in this study is shown in figure 4.4.

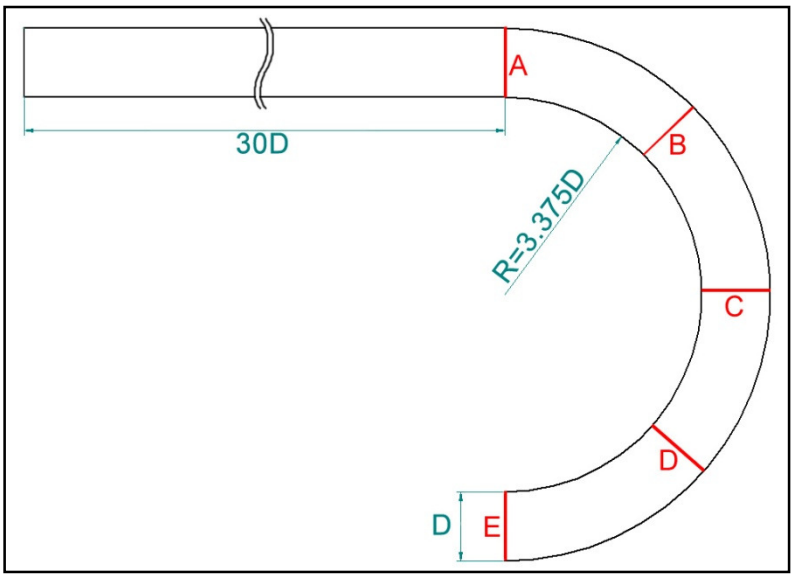

Figure 4.4. Geometry of ERCOFTAC test case: Square profile duct with 180° bend. Critical planar regions are also highlighted at 0° (A- Onset of Bend), 45° (B), 90° (C), 135° (D) and 180° (E- Outlet). (Source: Author).

4.3.2 Modelling

The numerical computation of turbulent flow within a square sectioned pipe with a 180 Degree bend has previously been conducted by Choi et al [86] respectively. In both cases the computational work was compared to experimental data by Choi et al [87] and an algebraic second moment closure model was combined with a mixing length model as an improvement on previous *k-ε* eddy viscosity models. As part of their study a number of significant assumptions and simplifications where made including modelling the domain about a central plane and employing a symmetry function.

Furthermore the total cells used in the CFD work by Choi et al had a total cell count of approximately 235,000. This was justified at the time thus:

> "*a minimum of about 25 nodes from the wall to the duct centre is sufficient to obtain a grid-independent velocity field at this level of turbulence modelling for bend flows without recirculation.*"

Whilst this approach, and the associated cell count is easily achieved using current computational technology, there is an opportunity to advance the numerical modelling of this engineering problem. To this end a number of corresponding decisions have been made, reflecting the objectives laid down in section 3.4. These include:

- Full three dimensional domain modelled
- High mesh cell count, incorporating boundary layer meshing
- Steady state and time dependent analysis
- Increased Inlet length (30D compared to 2D)

Full Domain Modelling

In this instance the previous numerical and experimental data is used to compare new CFD work using three different turbulence models, Renormalised *k-ε,* Reynolds stress model (RSM) and Detached Eddy Simulation (DES). The primary focus is to identify whether the Detached Eddy Simulation can be applied to Hydrocyclone modelling in order to increase modelling accuracy. As a result the assumptions of Chang and Choi have been ignored for the comparative study in order to identify secondary, cross centreline flows and to ascertain the significance of the inherent time dependent nature of the separated flow regime.

Increased Mesh Density

In order to establish the net benefits from each of the turbulence models there are two different domain meshes. The first of these meshes is an appropriate replication of that used by Choi, however it is a fully three dimensional domain incorporating an extended inlet region (discussed later). This domain will be used to establish the correlation between previous CFD work and the work presented here. The second of the two domain meshes has the same extended inlet and full three dimensional domain characteristics of the first, however the mesh density is significantly higher at

2.8 million cells. This mesh will primarily identify the abilities of the RSM and DES turbulence models to simulate the secondary, temporal flows within the SPD.

Steady State and Time Dependent Analysis

By their very nature the K-Epsilon and K-Epsilon RNG models provide a steady state solution to the modelled flow. While this is in keeping with the result presented for the algebraic second moment closure model (combined with a mixing length model) by Choi, both the RSM and DES models have the capacity to model time dependent flow regimes. As such a combination of steady state and time dependent flows will be analysed, the results for the time dependent simulation will be presented as both isolated 'snapshots' at a given time frame, as well as time averaged results for the duration of the modelled scenario.

Increased Inlet Length

Choi et al applied an experimentally derived inlet boundary profile to the CFD domain. Whilst this is an appropriate use of resources, for the purpose of this study the capacity for the entire system to be modelled to a suitable degree of accuracy is imperative. To this end the inlet conditions for the SPD have been modelled, an increase in the inlet length from two to 30 times the hydraulic diameter will ensure that the modelled boundary layer will be suitably formed prior to entering the 180° bend section. This inlet length increase is not an arbitrary increase, it was first discussed in the later work by Choi et al.

4.3.3 Methodology

Whilst the work of Choi et al utilised quadratic upstream differencing for convection in order to improve the impact of numerical errors the use of this approach was deemed to have no significant impact on the computed flow pattern at the 90 Degree plane [86]. As the 90 degree plane can be considered in isolation to a number of the potential numerical eccentricities of the original CFD, and the fact that this plane

exhibits a high degree of flow separation, it forms the basis of the comparison between the various CFD simulation results, including historical work and the experimental results of Chang et al. However a full comparative analysis of the DES turbulence model will be conducted for each of the remaining reference planes 45° and 130°.

Referring back to the objectives of this study the fundamental purpose of numerical simulation in ballast water hydrocyclone design is to accurately model the internal cyclone flow regime in order to determine shipboard system suitability without the need for costly experimental prototypes. In this respect the DES turbulence model has been chosen as it applies a RANS model close to the wall to predict the attached boundary layers while adopting a Large Eddy Simulation (LES) model in order to resolve the time-dependent, three dimensional large eddies thus incorporating the benefits of a higher accuracy model while reducing the necessary computational time. However in order to validate this statement the DES model has been compared with a number of other well known turbulence models. It is envisaged that the results of the test case simulations will ascertain whether DES can successfully be used to determine the flow regimes within a hydrocyclonic separator (hydrocyclone).

Meshing

As the simulation results of the test case are to be compared with previous work it is imperative that any purported improvements in the modelling can be clearly assigned to a specific characteristic of the model in this study. The use of a number of different turbulence models also gives rise to fundamentally different mesh structure requirements across the test simulations.

In addition there are two separate features of the previous CFD work that will be assessed, the first is whether there is strong secondary flows, previously neglected due to the use of a symmetry function, and the second is the capacity of the DES model to outperform the other turbulence models under scrutiny. For this reason

there are two different meshes utilised, both form the same geometry however. The two meshed domains are as follows;

1. Fully 3 dimensional, quadrilateral mesh at a density appropriate to historical meshes by Choi et al, albeit with a with a cell count of 518,175 (due to full 3D instead of symmetry). Mesh Reference - CM3D

2. Fully 3 dimensional, quadrilateral mesh at a significantly higher density with a cell count of 2,836,800. Mesh Reference - HDM

Whilst the meshes differ in cell count each mesh will be used for each of the turbulence models. Furthermore in a bid to identify the suitability of these meshes a separate mesh sensitivity study has been conducted. Throughout this study the meshing software GAMBIT, which is designed to operate specifically with the CFD package FLUENT, will be used.

Mesh Sensitivity

The purpose of the mesh sensitivity (MS) test is to identify whether changing from a lower density to a higher density mesh may be capable of resolving turbulence behaviour, in particular whether there is a specific configuration change that results in a vastly different numerical outcome. The occurrence of a step change in numerical outcome could be seen as an indication of incorrect starting cell size, such that smaller eddies may be only partially resolved, despite correct application of suitable turbulence model and boundary conditions. Conversely it indicates the point at which a higher density mesh is capable of resolving the eddies.

The domain used for the MS is split into two primary regions as shown in figure 4.5, a straight 30D long inlet (section A) and a 50° bent segment representing the first portion of the 180° bend (section B).

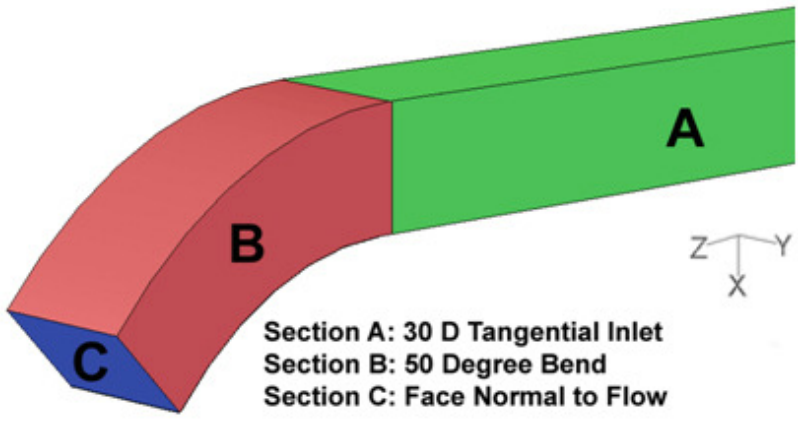

Figure 4.5. Schematic defining the regions of interest with the mesh sensitivity study. (Source: Author).

The mesh densities varied across each of the four tested domains (denoted as MS1, MS2, MS3 and MS4), however only two mesh density variations, and permutation of these, were assessed in a bid to define the critical region alongside the MS analysis. To this end the cell structure normal to the flow was maintained across all studies, and was based on initial studies that identified the necessary meshing required to pick up the secondary flow in the corners of the square profile using the DES turbulence model. The breakdown of the meshes employed for each MS domain is provided in table 4.4. A schematic of the streamwise mesh structure is also provided in figure 4.6.

Case	Section A	Section B	Section C		Total Cell Count
	Cell Count Streamwise	Cell Count Streamwise	Cell Count Normal to Flow		
			X	Y	
MS1	240	50	50	50	725,000
MS2	240	25	50	50	662,500
MS3	120	50	50	50	425,000
MS4	120	25	50	50	362,500

Table 4.4. Mesh structure for the four mesh sensitivity studies. (Source: Author).

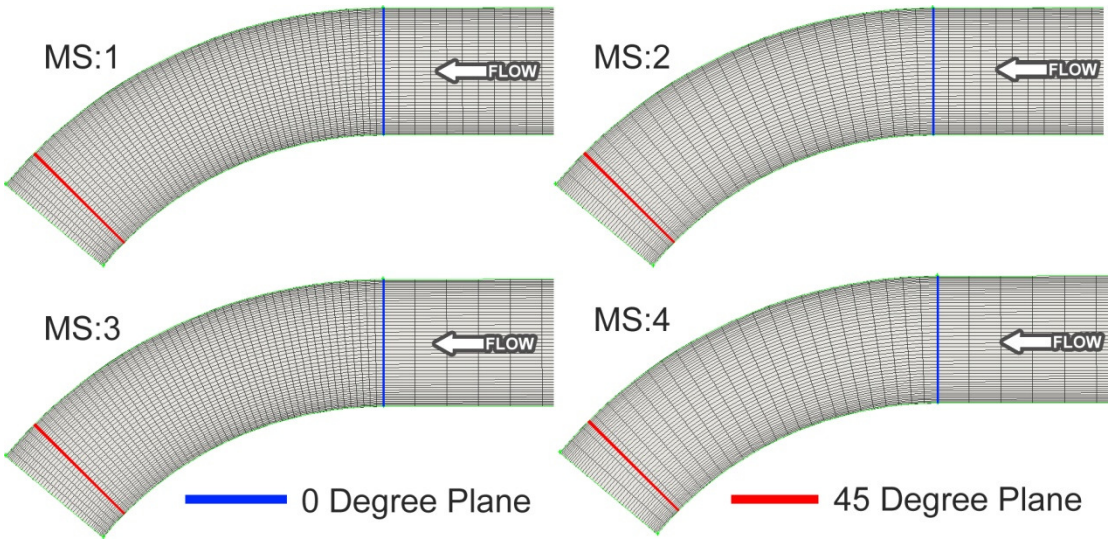

Figure 4.6. Streamwise mesh schematic used across the four mesh sensitivity test domains. (Source: Author).

In order to evaluate the effects of the mesh sensitivity analysis six data reference points have been selected. The location of the reference points for the mesh sensitivity analysis is defined in table 4.5, furthermore figure 4.7 identifies the reference points with respect to the domain geometry. The co-ordinates of the reference points are provided in Appendix B.

Reference Point	Section	Flow Regime
1	Within initial 50° section of the 180° bend.	Centre of flow, maximum velocity in the bend expected.
2		Inbound of the non-critical side walls.
3		Downstream of critical separation point on the lower curved wall.
4	Onset of Bend section, downstream of 30D inlet	Upstream (straight inlet side) of the critical separation point on the lower curved wall.
5		Centre of flow, maximum velocity in the inlet expected.
6		Corner of the non-critical side/top walls, potential are for secondary flow development.

Table 4.5. Mesh sensitivity reference point descriptions. (Source: Author).

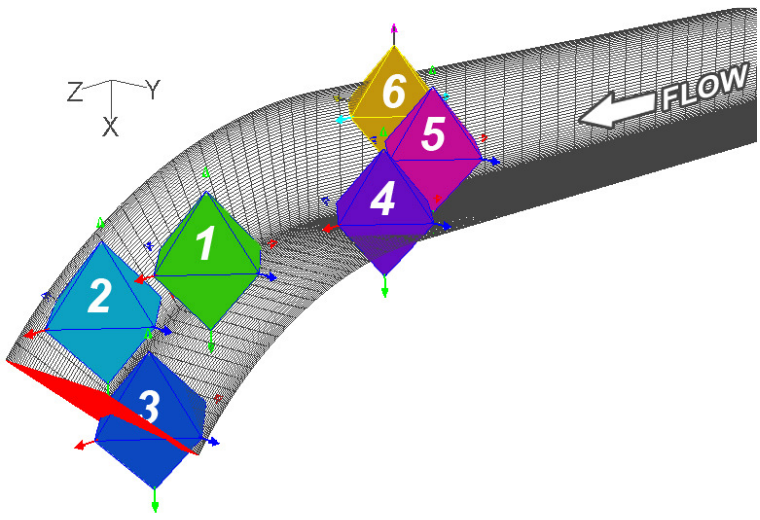

Figure 4.7. Mesh sensitivity reference point locations. (Source: Author).

Boundary Conditions

As with the primary test case common to each of the assessed turbulence models are the following boundary conditions. The domain fluid, Air, is used as standard such that the following parameters apply:

- Kinematic viscosity: $\nu = 1.72\times10^{-5}$ m^2/s.
- Inlet bulk axial velocity $W_B = 11$ m/s.
- Reynolds number based on the bulk axial velocity W_B: $Re = W_B D/\nu = 56{,}690$.
- ρ = 1.225 Kg/m^3
- μ = 1.7894e-05 Kg/m-s

These parameters have been modified in accordance with the data presented within the ERCOFTAC test case literature [8]. It is assumed that the most likely cause for the numerical disagreement in the reverse calculation of these parameters is due to numerical rounding. In particular the calculated value for the Inlet bulk axial velocity, with a Reynolds number of 56,690, gives rise to an Inlet bulk axial velocity of 10.85m/s. It is feasible that this has been reported as 11m/s in the literature. For the purpose of this study this minor numerical disagreement has been ignored.

Post Processing

The post processing capability of FLUENT enables the results of the DES simulations of each MS test to be compared allowing for temporal fluctuations in the flow regime. The unsteady state statistics, mean static pressure and mean velocity magnitude, have been presented in charts 4.1 and 4.2.

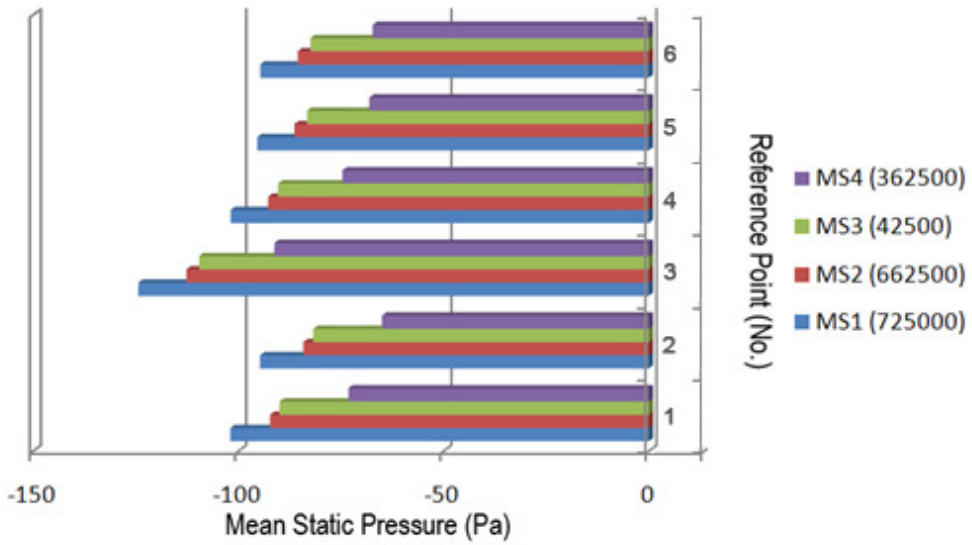

Chart 4.1. Unsteady statistics showing mean static pressure (Pa) for six reference points across four mesh studies. (Source: Author).

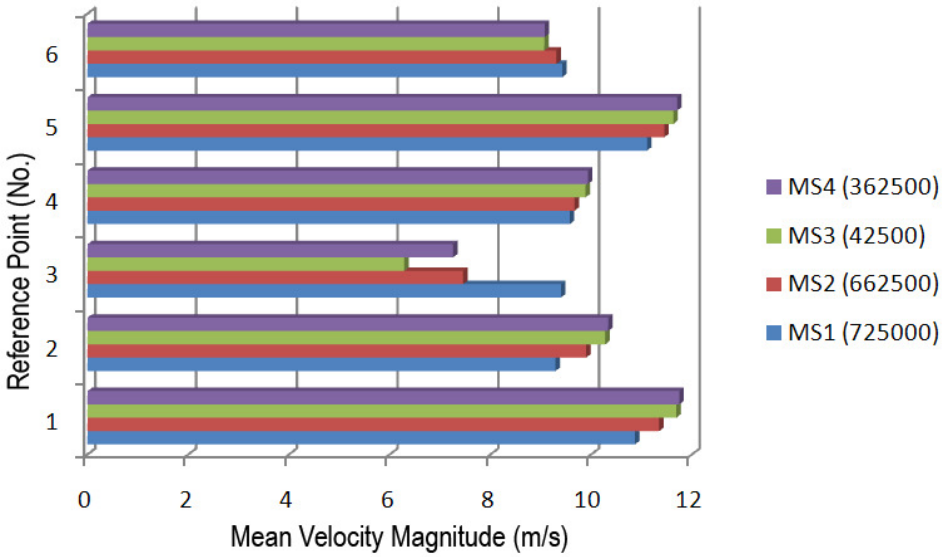

Chart 4.2. Unsteady statistics showing mean velocity magnitude (m/s) for six reference points across four mesh studies. (Source: Author).

Mesh Sensitivity - Discussion

Generally speaking MS4 reports higher mean static pressure and subsequently higher mean velocity magnitude at locations 1, 2, 4 and 5 within the domain. The reduced mesh density in both of the critical regions has resulted in less turbulent eddies being resolved and thus less impact on the initial starting conditions of the flow. This implies that the boundary layer development would be insufficient to accurately capture the flow separation at the onset of the bent section of the domain.

Reference points 4, 5 and 6 all report similar mean static pressures across the four MS tests, with points 5 and 6 near identical. In terms of the mean velocity magnitude the results indicate that a parabolic velocity profile has developed, shown by the higher mean velocity magnitude at point 5 (centre of flow) compared to points 4 (lower surface, inside bend boundary layer) and 6 (side wall boundary layer).

Of interest is the fact that MS2 and MS3 report similar results across all reference points. This indicates that the mesh in the straight section, whilst important for

correct boundary layer development, can be partially accounted for by a higher mesh density in the curved region.

The most significant difference across all tests and reference points applies to point 3. Whilst the mean static pressure follows a similar trend to other reference points the mean velocity magnitude is a noticeable outlier. Furthermore reference point 3 lies in the key region of interest (ROI) lying within the flow separation region in the bent segment of the domain.

Mesh Sensitivity - Impact

The findings from the MS tests have been used to determine the best compromise between computational cost and resultant accuracy for the mesh applied to the full test case analysis. In this respect the mesh for the test case will include a lower density region within the straight inlet in order to reduce computational times, with a high density mesh for the bend section. This high density mesh extends a distance of 2D upstream of the bend to account for boundary layer development upstream of the critical region and should prevent any interface issues resulting from the mesh density change from affecting the separation point. This equates to a cell structure consisting of 360 cells in the streamwise direction for the initial 28D straight inlet, a further 68 cells for the final 2D segment. The cell count for the 180° section is 360, equating to 2 cells per degree of arc. The final mesh for the full scale DES analysis (HDM) is shown in figure 4.8, highlighting the three meshed regions (streamwise).

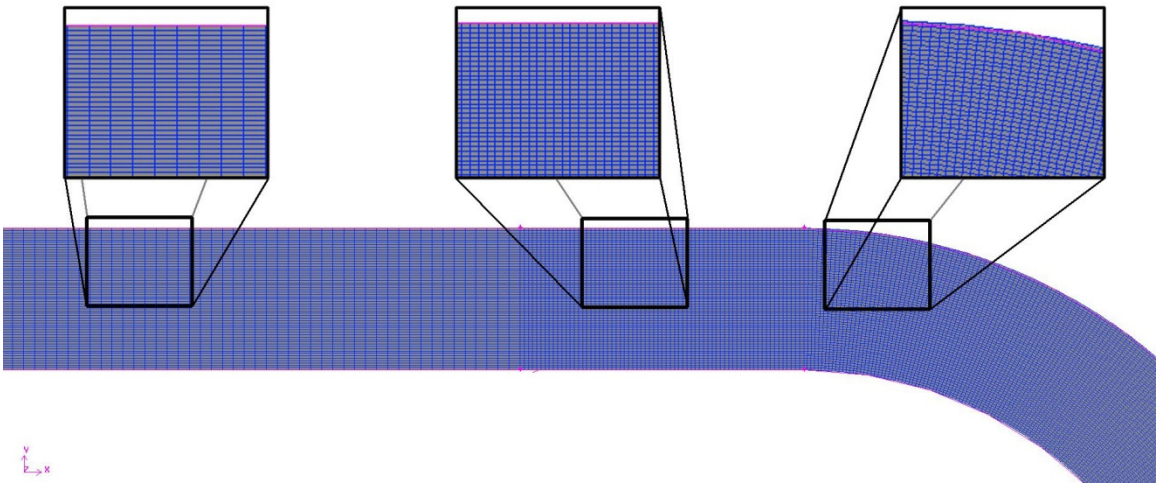

Figure 4.8. HDM Streamwise mesh structure employed for full scale DES analysis (including comparison with k-ε RNG *and RSM turbulence models). (Source: Author).*

For comparison the mesh structure as used by Choi et al is shown in figure 4.9. This mesh will be used to conduct a parallel study of each of the turbulence models as discussed previously. It should be recalled that this mesh, though comparable to that of Choi et al, is a fully three dimensional mesh and thus does not have the symmetry function of Choi applied. The fully 3D variation (CM3D) of the historical mesh equates to a cell structure consisting of 135 cells in the streamwise direction for the straight inlet with a further 90 cells for the 180° bent section, equating to 1 cells per 2° of arc.

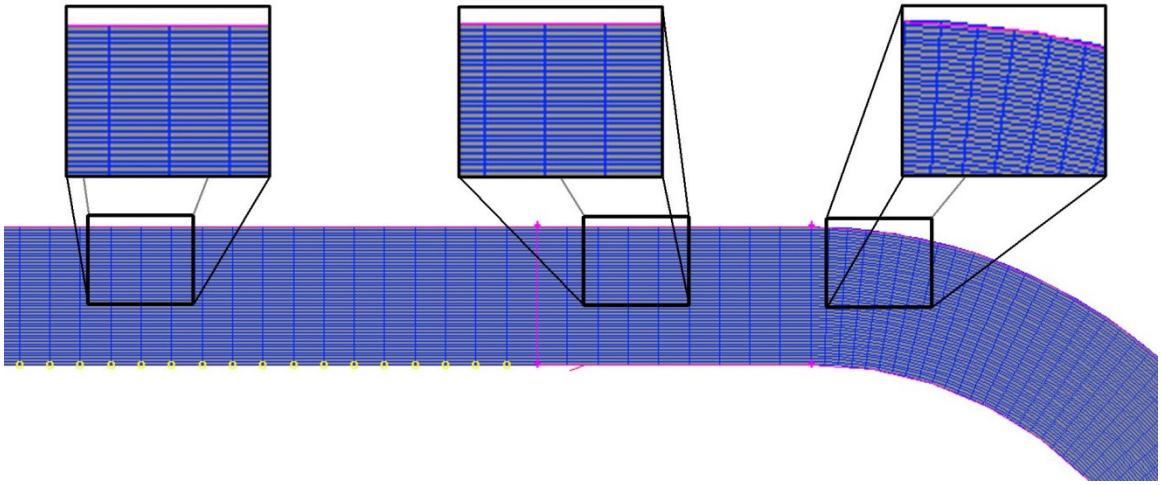

Figure 4.9. CM3D Streamwise mesh structure employed for historical CFD/DES analysis (including comparison with k-ε RNG *and RSM turbulence models). (SOurce: Author).*

For completeness the mesh structure normal to the flow for the CM3D consists of cells 49 x 49 square. By contrast the HDM used for the DES study consists of cells 60 x 60 square.

It should be noted that the higher density mesh has a minimum grid size equating to 1/3 of the inlet turbulent length scale. Whereby the inlet turbulent length scale is taken as 7% of the hydraulic diameter of the duct. This dense mesh should ensure that the small flow structures are resolved, a feature not expected to be picked up by the lower mesh density of the CM3D.

FLUENT Configuration of the comparative turbulence models

The variables associated with each of the assessed turbulence models varies across each model. To this end the boundary conditions and associated FLUENT parameter setup will be detailed for each model in turn and can be found in Appendix B.

The configurations tested and subsequently incorporated for analysis are listed below (see table 4.6). Their reference file is also detailed (Note: missing files within the sequence denote erroneous or non-required simulations. The full list can be found in Appendix B);

File Ref.	Turbulence Model	Cell Count (No.)	Termination Time (s)
1.1	DES	2,836,800	4.8015s
1.3	*k-ε* RNG	2,836,800	Steady State
1.4	RSM	2,836,800	Steady State
1.7	*k-ε* RNG	518175	Steady State
1.10	RSM	518175	Steady State
1.12	DES	518175	6.0s

Table 4.6. Test case simulation details and file reference. (Source: Author).

Common to each of the above configurations is the domain fluid, in this case standard Air, with a constant density of 1.225 Kg/m^3 and a constant Viscosity of 1.7894e-05 Kg/m-s, has been selected. Furthermore the conditions are set to utilise an operating pressure of 101325 Pascals (1atm).

Solution Controls

For the purpose of all CFD simulations within this study a first order upwinding scheme will be employed. The low mach numbers associated with the velocities in the two primary domains (SPD test case and Rietema cyclone) benefit from the higher stability associated with first order upwinding schemes. First order schemes tend to be extremely stable in low Mach systems and this presents convergence advantages in marginally stable solutions. Furthermore the quadrilateral, flow aligned mesh used for the test case domain minimises the numerical diffusion that can arise due to the use of first order schemes, as discussed in Chapter 3. Although the QUICK (Quadratic Upstream Interpolation Convective Kinetics)scheme can be applied to the test case mesh, the possibility of moving from a quadrilateral mesh to a tetrahedral mesh post test case analysis resulted in discarding QUICK as a viable discretization scheme for this study as it is not well suited to tetrahedral meshes. Whilst acknowledging the availability of second order upwinding, Power Law, QUICK and third order MUSCL (Monotone Upwind Scheme for Conservation Laws)

schemes, these discretization approaches have not been utilised for either SPD or Cyclone analysis. However it should be noted that Bounded Central Differencing is the standard discretization mode for Momentum when using a Detached Eddy Simulation. Furthermore the Pressure-Velocity coupling algorithm, SIMPLE (Semi-Implicit Method for Pressure-Linked Equations), has been chosen for its suitability for turbulent, separating flows, SIMPLEC (Semi-Implicit Method for Pressure-Linked Equations Corrected) is predominantly suited to simple, laminar flows. It is the intention that future DES only work may employ the PISO (Pressure Implicit Splitting of Operators) scheme for it suitability for transient applications, however as direct comparisons between simulation were to be established it was deemed incongruous to adopt the PISO scheme for the DES simulations in isolation. Figure 4.10 shows the menu for these controls.

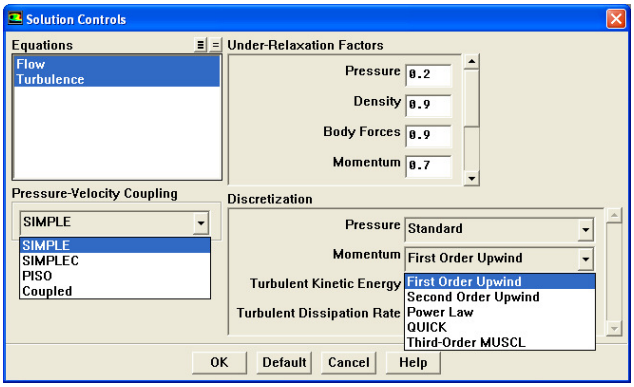

Figure 4.10. FLUENT Solution Controls menu. Pressure-Velocity Coupling and Discretization call out menus shown. (Source: Author, via FLUENT).

The turbulence modelling section of the FLUENT documentation with states that for modelling turbulence within swirling flows, including cyclonic flows, then the *k-ε* RNG, Realizable *k-ε* or Reynolds stress model should be adopted, and that the defining factor is the associated swirl number of the domain. Whereby the swirl number is ratio of axial flux of angular momentum to axial flux of axial momentum thus:

$$S = \frac{\int rw\vec{v} \cdot d\,\vec{A}}{\bar{R} \int u\vec{v} \cdot d\vec{A}} \quad [4.19]$$

In particular the recommendation by FLUENT is that for flows with a high swirl, S>0.5, then the RSM should be used [56].

However the documentation does touch on a number of comments referred to earlier, such that in cyclonic separators the near-wall turbulence is often a secondary issue at most and that the fidelity of the predicted simulation results are mainly determined by the accuracy of the turbulence model within the core region. For this reason the Spalart-Allmaras DES model has been selected as it provides sufficiently detailed analysis of the critical core region whilst minimising the computational cost of analysis of the near wall regions.

Results and Discussion

The data for the SPD simulations is presented across five rakes across the analysis plane (see figure 4.17). Each of the planes correspond with those referenced in the original ERCOFTAC test case, the rakes across all planes are as indicated. While there are five specific reference planes, 0° - 45° - 90° - 130° and 180° it should be noted that the 0° and 180° were not used by Choi et al and therefore do not form part of the comparative analysis. For reference each plane has five rakes (or lines of analysis), corresponding to the equation 2Y/D = [0, 0.25, 0.5, 0.75, 0.875]. The plane of symmetry (which can be seen in figure 4.11 falls in line with the rake at 2Y/D=0. As discussed previously the primary focus will be on the 90° plane.

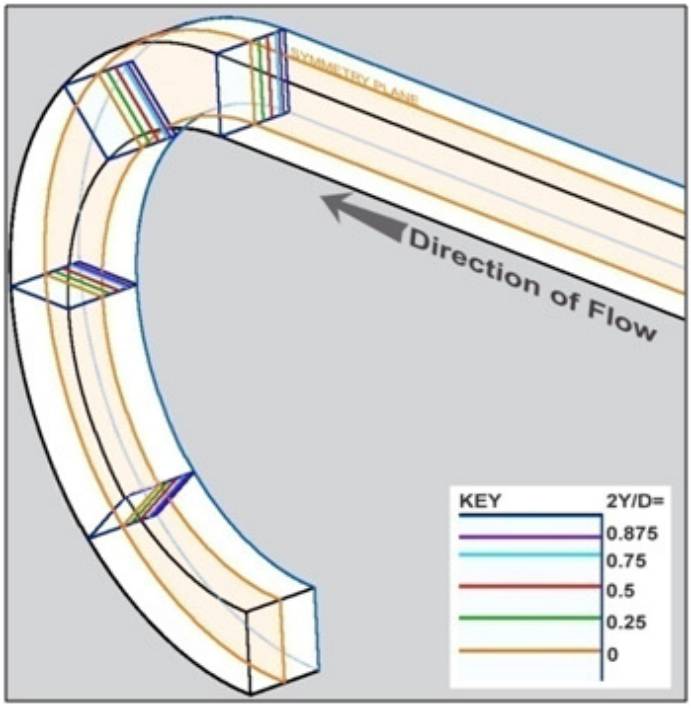

Figure 4.11. Location of reference rakes (2Y/D) on key planes. (Source: Author).

The primary comparative data source of the velocity profiles at the 90° Plane are given by Choi and are shown in figure 4.12. It should be noted that the five separate reference rakes have been plotted on a single chart by means of an amplified stepping of the data points, in each 2Y/D instance the mean bulk velocity (W/W_B) is stepped vertically by +0.25. This method of data presentation will be maintained for all data charts that are to be evaluated against the data presented by Choi et al.

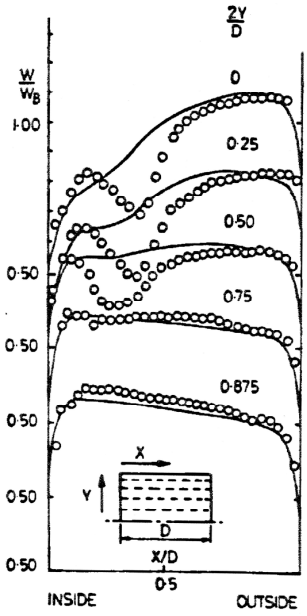

Figure 4.12 Streamwise mean velocity profiles on the 90° plane. Measurements are shown as point samples while the CFD work of Johnson (1984) is shown by a straight line.

One of the most significant findings of the earlier work was the inability of the numerical modelling to accurately model the “velocity hole” that occurs due to the separation of flow round the bend. In this respect a number of additional simulations have been conducted in order to identify whether any improvement in the numerical modelling is the result of turbulence model selection, increased mesh density, or higher performance computing. With regards to the turbulence model selection in particular the primary purpose is to ascertain whether the DES model is a suitable turbulence model for separating flows with strong secondary flow regimes.

The analysis has been separated into two sections. The first section will concentrate on the 90° reference plane and assess each of the turbulence models in turn, the second section will assess the results of the DES model for each of the remaining reference planes. In general the following aspects will be considered;

- Effects each of the turbulence models has on the reported result.
- Potential causes for discrepancy between experimental and simulated results.
- General engineering assumptions, and considerations for applying the test case findings to the hydrocyclone.

Results: Section 1 - 90° Reference Plane

The velocity profiles along the reference rakes (2Y/D = 0, 0.25, 0.5, 0.75 and 0.875) on the 90° Plane have been plotted in charts 4.3 -> 4.7. In all instances the charts represent the velocity profile from the inside bend towards the outside bend (see figure 4.13).

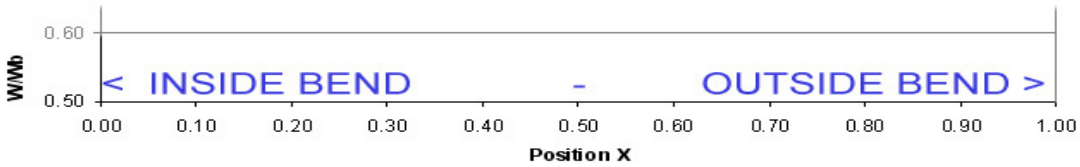

Figure 4.13. Chart position with respect to physical geometry. (Source: Author).

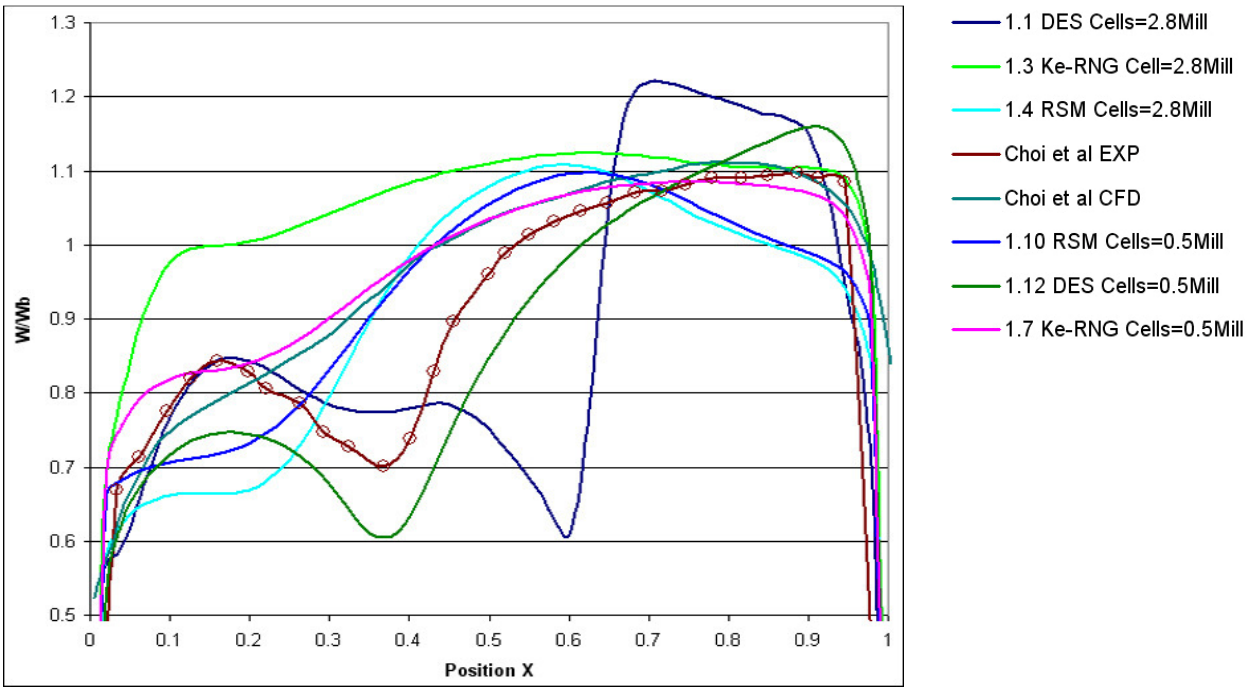

Chart 4.3. Numerical model comparison data for 90° Plane of the ERCOFTAC 180° Square Profile Duct. Rake 2Y/D=0 on 90° Plane. (Source: Author).

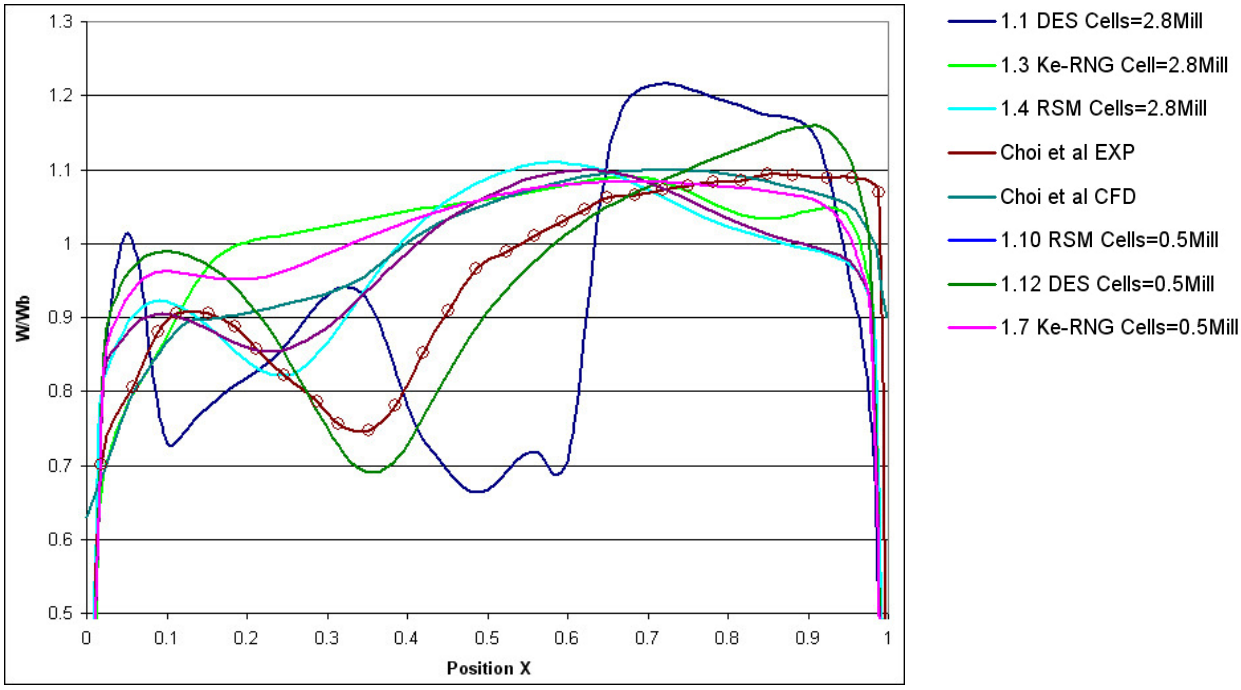

Chart 4.4. Numerical model comparison data for 90° Plane of the ERCOFTAC 180° Square Profile Duct. Rake 2Y/D=0.25 on 90° Plane. (Source: Author).

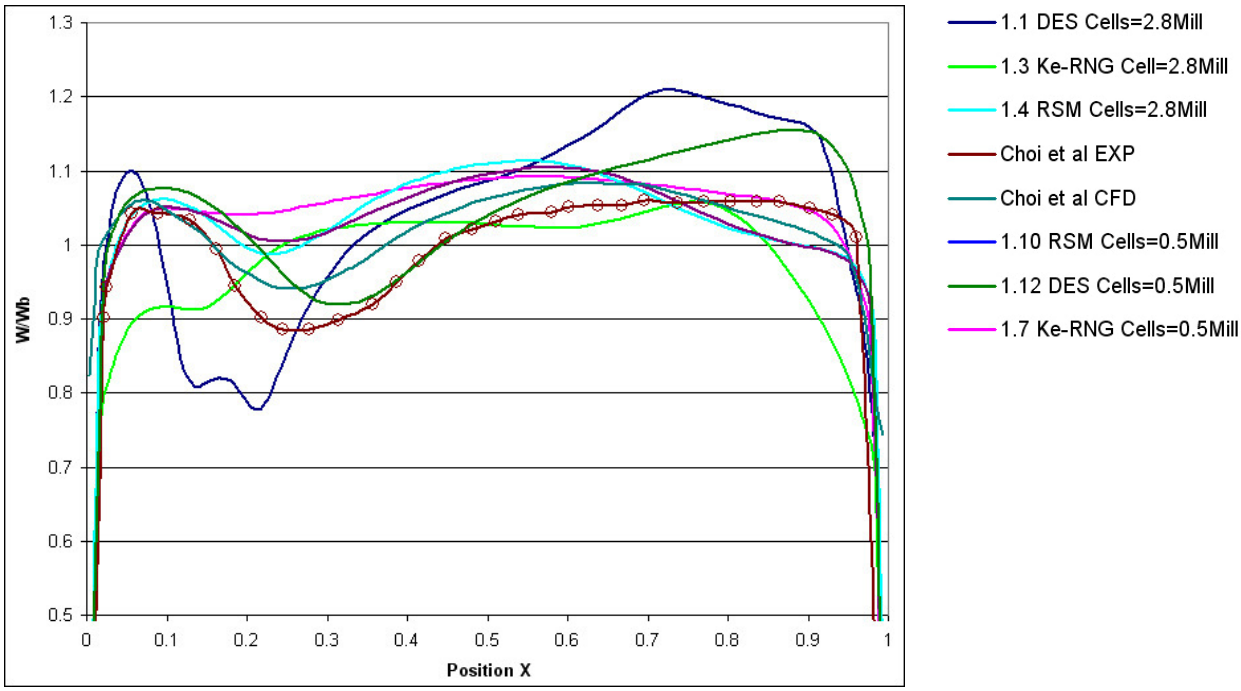

Chart 4.5. Numerical model comparison data for 90° Plane of the ERCOFTAC 180° Square Profile Duct. Rake 2Y/D=0.5 on 90° Plane. (Source: Author).

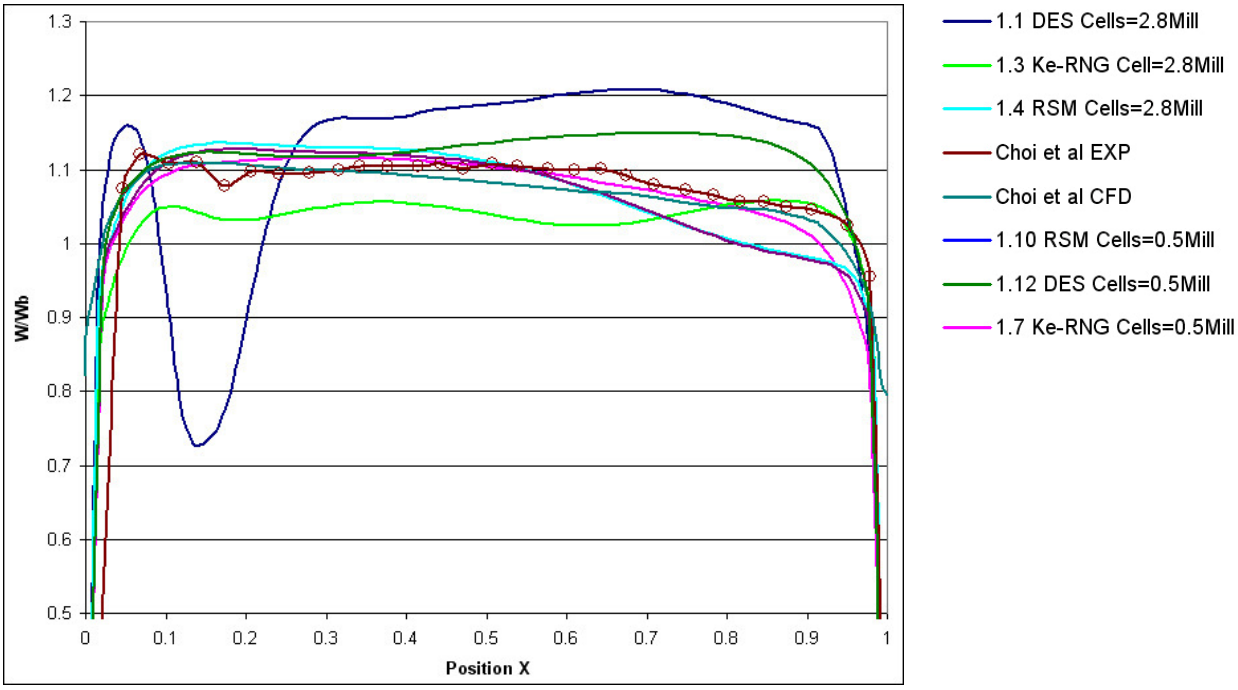

Chart 4.6. Numerical model comparison data for 90° Plane of the ERCOFTAC 180° Square Profile Duct. Rake 2Y/D=0.75 on 90° Plane. (Source: Author).

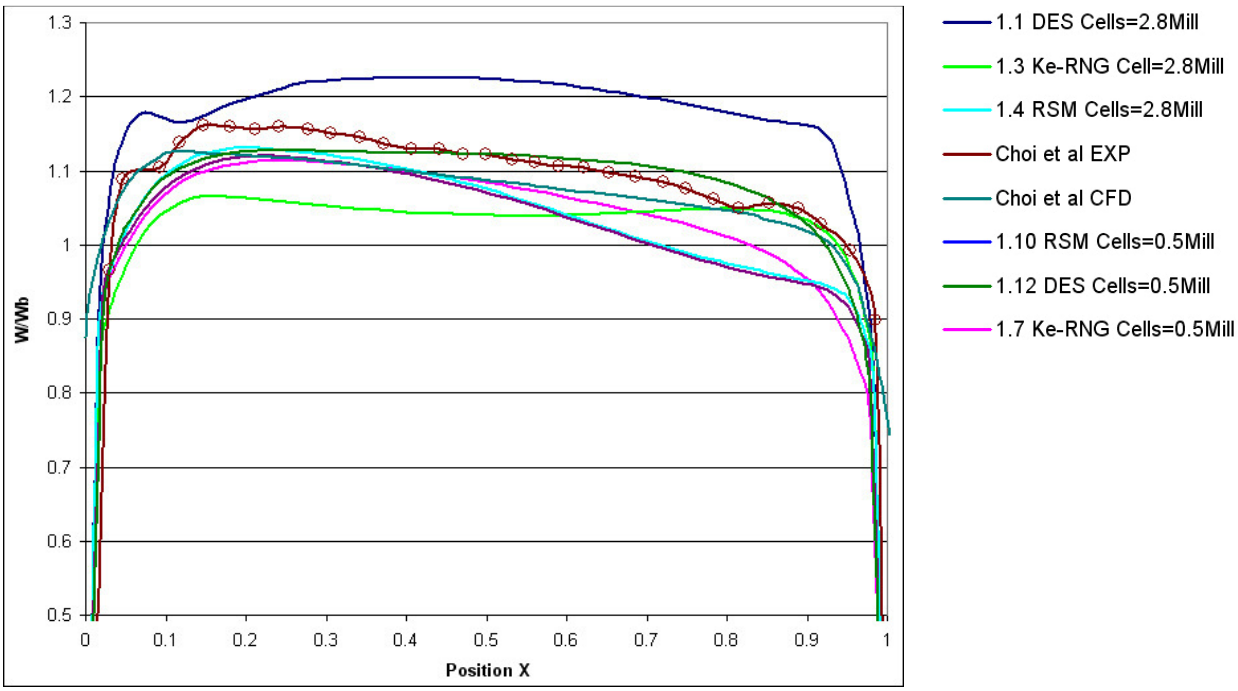

Chart 4.7. Numerical model comparison data for 90° Plane of the ERCOFTAC 180° Square Profile Duct. Rake 2Y/D=0.875 on 90° Plane. (Source: Author).

With regards to the analysis conducted using the higher density grids there is a reasonable correlation in most circumstances; however the HDM DES data shows

signs of additional complex flow phenomenon not presented in the previously published work (see figure 4.14C). It is feasible that the experimental data has been subject to a high degree of temporal averaging and therefore a possible cause of any discrepancy between the experimental and HDM DES simulation may be a result of this averaging process. Furthermore there is no comparative data for the complex secondary, time dependent flows. Again it is possible that the velocity vectors associated with these secondary flows may have been omitted from the data sets, however this is unlikely as it is known that there are complex secondary flows associated with both square profile ducts and highly separated flows and the measurement process of the experimental data (acquired using Lased Doppler Velocimetry, LDV) is likely to accommodate this. Finally, regardless of the nature of the complex secondary flows the data as presented is for mean streamwise (radial) velocity in isolation from the axial and tangential velocity components. Figure 4.14(A-F) demonstrate more clearly the velocity contours associated with the 90° plane, while figure 4.15(A-F) highlights the velocity contours on the plane of symmetry for each of the computational simulations.

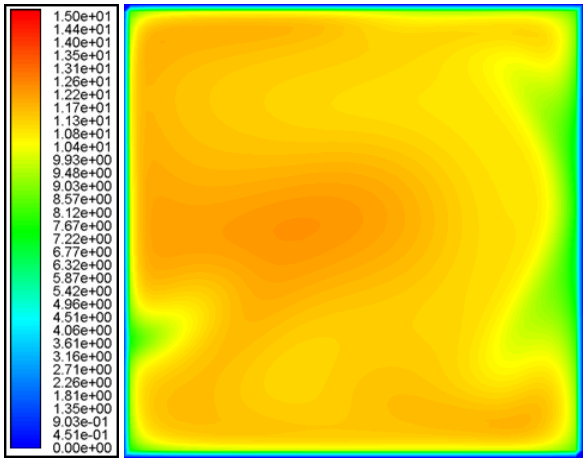

A) Run No 1.3. *k-ε* RNG. Cells: 2.8 Million. t=n/a

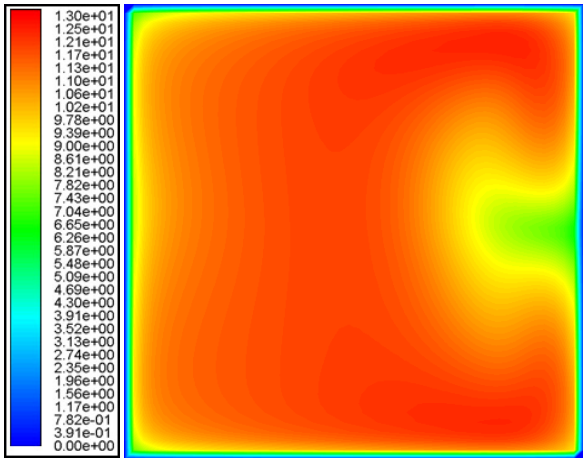

B) Run No 1.7. *k-ε* RNG. Cells: 0.5 Million. t=n/a

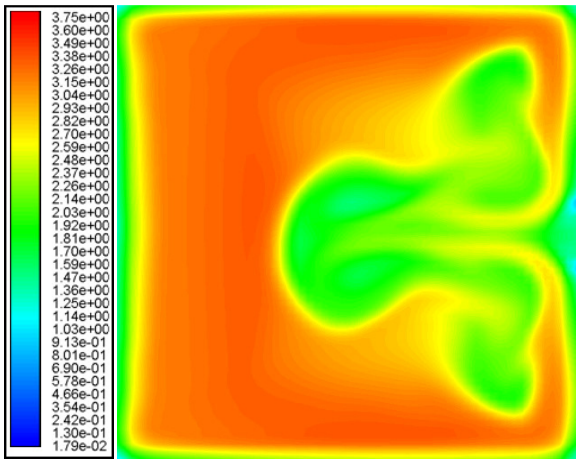

C) Run No 1.1. DES. Cells: 2.8 Million. t=4.5s

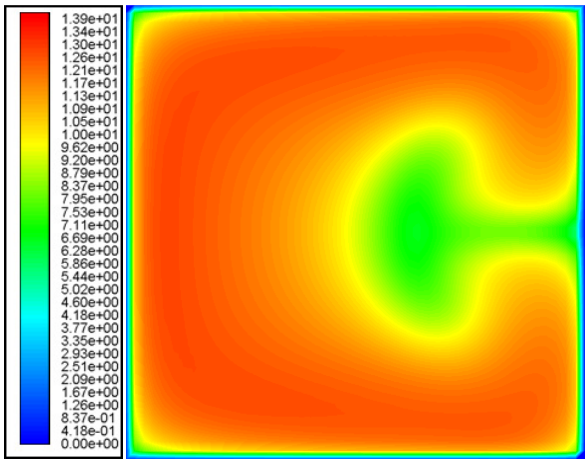

D) Run No 1.12. DES. Cells: 0.5 Million. t=4.5s

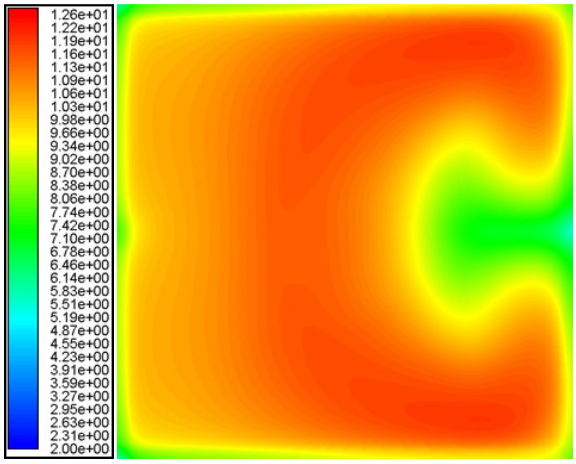

E) Run 1.4. RSM. Cells: 2.8 Million. t=n/a

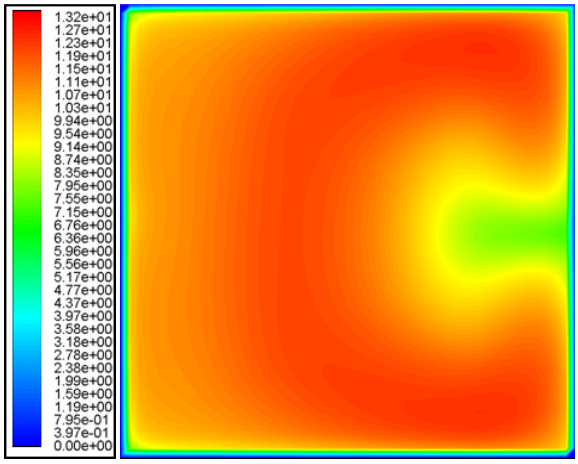

F) Run No 1.10. RSM. Cells: 0.5 Million. t=n/a

Figure 4.14 (A-F). Images show contours of velocity magnitude on the 90° Plane. Note: Image is shown with the inside edge of the bend on the Right Hand Side (RHS). (Source: Author).

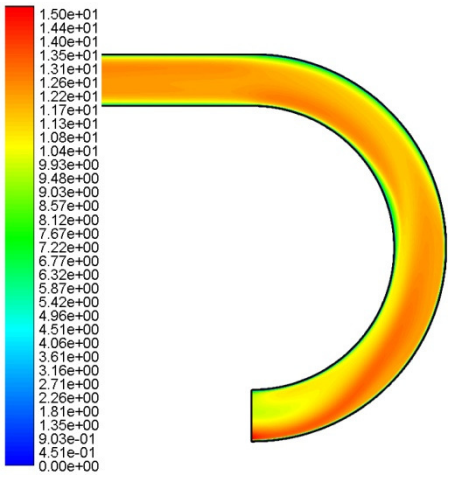

A) Run No 1.3. *k-ε* RNG. Cells: 2.8 Million. t=n/a

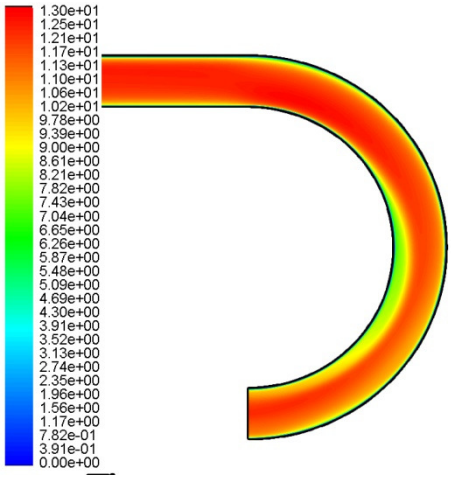

B) Run No 1.7. *k-ε* RNG. Cells: 0.5 Million. t=n/a

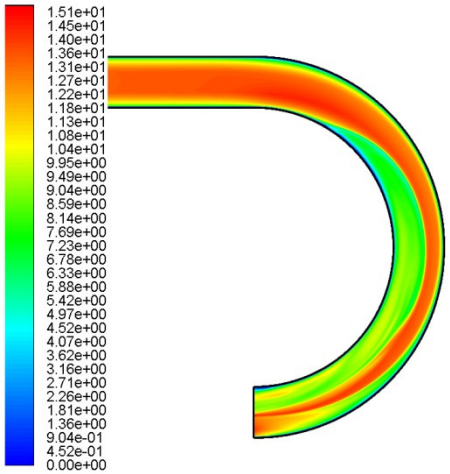

C) Run No 1.1. DES. Cells: 2.8 Million. t=4.5s

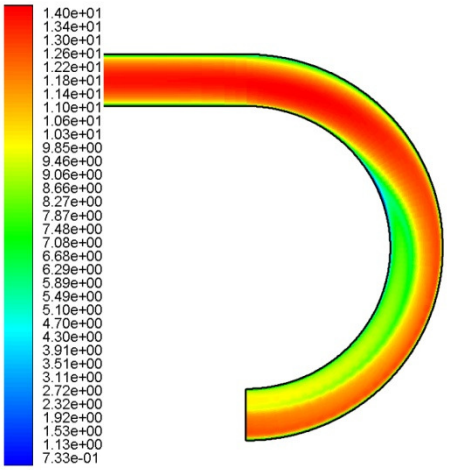

D) Run No 1.12. DES. Cells: 0.5 Million. t=4.5s

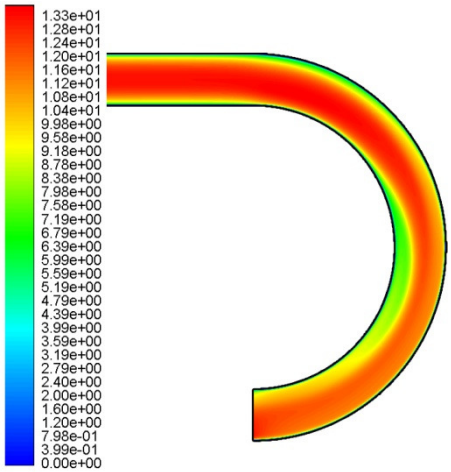

E) Run 1.4. RSM. Cells: 2.8 Million. t=n/a

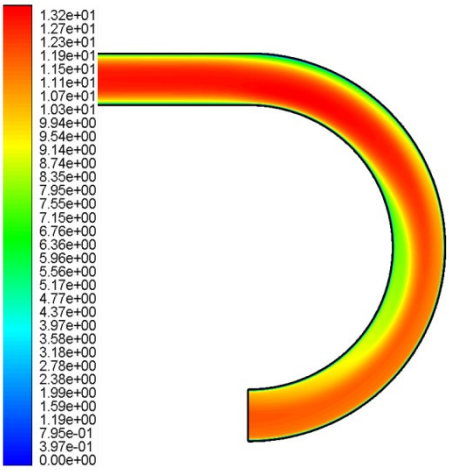

F) Run No 1.10. RSM. Cells: 0.5 Million. t=n/a

Figure 4.15(A-F). Images show contours of velocity magnitude on the Plane of symmetry. Images clearly show the point of flow separation round the bend. (Source: Author).

In a bid to establish any possible discrepancy with the SPD further review of the available experimental analysis was conducted. This review uncovered work by Suzuki and Kasagi [88], whose research was conducted in a bid to validate the use of Three Dimensional Particle Tracking Velocimetry (3D PTV) for flows in a SPD with a 180° Bend. This work was compared against the experimental LDV work of Chang [89], the same experimental work referenced by Choi et al. The 3D PTV data of Suzuki and Kasagi was found to be in accordance with the LDV work of Choi and Chang respectively. This agreement further strengthens the argument that the issues surrounding the HDM DES work lies with the mesh distribution of the HDM itself.

However from the analysis of the test case plots at 90° it is evident that the less dense CM3D mesh, when the DES turbulence model is applied, provides a simulation result that is generally in agreement with the experimental work. After critical review it was established that the simulation setup of both the HDM DES and C3DM DES work was in accordance with each other. Therefore the only variable between these simulations is the mesh itself. In order to establish whether the reported 90° planar data of the C3DM mesh is anomalous the remaining 45° and 130° planes have been plotted against the work of Choi et al (see charts 4.8, 4.9 and 4.10).

In practically all 2Y/D locations, across each of the reference planes, the CM3D DES work showed good agreement with the experimental data, furthermore the review highlighted the fact that the DES analysis, utilising the CM3D mesh, outperformed the *k-ε* RNG and Reynolds Stress Model analysis on both CM3D and HDM meshes at all 2Y/D reference positions.

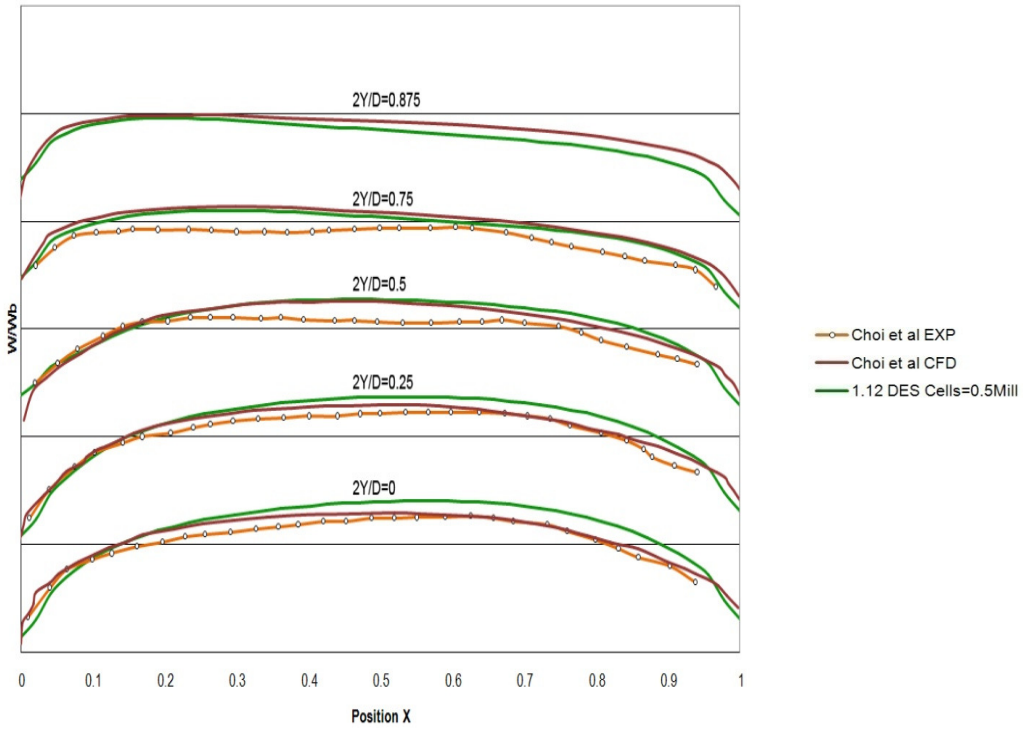

Chart 4.8. Comparison of the results from C3DM DES study to the reference data of Choi et al for the 45° plane. (Source: Author).

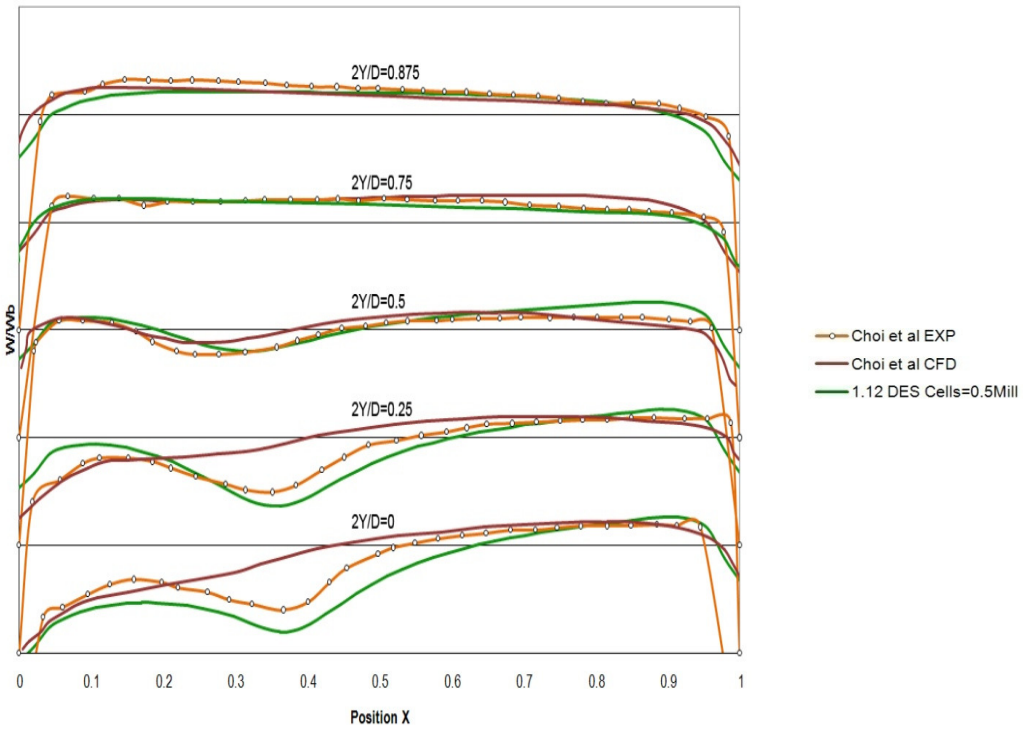

Chart 4.9. Comparison of the results from C3DM DES study to the reference data of Choi et al for the 90° plane. (Source: Author).

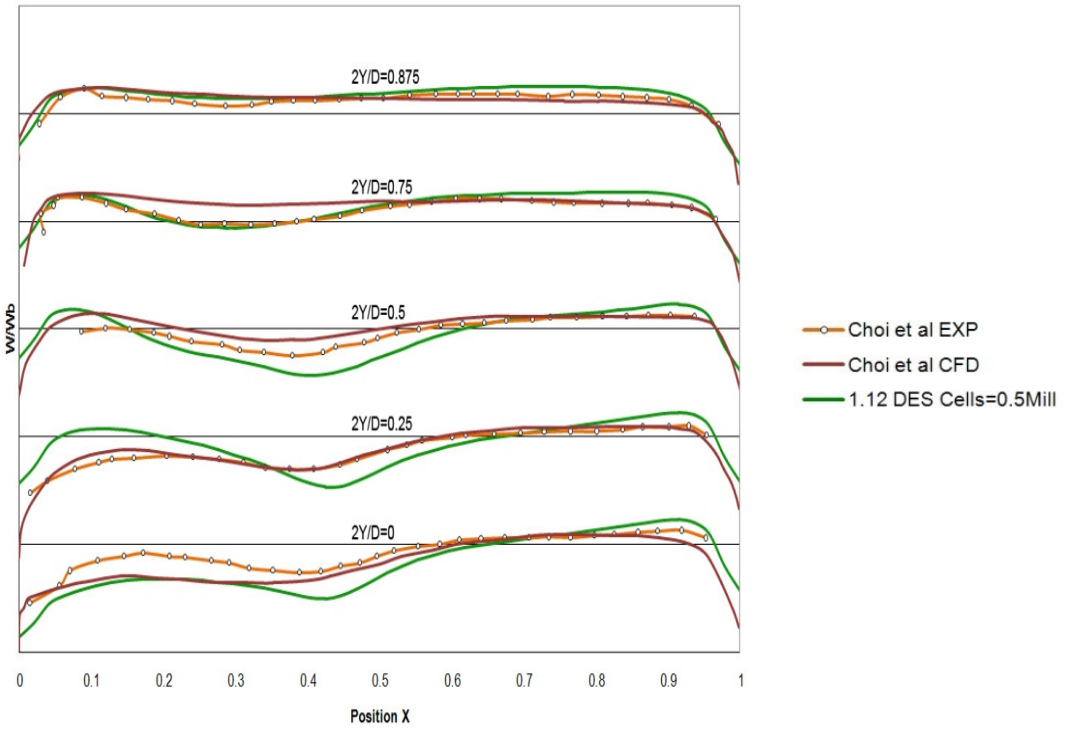

Chart 4.10. Comparison of the results from C3DM DES study to the reference data of Choi et al for the 130° plane. (Source: Author).

In order to establish further support for the lower density C3DM mesh for use with the DES model over a further study was conducted utilising the four mesh sensitivity simulations. The SPD 45° reference rakes were applied to the four mesh sensitivity domains (MS1, MS2, MS3 and MS4). The results were assessed against those for the experimental data, the early CFD work and the subsequent DES results from this study (with the exception of 2Y/D=0.875 for the 45° where the experimental data is not available). It is apparent from chart 4.11 that the results of any of the individual mesh studies in isolation would be considered viable to proceed with further analysis, however there was little characteristic information that would indicate the lower mesh density would result in a better correlation between the DES study and the reference data. Furthermore comparing the MS data to current available data yields little further gain (see chart 4.12).

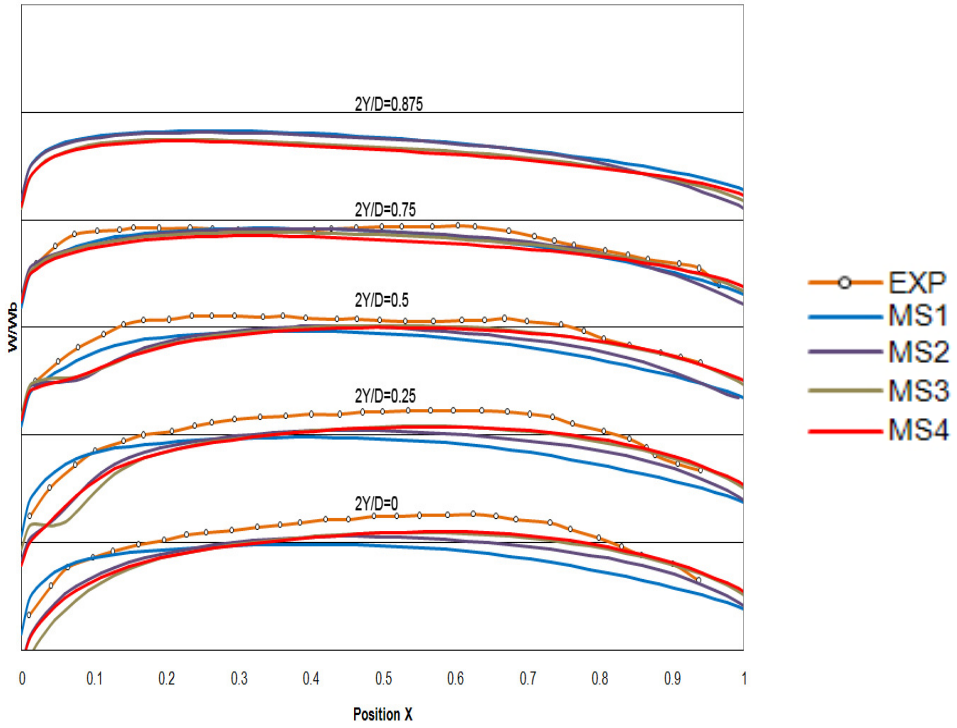

Chart 4.11. Comparison of the results from the four MS studies to the experimental data at the five reference rakes on the 45° plane. (Source: Author).

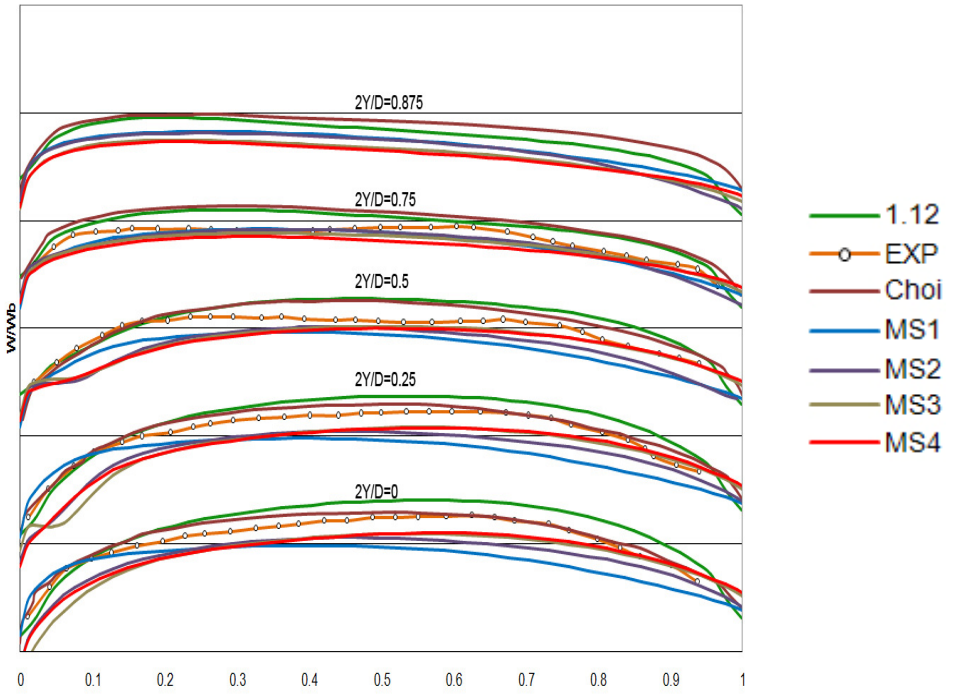

Chart 4.12. Comparison of the results from HDM DES and the four MS studies and to the reference data of Choi et al for the 45° plane. (Source: Author).

A combination of a lack of distinct flow features at the 45° plane, in conjunction with the fact that the mesh sensitivity studies were terminated early (at a time of approximately 0.5 seconds of flow) have meant that it would have been impossible to pre-empt the findings of the HDM and C3DM simulations without further computational time applied to the mesh study. However of interest is the fact that the MS3 mesh, which incorporates a low density mesh in the straight inlet section and a high density mesh in the bend section, exhibits velocity distributions that appear to highlight the onset of separation (see chart 4.13, 2Y/D= 0.25 and 2Y/D=0.5), however the MS1 mesh, which incorporates a high density mesh across both sections, does not show evidence of this velocity contour. One possible reason for this discrepancy is that despite the 11m/s flow rate (equating to 3 1/3 volumetric flow exchanges at a maximum outside bend distance of 3.3m) the boundary layer may not be sufficiently formed for the separation to occur.

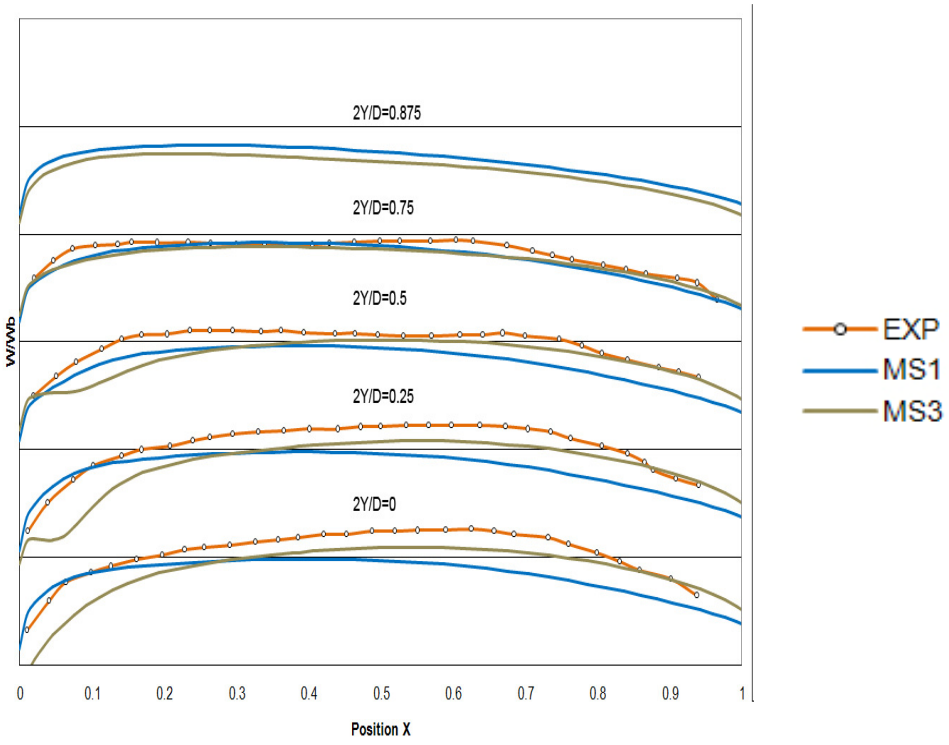

Chart 4.13 Comparison of the results for the two higher density MS studies (MS1 & MS3) to the reference data of Choi et al for the 45° plane. (Source: Author).

The implications and possible causes of all the SPD results will be discussed in Chapter 5. In summary it has been identified that a lower density mesh than initially

expected will produce results that are generally in agreement with the test data when the DES model is applied to separating flows. Accordingly the SPD test case has successfully validated the use of a DES turbulence model for flow regimes consisting of flow separation and strong secondary motion. Subsequently the DES model will be applied to a known hydrocyclone design.

4.4 Application of Test Case modelling to Cyclone modelling

4.4.1 Modelling

Of the two principal commercial cyclone designs in regular use, *Rietema* and *Bradley*, it is the Rietema cyclone that has been selected for this study on BWT. the selection of the Rietema optimum cyclone is due, in part, to its ability to separate higher capacities than its counterpart [42]. Whilst there are a number of Rietema geometries in operation, the design considered to be the optimum (via experimental study of parametric and geometric criteria [46-49]) will be used. This cyclone design, the Rietema Optimised Hydrocyclone (ROH), is based on a set of fundamental design ratios developed in order to produce a hydrocyclone with optimal dimensionless cut size (generally referred to as x_{50} the particle size whereby 50% of the particles will be removed) and return to underflow (the subsequent recovery of the separated particles) whilst minimising the effect on the capacity of the cyclone.

The basic schematic of the optimum Rietema hydrocyclone is shown in figure 4.16, the corresponding design ratio parameters are shown in table 4.7.

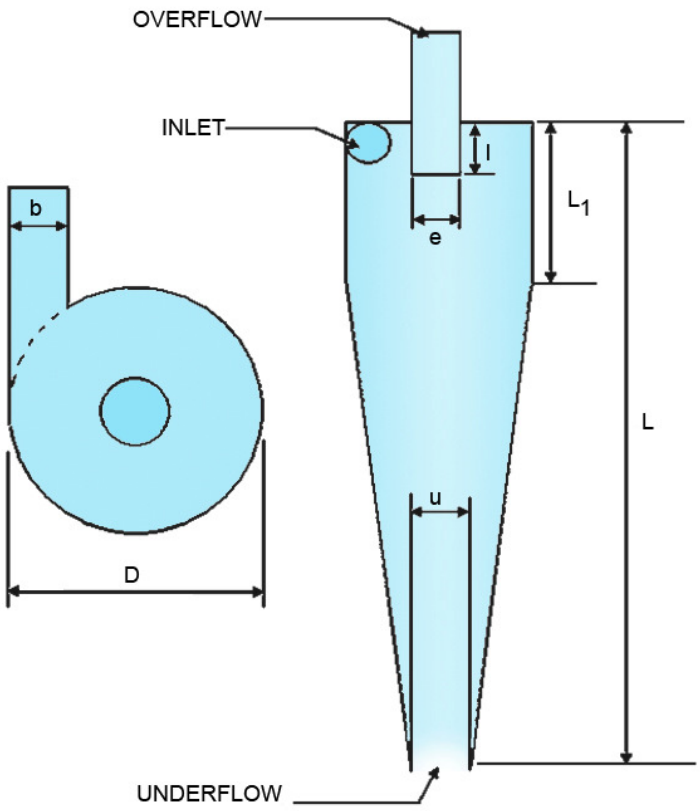

Figure 4.16. Schematic of the Rietema optimum hydrocyclone. (Source: Author).

Design Ratio	Value
L/D	~ 5
b/D	=0.28
e/D	= 0.34
l/D	~ 0.4

Table 4.7. Rietema optimum hydrocyclone design ratios. (Source: Author).

The characteristic dimension for the Rietema cyclone is the overall cyclone diameter, D. whilst the target use for hydrocyclones in this study is for BWT the CFD analysis will be conducted for a 75mm diameter cyclone, the same size used by Rietema. The scalable nature of the ROH cyclone will ensure that the results of this small scale cyclone compare favourably to a larger BWT cyclone.

In order to reduce the modelling complexity, and to ensure comparability between the ROH cyclone and the SPD test case an inlet with a rectangular profile inlet has been substituted in place of the circular profile of the idealised ROH design. The rectangular profile inlet with width and length of 17mm and 25mm respectively has a comparable hydraulic diameter to the circular profile where, for a rectangular profile, the hydraulic diameter is given thus:

$$D_h = \frac{2L \times W}{L + W} \qquad [4.20]$$

The resultant D_h is 20.24mm (1.2% larger than the circular profile inlet). It should be noted that whilst a square profile duct would have been physically possible, a larger proportion of the inlet flow would impinge on the outer surface of the vortex finder. By reducing the width of inlet from 20mm to 17mm this has been avoided. Figure 4.17 shows the physical differences between the idealised ROH cyclone and the SPD comparable ROH cyclone. Furthermore figure 4.18 compares dimensions between the two configurations.

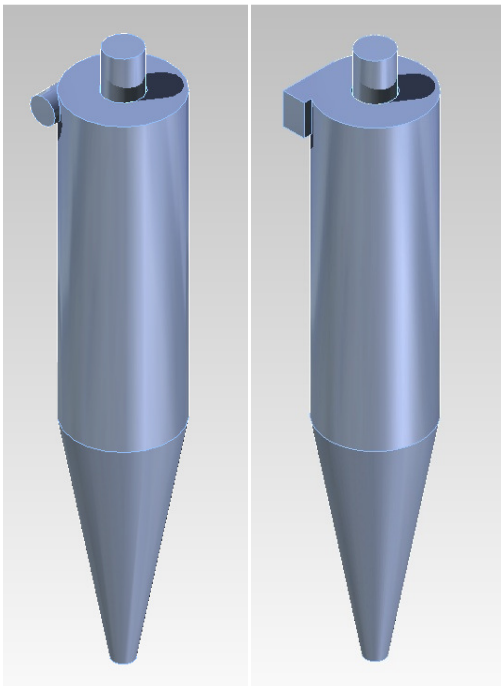

Figure 4.17. Physical differences circular and rectangular profile inlets of the cyclone designs. (Source: Author).

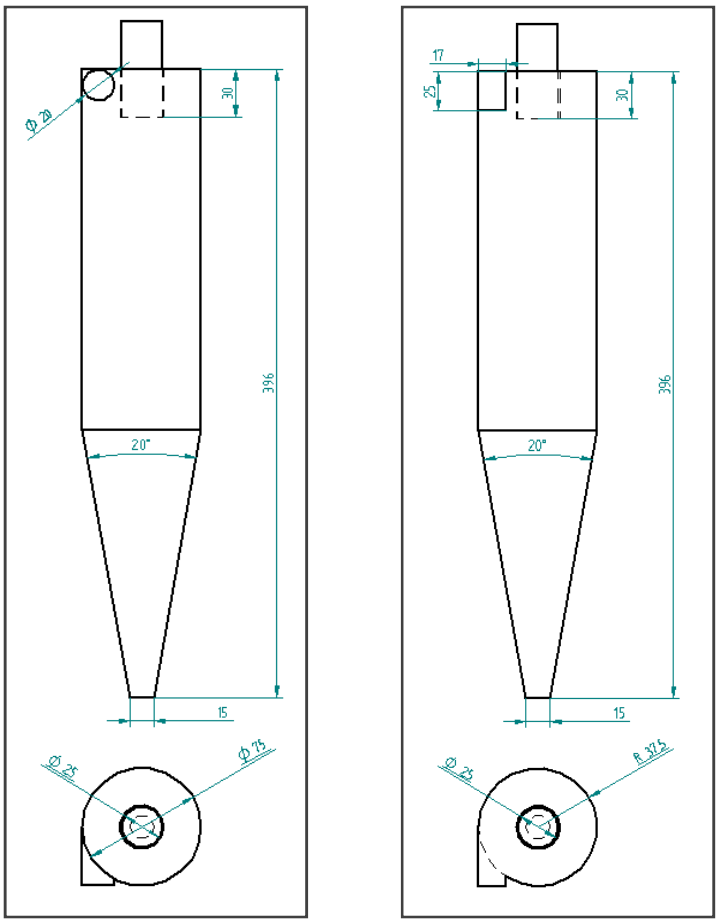

Figure 4.18. Dimensional differences circular and rectangular profile inlets of the cyclone designs. (Source: Author).

4.4.2 Methodology

Meshing

The test case data from the SPD indicated that there is sufficient resolution of flow regimes with a minimal grid density when using the DES turbulence model. The criteria to determine a "minimal grid density" has not been established, however for the purpose of this study the cell count per unit volume will be used to scale the ROH domain according to the criteria determined by the SPD domain. Furthermore the concept of a grid structure such that the cell faces are normal to the flow direction has been discussed. In order to further validate these concepts, with respect to the modelling of hydrocyclones for ballast water treatment, two meshes have been generated for CFD modelling of the Rietema optimised hydrocyclone.

The first of these meshed domains is a relatively low density quadrilateral mesh with the cell faces orientated in a 'polar' fashion, ensuring that the swirling flow within the cyclone encounters the cells at an angle as close to normal as possible. The second domain is a higher density mesh consisting of tetrahedral cells. The use of a tetrahedral mesh in this instance is to identify whether the careful design and associated computational cost for the meshing process can be avoided by simply increasing the mesh density. In this instance it is only with the use of tetrahedral cells that the automatic mesh generation is capable of meshing the domain with minimal user input. Comparative images of the inlet, upper cylindrical and outflow sections of the cyclone for each of these two domains are shown in figure 4.19.

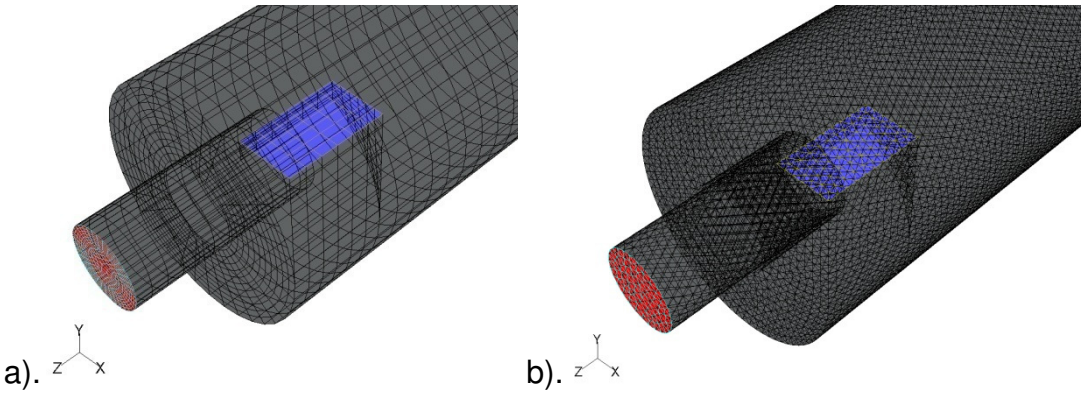

Figure 4.19. Mesh structure at the inlet segment of the Rietema Optimised Hydrocyclone model a) 17272 Quadrilateral cells, b). 310048 Tetrahedral cells. (Source: Author).

Boundary Conditions

As the primary purpose of this study is to assess the viability of CFD, and the DES turbulence model in particular, for the design of shipboard BWT the initial boundary conditions applied to each of the above meshed domains are identical to the test case discussed earlier.

Results

The results for the two mesh variations of the ROH are presented for a series of reference lines taken at eight Z axis positions within the domain as shown in figure 4.20.

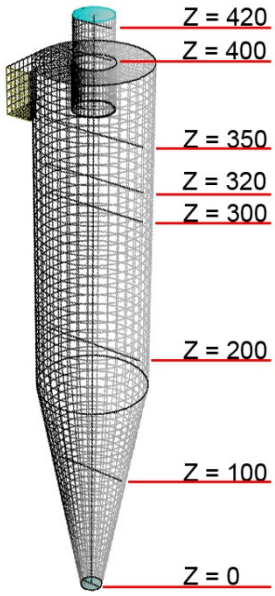

Figure 4.20. Location of reference positions with respect to the ROH geometry. (Source: Author).

As a result of the earlier mesh density analysis and the subsequent findings of the SPD test case a grid, coarser than originally envisaged, was applied. The principal intention is to mitigate any possible exaggeration of flow characteristics. Furthermore as numerical diffusion has been witnessed previously, it is critical that steps are taken to avoid or minimise the potential for this to occur. For this study the simulation duration was such that a minimum of 10 volumetric exchanges where conducted, the simulations where terminated after this period. The data set for the time period equivalent to six complete volumetric exchanges of fluid was then compared. This time period was selected on the basis of the mesh sensitivity study in section 4.3.

In order to evaluate the modelling more thoroughly the initial simulations presented employ air as the domain fluid. The characteristics of this domain fluid are in keeping with those of the SPD. The results presented in charts 4.14 and 4.15 show the velocity contours at the key reference locations for both high density tetrahedral mesh and the more coarse quadrilateral mesh.

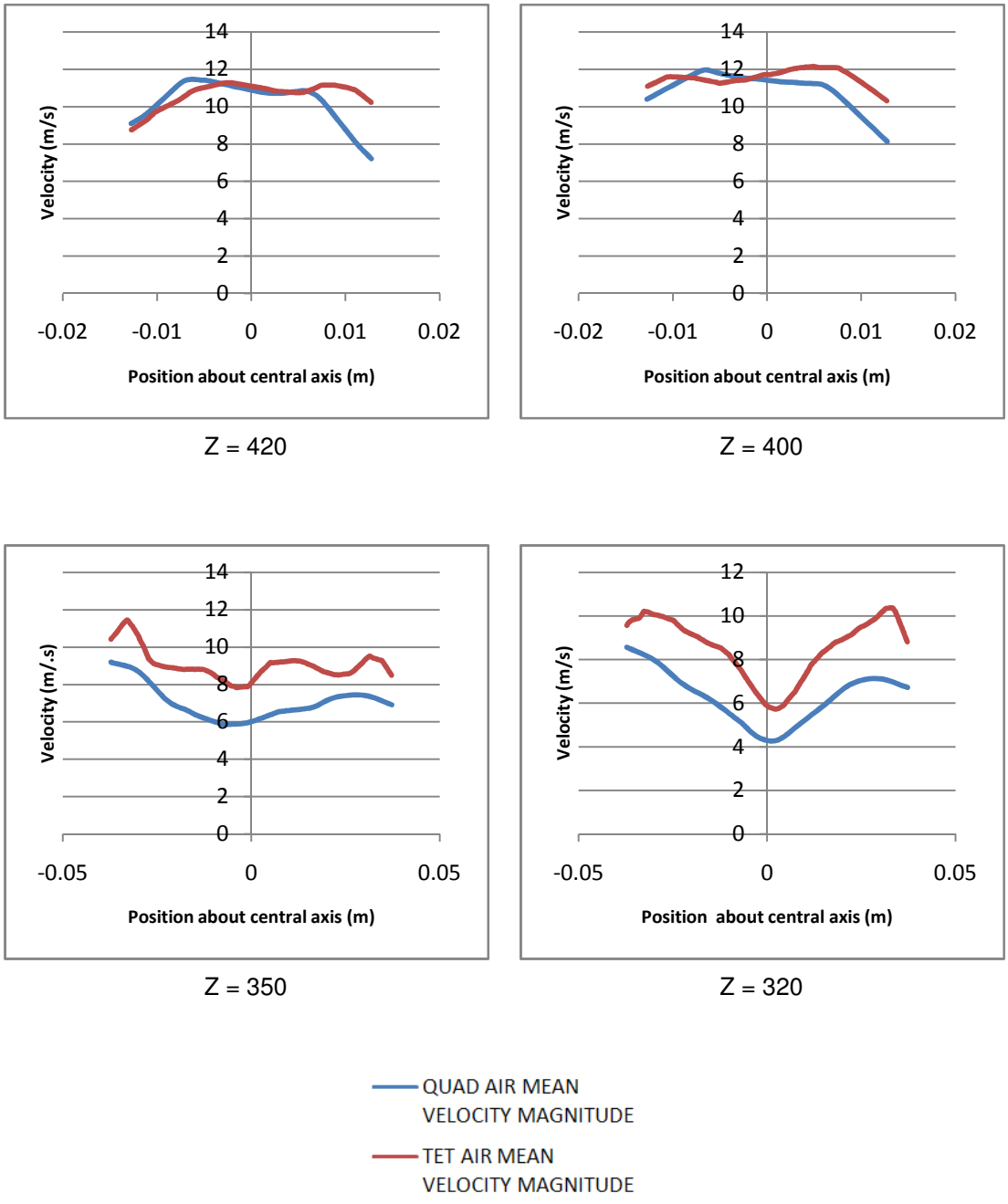

Chart 4.14. Velocity distributions across reference locations z=420 to z=300 for quadrilateral and tetrahedral meshes of the rectangular inlet ROH using air as the domain fluid. (Source: Author).

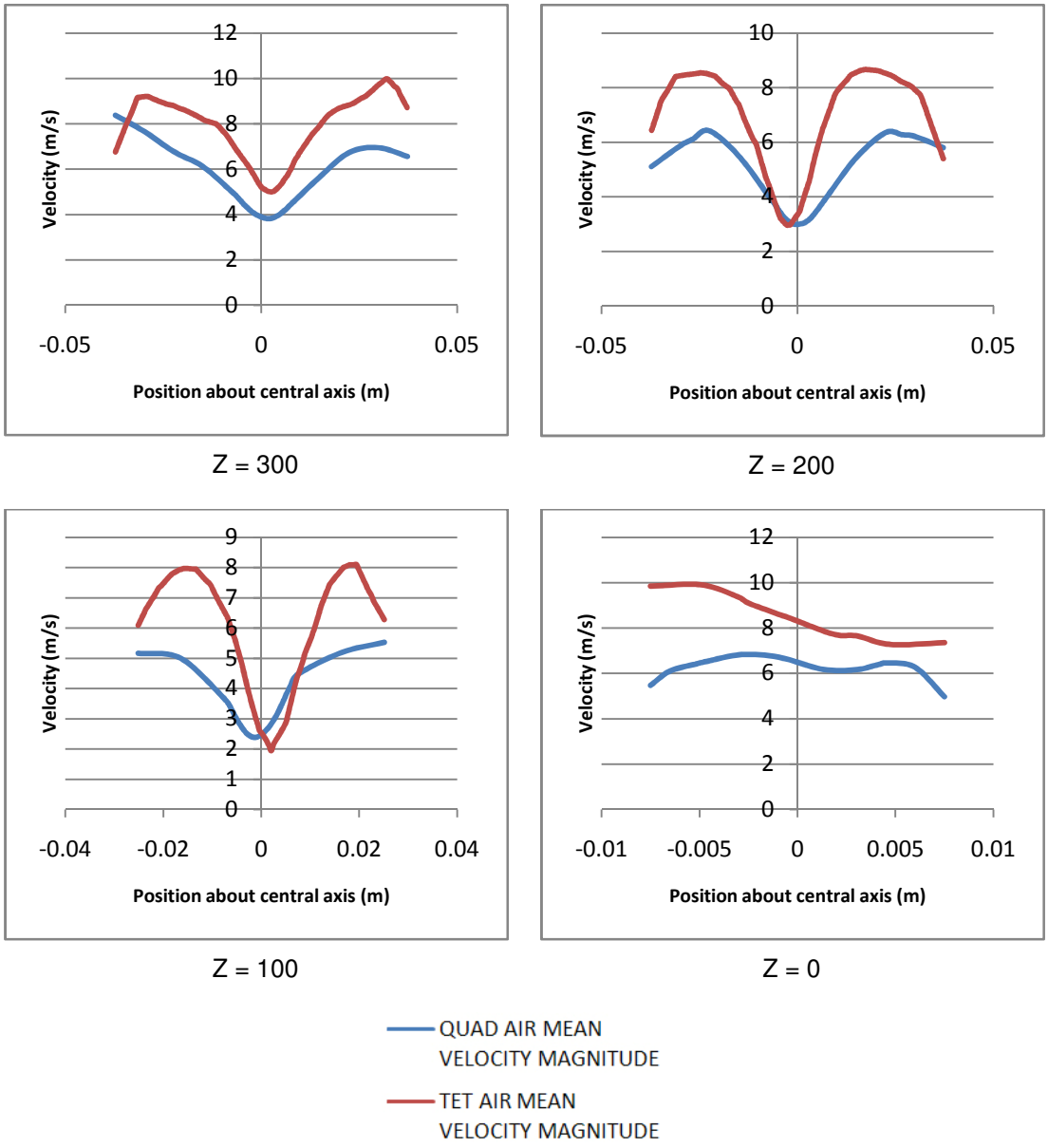

Chart 4.15. Velocity distributions across reference locations Z=300 to Z=0 for quadrilateral and tetrahedral meshes of the rectangular inlet ROH using air as the domain fluid. (Source: Author).

In order to visualise the velocities more clearly the data for the velocity magnitude at the reference positions has been applied to a schematic of the cyclone (see figure 4.21), showing more clearly the flow field within the domain.

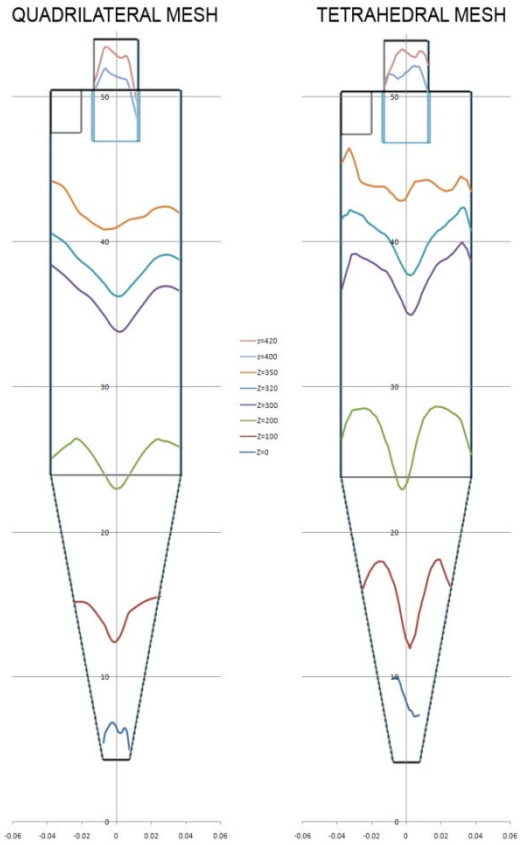

Figure 4.21. Velocity distributions across reference locations applied to a schematic of the hydrocyclone. Data from Quadrilateral and Tetrahedral meshes (clearly marked) are shown. Both simulations utilise air as the domain fluid. (Source: Author).

The resultant velocity distributions show verisimilitude when the inlet and boundary conditions are applied as per the SPD test case. However the tetrahedral mesh reports a more complex velocity fluctuation, despite time averaging of the results. The indications are that the numerical diffusion exhibited by the higher density SPD case is manifesting itself in the tetrahedral domain, whether this is due to the higher density, or the irregularity of the tetrahedral mesh itself is unknown. However the results of the quadrilateral mesh display generic velocity profiles which correspond to those published by both Hoffman and Svarovsky. As a result the modelling progresses to utilising the quadrilateral mesh with boundary conditions adjusted to match those of Rietemas optimum hydrocyclone analysis, identified as experiment number 153 in the literature [48]. The results for mean velocity magnitude at the reference locations are presented in charts 4.16 and 4.17. Likewise the results for mean static and total pressure distributions are shown in charts 4.18 and 4.19.

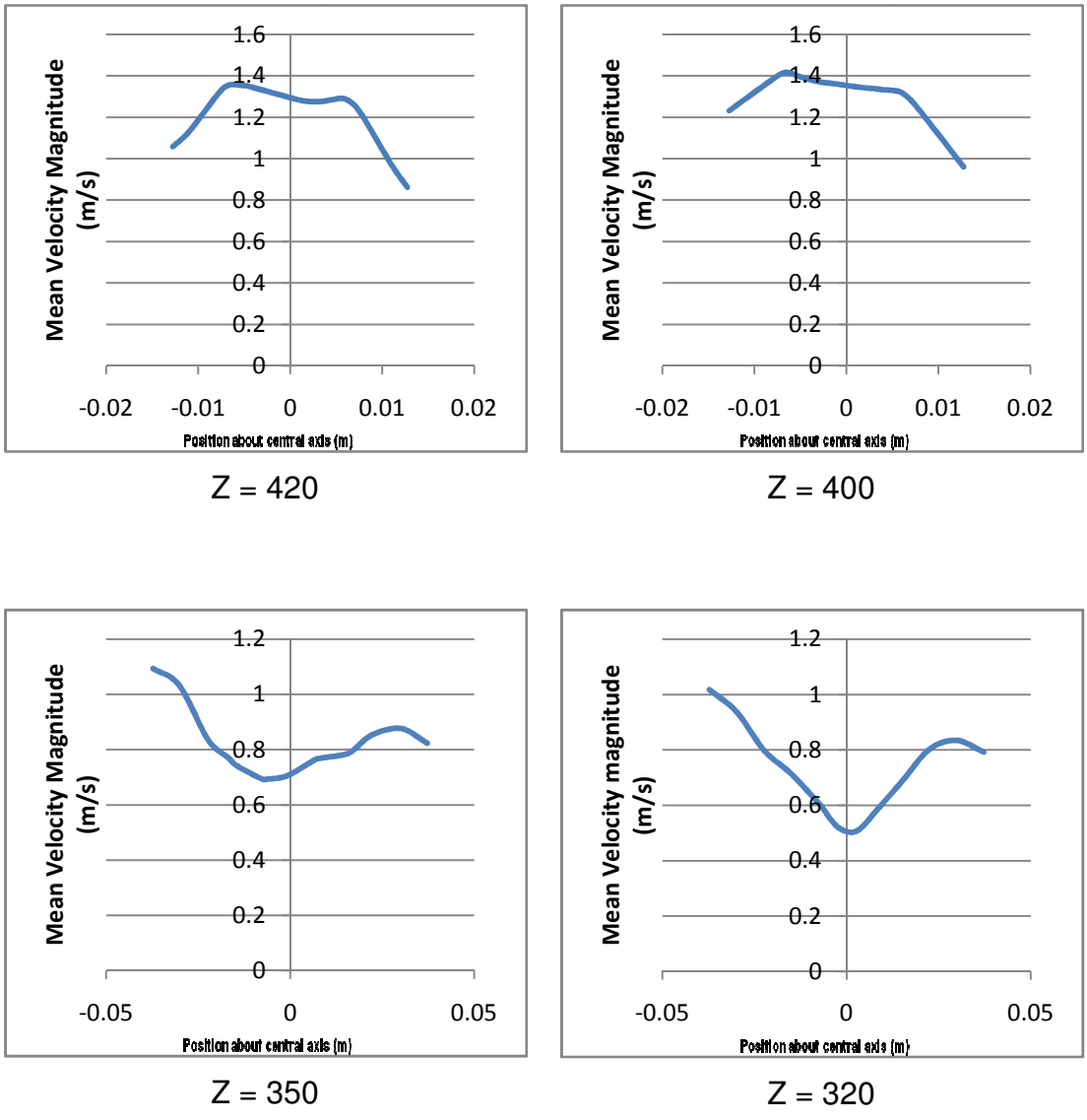

Chart 4.16. Mean velocity distributions across reference locations Z=420 to Z=320 for quadrilateral mesh simulations of the rectangular inlet ROH using boundary conditions as defined by Rietema experiment 153. (Source: Author).

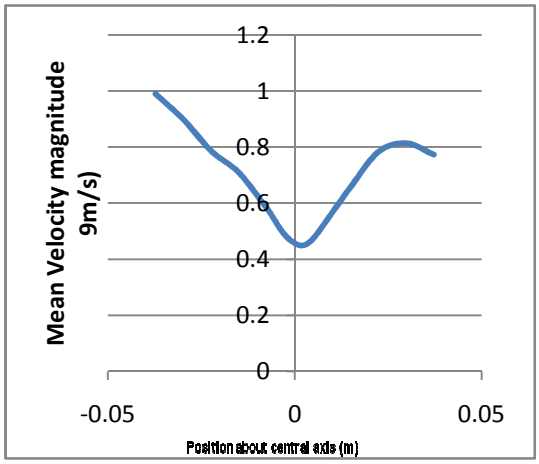

Z = 300

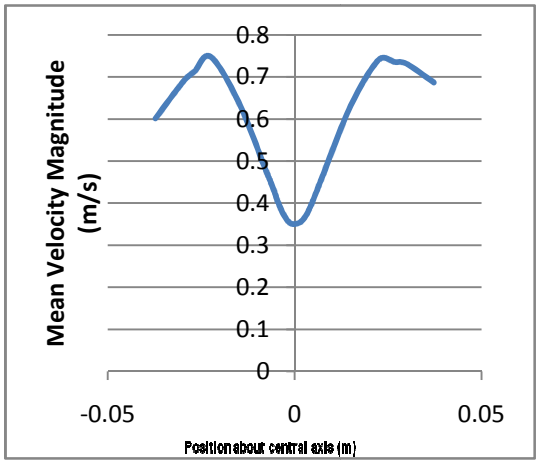

Z = 200

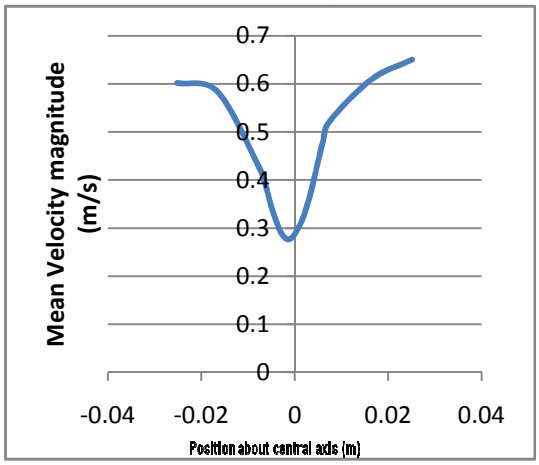

Z = 100

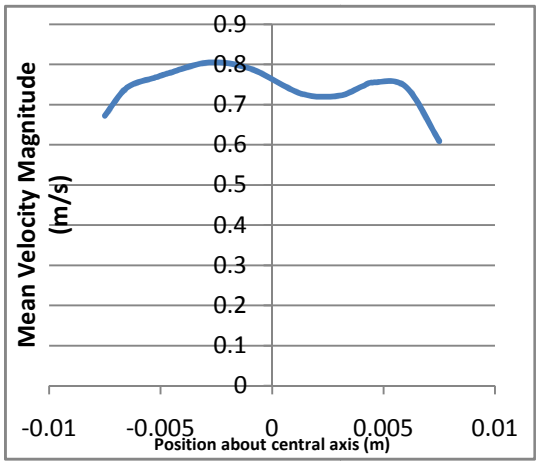

Z = 0

Chart 4.17. Mean velocity distributions across reference locations Z=300 to Z=0 for quadrilateral mesh simulations of the rectangular inlet ROH using boundary conditions as defined by Rietema experiment 153. (Source: Author).

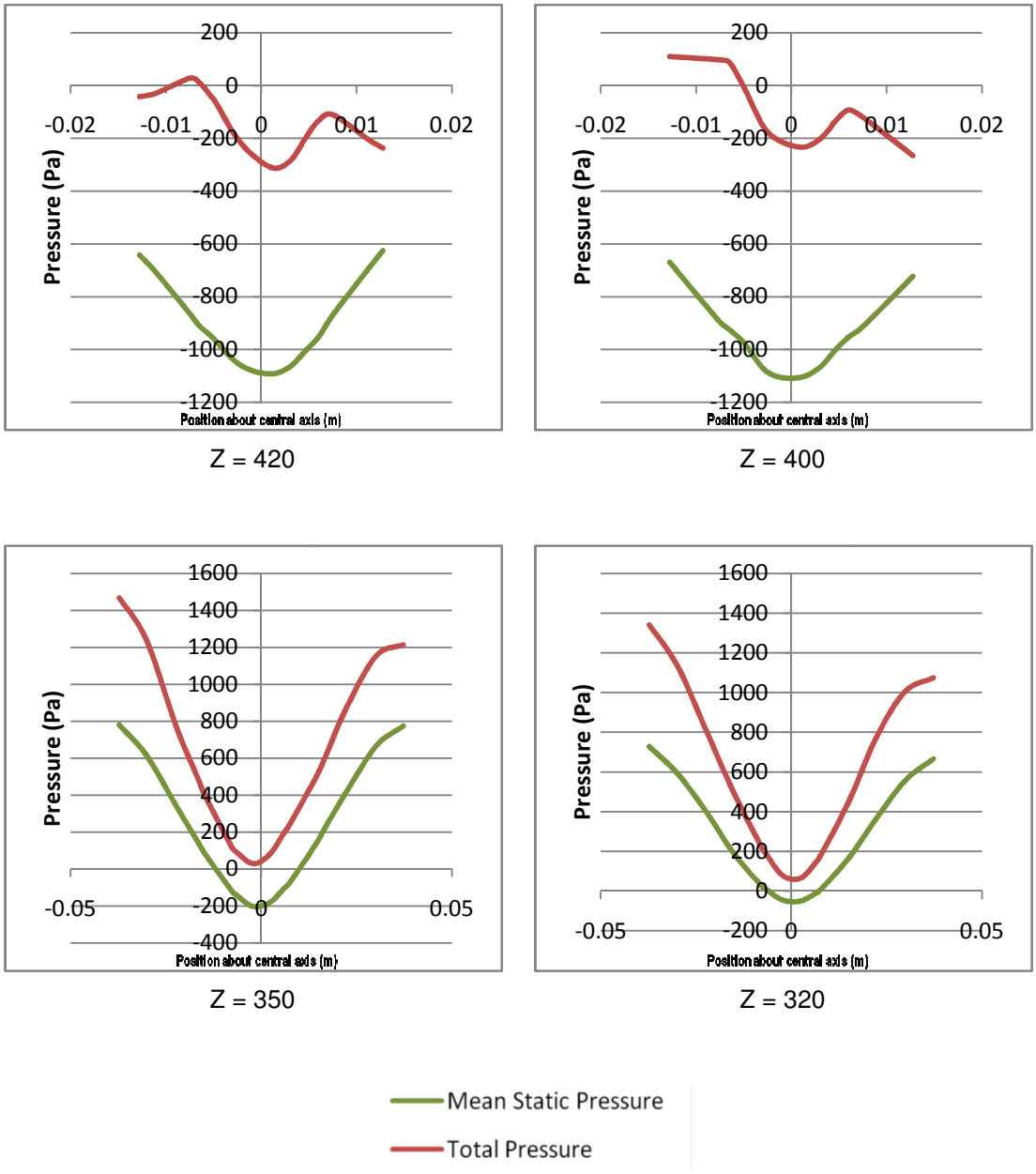

Chart 4.18. Pressure distributions across reference locations Z=420 to Z=320 for quadrilateral mesh simulations of the rectangular inlet ROH using boundary conditions as defined by Rietema experiment 153. (Source: Author).

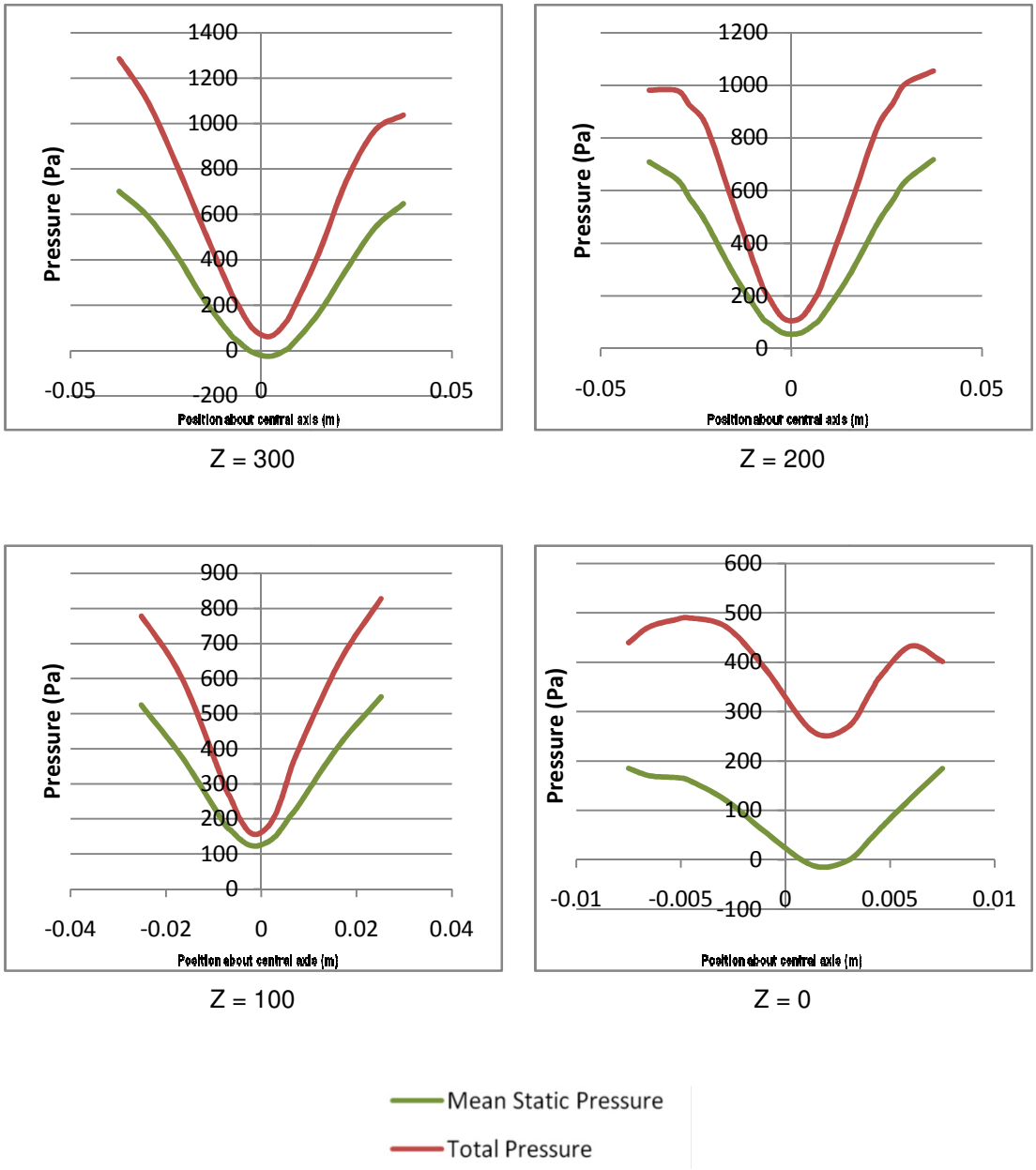

Chart 4.19. Pressure distributions across reference locations Z=300 to Z=0 for quadrilateral mesh simulations of the rectangular inlet ROH using boundary conditions as defined by Rietema experiment 153. (Source: Author).

To further validate the use of the DES turbulence model for the ROH the quadrilateral domain mesh was used to perform further kε RNG and RSM simulations. Figures 4.22 and 4.23 show the contours of velocity magnitude and contours of total pressure on the plane of symmetry normal to the inlet flow for each of the three turbulence models.

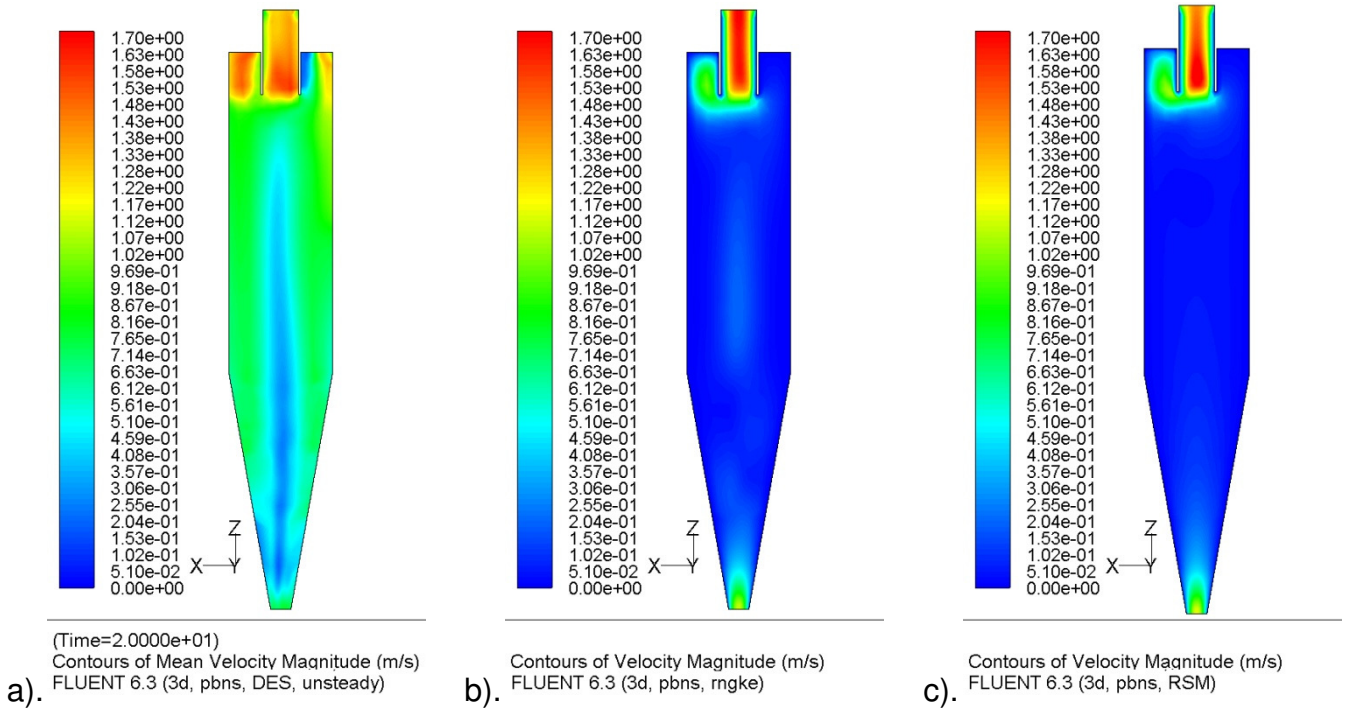

a). b). c).

Figure 4.22. Contours of Velocity Magnitude (m/s) on the central plane normal to the inlet flow direction at a velocity of 1.3m/s with an 80/20 ratio for overflow/underflow outlets. Turbulence models are a). Detached Eddy Simulation, b). kε Renormalised Group, c). Reynolds Stress model. (Source: Author).

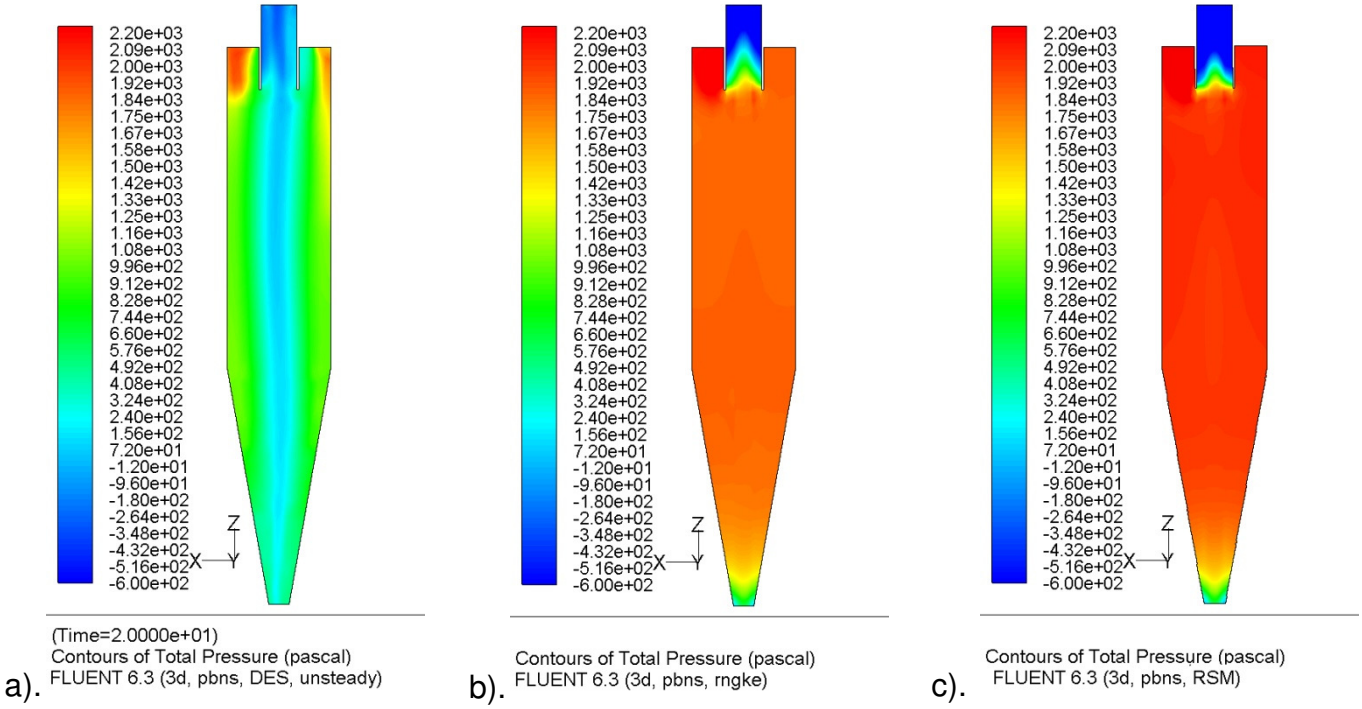

a). b). c).

Figure 4.23. Contours of Total Pressure (Pa) on the central plane normal to the inlet flow direction at a velocity of 1.3m/s with an 80/20 ratio for overflow/underflow outlets. Turbulence models are a). Detached Eddy Simulation, b). kε Renormalised Group, c). Reynolds Stress model. (Source: Author).

The low pressure, low velocity region representing the formation of an air core is clearly identifiable on the contour plots of the DES simulations. The fully converged simulations for the kε RNG and RSM turbulence models fail to model this flow feature. While this study does not determine the separation efficiency of the hydrocyclone design these contour plots clearly indicate that the DES turbulence model results, for both velocity and pressure contour plots, are more in keeping with the flow regimes identified in the literature [43] for hydrocyclonic separation. The DES plots clearly show the low velocity, low pressure central core indicative of the formation of an air core. Of note is the fact that the RSM model does not show the same potential for resolving complex flow features when applied to swirling flows, with a low density mesh, when compared to the earlier highly separated flows of the SPD, again this is a feature that has been noted in the literature [65].

4.5 Chapter Summary

In this chapter the main technical work has been presented. The concept of cyclone modelling has been address with respect to both analytical and computational models, furthermore the limitation surrounding the use of analytical models have been detailed, highlighting the requirement for robust computational modelling for the BWT engineer.

In terms of computational modelling a thorough analysis of the DES turbulence model has been applied to a test case provide by the European Research Community On Flow, Turbulence and Combustion (ERCOFTAC). This has formed the basis of turbulence model analysis and has enabled the DES model to be applied to the Rietema Optimised hydrocyclone design. The results of which have been presented.

CHAPTER 5: DISSCUSION

CHAPTER CONTENTS

5.1 Introduction

The focus of the discussion is split between three key criteria with an emphasis towards fully answering the requirements of the ship board ballast water treatment design engineer. To this end the following questions will be discussed:

1. To what extent can you use hydrocyclones for BWT? What are their limitations/applications/viability etc?
2. What is the design process and how are the analytical and numerical models combined to develop a successful design?
3. What key methods for numerical modelling has the study identified? What are the limitations for numerical modelling of hydrocyclones?

5.2 On the use of hydrocyclones for ship board Ballast Water Treatment

In order to establish the application of hydrocyclones to ship board use, and thus identify their viability and limitations, it is necessary to understand the selection criteria and influencing parameters of ship board waste management selection.

Most on-board waste management technologies for different types of waste such as solid, liquid or air have been developed from technologies used in other industries. However for onboard installation this equipment often requires modification. Certain design restrictions need to be followed which are common to all waste management when assessing their suitability for various ships. Common parameters are mainly; on-board safety, size, maintenance envelope, processing rate, reliability, maintainability, shock, footprint, vibration, weight, acoustics, electromagnetic interference and electromagnetic compatibility, shipboard services, human factors, and cost. The criteria, such as weight, footprint, and operational envelope are defined by the boundaries of ship interfaces.

A number of parameters are particularly applicable for equipment retrofit due to important implications such as high unit time, ship downtime for installation of the new control technology, limited space on the existing ship, increased fuel use (typical for heat treatment for ballast water and water injection or emulsion systems) and potential engine damage (possible with exhaust gas recirculation that routes exhaust gas particulate matter through the charge air system).

Identifying these boundaries at an early stage helps in the development of detailed guidance for equipment location, arrangement, and installation; therefore allowing concurrency of equipment design with ship installation planning. Most of these factors are taken into consideration in the equipment development by the manufacturers. However for shipyards to choose certain systems, for new build or retrofit, it is important that the system fits comfortably within the constraints of the vessel. In addition all materials and components should meet the standard performance requirements as well as anticipated extreme ship board environmental conditions. The following factors are a guideline for choosing waste treatment equipment for retrofit:

- Size and type of the equipment based on the amount and type of waste to be treated onboard. For example it might be more cost effective to install common equipment that treats both grey and black water, or to install a number of smaller units working in parallel resulting in a more simple installation.

- Utility requirement: Availability of electrical energy to meet overall energy demand, water requirement, utility air pressure and volume.

- Modularity: Most waste management systems consists of designs with modular treatment units with several parts that can be installed or replaced as stand-alone units. All systems constitute a primary treatment unit for separation of different waste products such as filters, screens and macerator pumps and secondary treatment units for treating the effluent to safe levels that can be discharged safely.

Secondary units may be UV disinfectant units, electrolysis equipment, heat treatment units, biocides, chemical treatment units etc.

The above mentioned factors should be matched to vessel characteristics to ensure that the chosen waste management system performs to its intended purpose.

5.2.1 Retrofitting of BWT - Scope and Cost

The work involved in a retrofitting of a system is based on ship type and technology of the system. At present worldwide BWT installations have been made by the technology developers, primarily as marketing and developmental platforms. As a result the data contained in table 5.1 is indicative only, showing cost information for known treatment technologies that have been installed onboard operational ships. The estimates are based on the information supplied by various technology developers and research partners through the FP6 SHIPMATES project.

Technology /Vessel	Equipment US $	Installation US $	Testing per voyage US $
Hydrocyclone +UV			
Container	200,000	220,000	67, 000
Passenger Vessel	105,000	15,000	Not available
Passenger Vessel	130,000	65,000	67,000
Passenger Vessel	128,000	19,000	Not available
100micron Filter +UV			
Passenger Vessel	173,000	Not available	63,000
Deoxygenation			
Integrated Tug-Barge	300,000	50,000	100,000
Container	290,000	170,000	100,000
Chlorine Dioxide			
Integrated Tug-Barge	237,000	157,000	80,000

Table 5.1 System Installation Cost Information for specific vessels. (Source: Author).

A BWT consisting of a Hydrocyclone with secondary UV system has been installed on two ship types and different vessels within different time parameters. There are

therefore obvious differences in the cost of installation. Due to commercial sensitivity it is not possible to get a detailed breakdown of cost associated with these installations and the associated differences between the two systems. However it can be assumed that some costs are for the representative technologies installed under research and development conditions, and are expected to decrease as they become commercially available. Equipment costs cover the purchase of the technology or system. The installation costs include, but are not limited to labour and materials, factors that vary depending on the geographic location where the work was performed.

Developers were unable to provide estimates for technologies that are currently being tested and might be installed onboard in the long term on new vessels. Other currently available technologies are still in prototyping stage and there are few studies available to provide any information on procedures and potential cost of implementing BWT onboard. Most studies reflect effectiveness of the technology in the laboratory or land based tests and thus costs are associated with research and development. Whereas retrofits can be very complex, costly and time consuming on most type of ships. Even when space is available – piping and controls are not trivial. Retrofits are difficult to do when a ship is in service especially where the work involves creating space for extra equipment or other significant alterations to the existing layout of the vessel.

Therefore the retrofit costs not only depend on the amount of direct work for the installation but the extra work that is involved in the modification of the existing pipe layout, ballast tanks, accessing the space and much more that is difficult to estimate in advance. Moreover depending upon yards' capabilities and work culture there will be variations in the time and costs quoted to do the same job. Retrofitting procedures and generic cost estimates for the retrofit or new build vary with different vessel types (e.g. bulk carrier, tank vessel, container vessel). Even with a class each ship can have a different layout and the retrofit work cannot necessarily be replicated for another ship.

After installation cost the next most important factors for consideration are the biological efficiency and associated operating cost. This is surmised in table 5.2.

Technology	**Time/flow rate Biological effectiveness**	**Biological effectiveness %**	**Operational Costs (US cents per m^3 water)**
Ballast Exchange	N/A	85%-99%	~2.85
Heat treatment	>80 Hrs @ 45° C	99% @ 70° C	~3.55
Screening /Filtration	50tonnes/hr (test)	82-95%	~0.61
Hydrocyclones	3000m3/h	>90%	~0.38
UV Irradiation	350m3/h	85% minimum	~0.05
Sonic methods	Unknown	~40% at present	Unknown
De-oxygenation	72Hrs @ 5° C	~86%	Unknown
Chemical Biocides	up to 48 Hrs	100%	<0.20
Electro-ionisation	<10mis	~95% in Laboratory Tests	Unknown
Ozone	5-10mins	88.89% max in trials	Unknown
Gas Supersaturation	>30 Days	80% @ 30 days	0.02-0.05

Table 5.2. Treatment technique operating cost and effectiveness (Various IMO Sources)

With the aforementioned installation requirements and associated cost the argument supporting the use for hydrocyclones as a stage in an onboard BWT can be shown. For the following analysis the BWT technologies identified in the literature review have been allocated a reference letter (see table 5.3)

BWT Technology	Reference	BWT Technology	Reference
Hydrocyclone	A	Ballast Water Exchange	F
Chemical Biocides	B	Sonic methods	G
Ozone	C	UV Radiation	H
De-oxygenation	D	Heat Treatment	I
Gas Super-saturation	E	Screens/Filters	J

Table 5.3. Assigned Reference letter to each BWT technology. (Source: Author).

As stated previously it is impractical to fix a specific BWT to ship class due to the variation of ship design within each class. However an approximation can be determined to select the best BWT technology for a ship type based on the technology best suited to ballasting/deballasting flow rate, availability of existing operational resources and the installation requirements. Each technology has been assessed under these criteria and the results are detailed thus:

Shipboard ballasting capacity (including associated ballasting/deballasting flow rates) are broken into three key capacity ranges design to account for the primary size ranges of ballast tanks across commercially operational vessels. The suitability of each BWT is shown in table 5.4.

Ballast Capacity (m^3)	>5,000	5,000 - 25,000	20,000 - 100,000+
Ballast Water Treatment	A-J	A - G, H -J	A, F, H, J

Table 5.4 BWT with respect to Ballast Capacity. (Source: Author).

Many BWT technologies have a specific resource dependence which would need to be rectified on many ships. The resources required by each treatment is summarised in table 5.5.

Utility Requirement	Resource Dependant BWT
Electric Power	G, H, J
Steam	I
Consumable Storage	B, D, E
No additional Resource Req. Uses available ballast water pumps.	A, F, J

Table 5.5. Treatment Utility Requirements. (Source: Author).

Finally the ship size and ballast tank capacity also highlight the differences within class and suitable BWT technology may be matched accordingly. Each of the BWT technologies would necessitate the following installations, shown in table 5.6.

Installation Required	**Treatment**
Pipe Modification	A, H, I, J
Electrical cabling	G, H, J
Storage	B-E
Control System	D - J
None	F

Table 5.6. Treatment Installation Requirements. (Source: Author).

5.2.2 The argument for hydrocyclone use as a BWT technology

Whilst the focus of the previous section is on the retrofitting of BWT technologies to existing vessels, the main discussion points surrounding resource dependence and installation requirements are valid for new build vessels as well. The hydrocyclone has been identified as a technology with minimum resource requirements, it is an inline system with no moving components and no external control requirements. In most cases the major requirement for the unit would be suitable space allocation and suitable piping to and from the cyclone. The high installation costs outlined are primarily due to the reworking of existing ballast piping, a feature that would not be necessary on new build vessels.

As discussed in Chapter 2, the hydrocyclone offers a reasonably high biological effectiveness however it is not capable of meeting the IMO requirements as a standalone system. A well designed hydrocyclone can ensure minimal secondary BWT requirements, and UV radiation systems have successfully been mated to Hydrocyclones onboard vessels. The additional benefits of hydrocyclones discussed in chapter 2 ensure that as well as the biological benefits of their use, there is also a strong commercial case for their installation.

5.3 The design process of BWT hydrocyclones

There are a plethora of design variables available to the hydrocyclone designer and in this respect the use of an analytical model prior to numerical modelling is advised. Many BWT systems will be provided with a specific working envelope and can be adjusted for use onboard specific vessels. However in many cases this may result in a non optimised system, subsequently effecting the biological removal efficiency of the BWT system as a whole. In this respect the simplicity of the hydrocyclone as a physical unit pays dividends, individually tailoring a hydrocyclone design to match the flow characteristics of a specific ship can ensure a fixed working environment for secondary BWT systems.

Analytical models, such as the Muschelknautz model outlined in Chapter 4, are not capable of providing definitive flow characteristics for individual cyclone designs, however they are able to impart an understanding on the cyclone engineer on the effects of specific design changes. The analytical models are built upon the equations of particle separation and the theory of fluids, they further include empirical observation collated over a number of long term research programmes. The resulting models can be used as a suitable starting point in order to produce full three dimensional numerical models. For example, the cyclone engineer will know that in order to increase the capacity of a hydrocyclone the physical design requires either; an increase in the cyclone diameter, inlet diameter , outlet diameter, overall body length, or a reduction in the vortex finder length. The analytical models can identify the exact effects of these design changes much more rapidly than numerical modelling. Careful classification of the initial problem, and subsequent developmental work utilising an analytical model can reduce the time spent on numerical modelling.

As such the recommended design process for BWT hydrocyclones is outlined below.

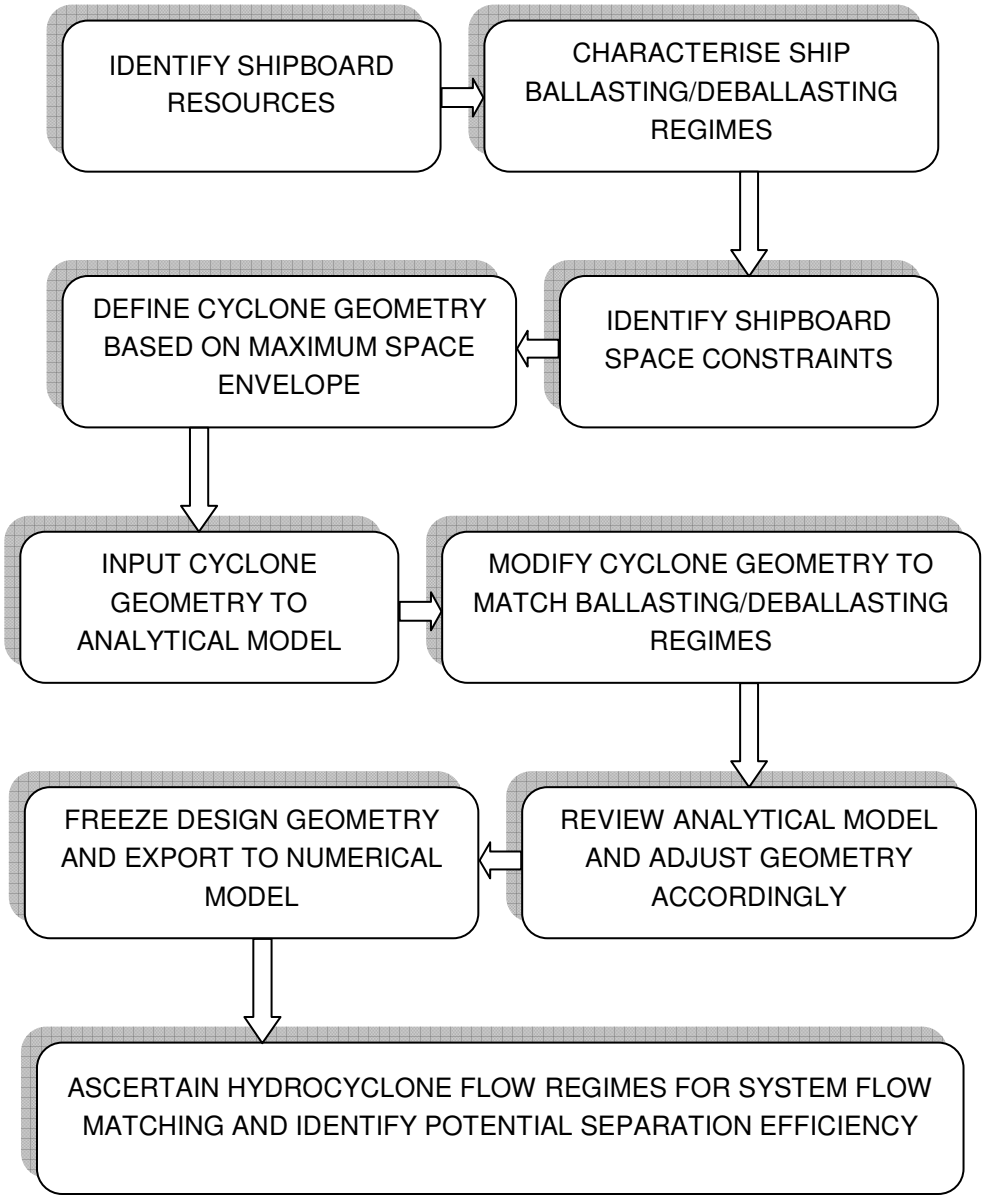

Figure 5.1. BWT Hydrocyclone design process - Ship review > Analytical model > Numerical model. (Source: Author).

Whilst the process model for cyclone design follows a simplistic, linear approach, it should be noted that the many commercial cyclones utilise adaptable geometries in order to achieved the required separation characteristics. This practice has evolved primarily due to the limitations of the analytical model. Until recently computational modelling has not been a cost effective option for industrial design of cyclones. The relatively low cost of computational software, and the development of more complex

turbulence models has enabled a small proportion of fluids analysis to move out of the research realm and into the commercial industrial environment. In this regard cyclone design is still heavily research orientated, however by utilising a cyclone of known design CFD can be applied to ensure suitable scalability for onboard ship usage.

5.4 Numerical modelling of hydrocyclones

5.4.1 Fundamental outcomes

It has been established that the selection of a suitable turbulence model is a fundamental aspect of cyclone analysis. Furthermore the selected turbulence model requires a significant understanding on the part of the engineer to ensure that the appropriate boundary conditions and domain modelling is used for the specific turbulence model.

This study has focussed on the application of the Detached Eddy Simulation turbulence model, primarily as a means to reduce modelling complexity without minimising the effective modelling of the main body of flow within the cyclone. The SPD test case has been utilised heavily as an approximation for the inlet condition of the cyclone. The strong separation and resultant secondary flows exhibited within the duct provide an ideal tool for analysis of the turbulence models.

Furthermore the intricacies of mesh development have been clearly highlighted through the SPD test case and the lessons learnt have been applied to a cyclone of known geometry. The following discussion concerns the DES turbulence model as applied to SPD and ROH domains.

The SPD simulation has identified the potential increased diffusivity as a result of high mesh density as discussed within the literature. It has also been noted that as the DES approach employs a less rigorous equation to model the near-wall this may also result in an incorrectly formed boundary layer at the point of separation. The

simulations conducted used a long flow time in excess of 18 complete volumetric flow exchanges in an attempt to negate this effect. In addition it is possible that the time dependent nature of the LES aspect of the DES model may prevent a completely developed flow from arising as flow structures may develop periodically or even intermittently. Furthermore the implicit filtering mechanism of the FLUENT software may result in numerical errors during the resolution of individual time steps which would adversely affect the boundary layer and subsequent flow separation. In order to lessen the effect of conditions the inlet domain has been extended, this should enable the boundary layer to fully develop prior to the flow entering the curves section of the domain where separation occurs. This increased inlet length coupled with the high number of complete volumetric flow throughs should mitigate these effects.

For the SPD analysis the Renormalized *k-ε* model show little evidence of picking up the complex secondary flows exhibited by the DES and RSM models, however this was an expected result. The Reynolds Stress Model however exhibited a flow which was reasonably indicative of the experimental measurements considering the relatively low computational cost of the model. However in both cases the simulations were conducted under steady state conditions and the inability to accurately model specific time dependent aspects of the flow was deemed to be detrimental to their for ballast water hydrocyclone design.

The high density 2.8 million cell DES model shows significantly more detail than its Renormalized *k-ε,* and RSM counterparts, where the velocity gradients of the latter models show evidence of “smoothing”. However the results of the DES model, even after time averaging, show more complex flow features than the corresponding empirical data. In this instance there is a clear indication that the results of the high density DES model alludes to the numerical diffusion discussed earlier. However the more coarse DES mesh returns results in keeping with the empirical data. This evidence suggests that with the more coarse mesh the modelling error has been significantly reduced, whilst the increased numerical error has not changed significantly enough to prevent its validity.

A possible explanation for the grid size dependency lies in the fact that the Smagorinsky Sub Grid Model (SGM) is likely to form part of the LES component of the DES model. One significant requirement for correct usage of the Smagorinsky SGM is that the grid size should be in the inertial sub range of the energy spectrum (see figure 5.2). In refining the mesh beyond this point the smallest scales resolved by the mesh are heading towards or close to the Kolmogorov scale and towards the end of the energy spectrum. Thus the assumptions of 'production equals dissipation' as assumed in the derivation of the Smagorinsky model is no longer valid, hence there is a mechanism for the introduction of additional modelling errors.

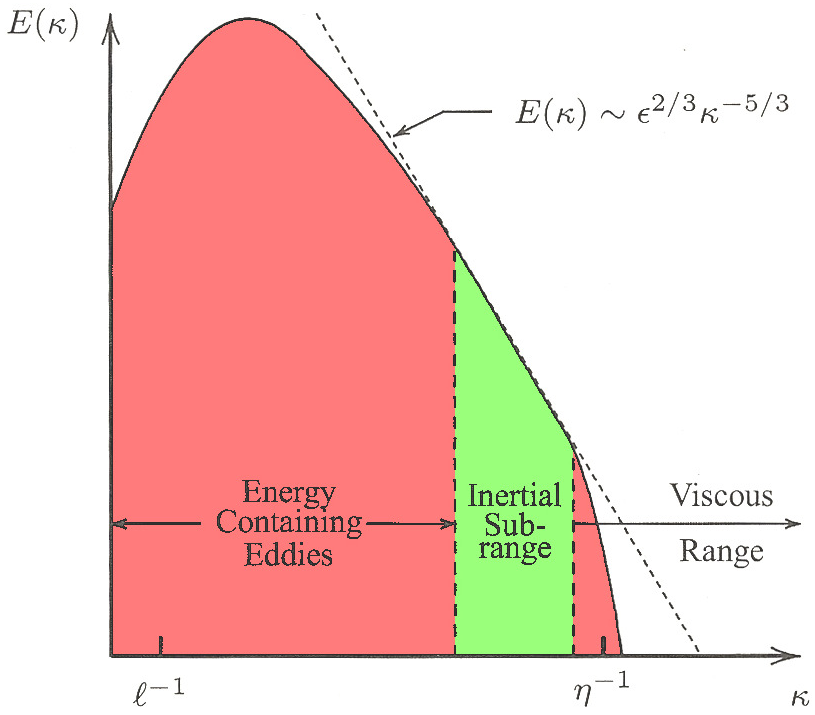

Figure 5.2. Energy Spectrum for a turbulent flow with the inertial sub-range highlighted (green). (Source: Author).

In order to establish the fundamental processes it is necessary to identify both the dissipation and diffusivity aspects of turbulent flow. Turbulent flow is by nature automatically dissipative, the inherent kinetic energy of the system is contained initially within the small, dissipative, eddies. This energy is transformed to become the system internal energy. These small eddies are not the starting point for the energy however, they themselves receive the kinetic energy from slightly larger

eddies. This process scales up such that these slightly larger eddies receive their energy from even larger eddies to the point whereby the largest of the eddies directly extract their energy from the mean flow. This process of transferred energy from the largest turbulent scales (eddies) to the smallest is referred to as the energy *cascade process* and it is the fundamental operation of this process that this detailed in figure 5.2. Diffusivity on the other hand is present within all flows, however the diffusivity of the flow increases within turbulent flows. The diffusivity itself is the spreading rate of flow features such as boundary layers, point source injections, jets, etc. The presence of a turbulent flow field increases the exchange of momentum within these flow features e.g. boundary layers. According to Tennekes and Lumley [90] this has the ability to reduces or delay separation at bluff bodies. The increased diffusivity also increases the resistance in internal channel or pipe flows.

Relating these two key aspects of turbulent flow conditions to the SPD and ROH simulations it is clear that there are a number of key geometrical features present in both domains that would be effected by incorrectly computed flow dissipation and diffusion. Of primary concern is the inlet pipe flow on both simulations and the separation about the curved segment of either the SPD or the interior vortex finder of the ROH. In this respect the lower density mesh appears to reduce the diffusivity through the mechanism discussed. As the grid size of the high density mesh may move away from the required inertial sub-range for the Smagorinsky component of the DES model, there is potential for the viscous stresses at the smallest scales to become too large and dissipating the kinetic energy into internal energy. This dissipation is proportional to the kinematic viscosity times the fluctuating velocity gradient up to the power of two. Since the kinetic energy is destroyed by viscous forces it is natural to assume that viscosity plays a part in determining these scales; the larger viscosity, the larger scales. incorrect grid sizes therefore plays a significant part in determining the amount of energy that is to be dissipated.

5.4.2 Handshaking

Initial investigations were not concerned with the interchange between the RANS and LES components of the DES model, and in this respect the mesh structure required was overlooked. A review of velocity plots from the SPD test case indicates that the interchange 'handshaking' may not currently be optimised as shown by the sharp velocity gradients at the inner and outer regions (indicated by low and high X position on charts 5.1 and 5.2). While this is not a deep concern for the existing study, it would be prudent for a detailed study to be conducted into the effects of this handshaking. For the purpose of this study the primary benefit obtained through the use of the DES model in this guise is the ability to model the main body of flow with an LES type turbulent model, without the mesh constraints a full LES analysis would impose. In this respect whilst it is possible that the boundary layer handshaking has been insufficiently modelled, the flow features main focal region within the duct, the separation inducing secondary flow features at the 90° have yielded significant improvements over the CFD work conducted by Choi et al. The two primary reference locations, plane of symmetry (2Y/D=0) and neighbouring reference location (2Y/D=0.25), have been shown in charts 5.1 and 5.2. In both cases the profile of the velocity distribution modelled by the DES provides a very close match to the experimental data. However the DES model predominantly reports lower velocities than the experimental work. this further validates the concept of artificially increased dissipation of the stored energy within the system, however this may be due to incorrect transfer of the system energy from the RANS boundary layer into the LES region as the primary flow variables within the RANS region are time averaged and unsteady flow phenomena are not present.

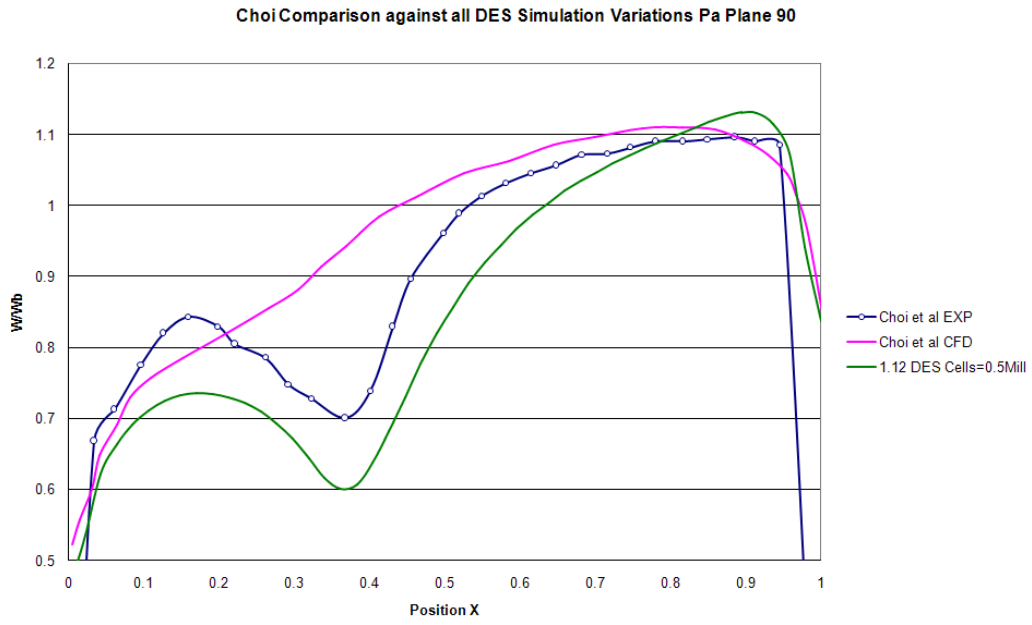

Chart 5.1. Comparison data of Experimental, DES and optimised Kε model with Wall functions for 90° Plane of the ERCOFTAC 180° Square Profile Duct. Rake 2Y/D=0 on 90° Plane. (Source: Author).

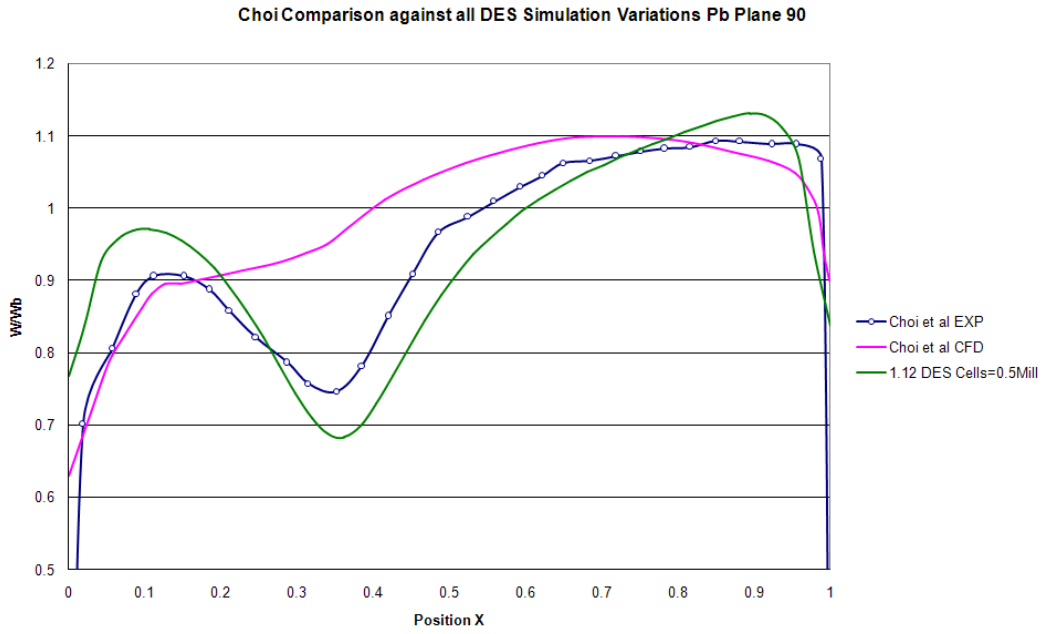

Chart 5.2. Comparison data of Experimental, DES and optimised Kε model with Wall functions for 90° Plane of the ERCOFTAC 180° Square Profile Duct. Rake 2Y/D=0.25 on 90° Plane. (Source: Author).

5.4.3 Implications on Ballast Water Treatment modelling

While the technical issues related to the use of CFD have been discussed, the implications on the development of BWT have yet to be addressed. The principal concern is whether the use of CFD can reduce the complex processes involved in the design of hydrocyclones suitable for BWT use.

In this regard the successful deployment of the DES turbulence model to more accurately model the highly separated flows of the SPD, in comparison to previous CFD analysis. These findings indicate that the DES model is suitable for the flow regimes exhibited by the hydrocyclone, and the modelling of a hydrocyclone of known geometry has been presented.

The modelling requirements for hydrocyclone domains have been found to be more relaxed than initially thought, a feature that lends itself well to the rapid development of hydrocyclones tailored to individual vessel requirements.

5.5 Chapter Summary

The main sources of numerical error have been discussed and the implications and primary findings of the CFD work have been outlined. Furthermore a detailed justification for the use of hydrocyclones as the main BWT technology onboard ships has been outlined. The process for utilising CFD as a design tool, in conjunction with the existing analytical design tools for hydrocyclones has been presented.

CHAPTER 6: CONCLUSIONS

CHAPTER CONTENTS

6.1 Ballast Water Treatment

The development of waste management systems is moving at a swift pace due to the forthcoming international legislation. However despite the urgent need for readily available systems there are a number of factors which hinder the maritime industries. The individual nature of each vessel in operation has influenced the modular design aspects of waste treatment systems. While this setup allows for a vast array of system designs it also complicates the selection and testing of systems. The BWT efficiency required of these systems leaves little room for error. To this end it is currently necessary to ascertain the effectiveness of prototype systems based on their ship board installations rather than laboratory test results.

This study has outlined some of the overriding factors which will influence the selection of certain treatment types based on the vessel in question. Due to the individuality between ship types, various treatments systems are not always suitable for each ship type, essential parameters that help the selection of a matching treatment system for each ship type is presented. Most systems consist of two stage treatment. Primary stages usually include the physical separation of all debris and macro scale organisms. This study has reinforced earlier suggestions that the Hydrocyclone (Cyclonic separator) is likely to be a crucial component of any ship based BWT.

Of the 85,000 vessels in operation the majority of these are potentially well suited to the installation of a hydrocyclonic separator for BWT. Nearly all vessels listed in figure 6.1 can accept the installation of a hydrocyclone in line with their ballast system, the exceptions include unknowns categorised under 'Other' and a small percentage of ferry's.

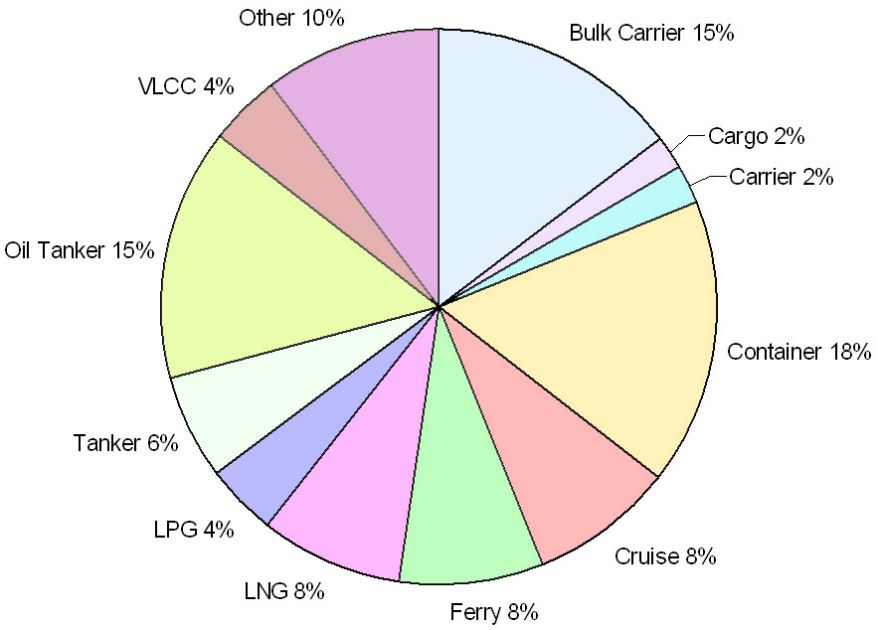

Figure 6.1. Worldwide ship demographic data. (Source: Author).

6.2 Computational Fluid Dynamics

The primary aim of this study was to establish the potential use of Computational Fluid Dynamics, and in particular to identify a suitable turbulence model for the design of Ships ballast water hydrocyclones. To this end a comprehensive analysis of three turbulence models (Kε-RNG, RSM and DES) has been conducted in order to analyse their suitability.

Initial work focused on the modelling of flow within a square profile duct with a 180° bend. The results have been compared to data published by the *European Research Community on Flow and Turbulence And Combustion.* In this respect the time dependent nature of the DES model was shown to identify secondary flows more accurately than previous *k-ε* numerical work, furthermore the application of a coarse mesh DES analysis resulted in modelled flow which closely approximated the time averaged experimental results of Chang et al for the same domain geometry.

6.2.1 Critical findings

I. Domain Modelling: The high grid dependence of the LES components of the DES turbulence model require significant thought to be applied to the generation of grids. Highly irregular tetrahedral meshes promote artificially high numerical diffusion and lead to modelled flow features more complex than those identified by experimental methods. Furthermore it has been found that high density meshes do not necessarily promote increased modelling accuracy, such that the grid size moves away from the inertial sub-range of the energy cascade required by the Smagorinsky sub-grid model. The potential for increased numerical dissipation and diffusivity can result in overly complex modelled flows that will hinder the successful development of suitable engineering solutions to design problems. The volumetric grid density identified from the square profile duct test case was then successfully applied to the Rietema optimised hydrocyclone design. This was subsequently verified utilising boundary conditions in keeping with those of the ERCOFTAC test case.

II. Inlet conditions: Whilst it is well known that incorrect inlet boundary conditions can have an adverse effect on the modelled flow, the square profile duct test case highlighted the benefit of complete system modelling. In this instance the test case data presented an inlet geometry of length two time the hydraulic diameter. The resulting modelled flow domain was of insufficient detail in the separated flow region to be useful, however upon investigation within the literature it was found that a correct boundary conditions can be achieved by utilising an inlet of length thirty times the hydraulic diameter. These findings where applied to the modelling of the Rietema optimised hydrocyclone design. As with the findings centred on the grid dependency of the DES model the inlet domain conditions where independently verified against the work conducted on the square profile duct.

III. RANS/LES Handshaking: Whilst not addressed within this study the results from the computational work on the square profile duct indicate that there is

significant advantage to be gained from optimising the domain grid to enable a smooth transition between RANS and LES components of the DES turbulence model. The energy transfer between the steady state analysis of the boundary layer and the transient analysis of the main flow could be a potential source of error, and may be responsible for the reported reduced bulk velocities of the main flow within the square profile duct.

6.3 Shipboard Hydrocyclones

With the continued reticence exhibited by ship owners and operators to install BWT technologies onboard their vessels it is imperative that an economic argument for treatment systems can be put forward. In this regard the hydrocyclone has been identified as a technology with minimum resource requirements, with no moving components and no external control requirements. Requiring only installation space and connection into existing piping systems. Whilst the hydrocyclone offers a reasonably high biological effectiveness in isolation it is its added benefits that may result in acceptance by the ship owners and operators. These benefits are centred on the removal of vast quantities of particulate matter from the ballast uptake resulting in significant reduction in transported sediment within the ballast tanks. In many cases this sediment can be uniformly distributed across the lower surfaces of all ballast tanks and is regularly between 100 and 200mm deep. The removal of the vast quantity of this sediment by the hydrocyclone during the ballasting process will reduce the frequency of replacement antifouling within the tanks. Furthermore the reduction in deadweight of the vessel can increase load bearing capabilities and reduces baseline fuel requirements.

CHAPTER 7: RECOMMENDATIONS

CHAPTER CONTENTS

7.1 Recommendations for future work

The research work presented within this study was primarily concerned with the successful application of the DES turbulence model. At the onset of the study the DES model offered a new approach to turbulence modelling and its suitability to particular applications had not been ascertained. Through the work presented here, in conjunction with research conducted elsewhere, the DES model is becoming better known. In this regard there is enhanced understanding of its uses and limitations. The following areas are proposed by the author as potential avenues of research for follow on work.

7.1.1 Particle analysis

The computational modelling of the hydrocyclone presented in this study was primarily concerned with establishing correct numerical representation of the known flow features exhibited by the cyclonic flow. In this respect the fluid applied to the domain has been assumed to be a single phase continuum. In reality the fluid would consist of a multiphase continuum fluid with an interspersed discrete phase. Whilst it is assumed that the discrete phase would have no interaction with physics of the continuum fluid the separation characteristics of the hydrocyclone can only be ascertained through the introduction of this discrete phase. The proposal in this instance is to develop the existing hydrocyclone modelling to incorporate particle analysis techniques in order to establish the suitability of the DES model for complete hydrocyclone separation modelling.

7.1.2 Dean Flow

In most real hydrocyclone installations the inlet piping often takes a 90° or 180° bend prior to entering the cyclone body. In this instance Dean flow separation refers to the inertial lift and viscous drag forces acting on particles of various sizes to achieve differential migration, and hence separation. The dominant inertial forces and the

Dean rotation force would cause the larger particles to establish an equilibrium position as a result of force balancing. Equally the Dean forces will result in migration of the smaller particles to a distinct position resulting in the formation of two separate particle streams within the fluid body. These can then be separated by a fluidic manifold. It has come to the attention of the author that the correct priming of the inlet flow through the use of dean flow characteristics in the inlet pipe could potentially move the inbound particulate into a region of the inlet pipe whereby particulate short circuiting can be minimised. The concept of dean flow vortices for flow separation of suspended particles has only recently been investigated with regards to large industrial applications [91, 92]. At present most cyclone analytical models assume a short circuit of between 6 and 10% of the inlet fluid. Potentially this introduced a limiting factor of, at best, 94% removal of suspended material if the inlet fluid is homogenised. The proposal in this instance is to develop the concept of dean vortex particle separation such that the existing inlet pipe curvature can be tailored to promote increased particle separation efficiency from the hydrocyclone. Furthermore a better understanding of dean flow separation may yield installation protocols to prevent the flow focussing particulate into the region that is likely to undergo short circuiting.

7.1.3 Cyclone Scale up

Whilst much has been discussed on the nature of parametric scaling of cyclones there has been little computational evidence to suggest that CFD itself can be used as a verification tool for the correct scaling of cyclone. This study assumed the analytical approaches to cyclone scaling are transferrable to the computed flow regimes of the hydrocyclones modeled. However without a comprehensive study this assumption may not be viable, the suitability of specific turbulence models may only be valid for specific physical sizes. The proposal in this instance is to identify whether the benefits of individual turbulence models are as applicable as the analytical models to a cyclone scale up.

CHAPTER 8: REFERENCES

1. National Oceanic & Atmospheric Administration. *Field Work Images*. Great Lakes Environmental Research Laboratory 2005 [cited; Available from: http://www.glerl.noaa.gov/.
2. McCluskey, D.K. and A.E. Holdo, *Ballast Water Treatment Literature Review - Second Quarter Report.* 2005, University of Hertfordshire.
3. McCluskey, D., A.E. Holdo, and R. Calay. *A Critical Review of Ballast Water Treatment Techniques in Development*. in *Ensus 2005*. 2005. Newcastle: School of Marine Science and Technology, Newcastle University.
4. McCluskey, D., A.E. Holdo, and R. Calay. *An Overview of Ballast Water Treatment Methods*. in *ASME PVP2005*. 2005. Denver, Colorado USA: ASME Pressure Vessels and Piping Division Conference.
5. McCluskey, D., A. Holdo, and R. Calay, *A Review of Ballast Water Technologies.* Journal of Marine Design and Operation, 2006. **B**(9): p. 21 - 29.
6. McCluskey, D.K. and A.E. Holdo, *Work-Package 5 Deliverable 5.3 Report on developments of new modular waste management systems & Guidelines for waste management systems and techniques*, in *SHIPrepair to MAintain Transport which is Environmentally Sustainable*. 2006, Shipbuilders & Shiprepairers Association.
7. McCluskey, D.K., A.E. Holdo, and R. Calay, *Work Package 5 Deliverable 5.2 Definition of Parameters to allow modular packages appropriate to ship types and required systems*, in *SHIPrepair to MAintain Transport which is Environmentally Sustainable*. 2006, Shipbuilders & Shiprepairers Association.
8. McCluskey, D.K., *Work Package 5 Deliverable 5.1 Report on LCA of new modular waste management systems*, in *SHIPrepair to MAintain Transport which is Environmentally Sustainable*. 2006, Shipbuilders & Shiprepairers Association.
9. Raaymakers, S. and L. Gould, *Ten of the Most Unwanted*, in *GloBallast Awareness Materials*. 2001, International Maritime Organization.
10. Global Invasive Species Database. [cited; Available from: http://www.issg.org/database.
11. Drake, J.M. and D.M. Lodge, *Global hot spots of biological invasions: evaluationg options for ballast-water management.* Proceeding - Royal Society of London. Biological Sciences, 2004. **271**(1539): p. 575 - 580.
12. Ahlenius, H. and UNEP/GRID-Arendal. *Major pathways and origins of invasive species infestations in the marine enviroenment.* UNEP/GRID-Arendal Maps and Graphics Library 2008 [cited; Available from: http://maps.grida.no/go/graphic/major-pathways-and-origins-of-invasive-species-infestations-in-the-marine-environment.
13. Raaymakers, S. *1st International Ballast Water Treatment Standards Workshop, IMO London, 28-30 March 2001: Workshop Report*. in *GloBallast Monograph Series No.4*. 2002. IMO London.
14. Maryland Department of Natural Resources. *Lifecycle of the Blue Crab*. 2005 [cited; Lifecycle of the Blue Crab (Modified)]. Available from: http://www.dnr.state.md.us/baygame/bluecrab.asp.
15. Globallast. *Globallast Webpage*. 2005 [cited; Available from: http://globallast.imo.org.
16. Rigby, G., A. Taylor, and G. Hallegraeff. *Ballast Water Treatment by Heat - an Overview*. in *1st Ballast Water Treatment R&D Symposium*. 2003: IMO London.

17. Glosten-Herbert Hyde Marine, *Full-Scale Design Studies of Ballast Water Treatment Systems*. 2002.
18. Sutherland, T., et al. *The Influence of Cyclonic Separation and UV Treatment on the Mortality of Marine Plankton*. in *1st Ballast Water Treatment R&D Symposium*. 2003: IMO London.
19. Mackey, T.P. and D.A. Wright. *A Filtration and UV Based Ballast Water Treatment Technology: Including a Review of Initial Testing and Lessons Learned Aboard Three Cruise Ships and Two Floating Test Platforms*. in *Ensus 2002*. 2002.
20. OptiMarin AS. *OptiMarin AS: MicroKill UV*. 2008 [cited; Available from: http://www.optimarin.com/visartikkel.asp?id=907.
21. Sassi, j., et al. *The Development and Testing of Ultrasonic and Ozone Devices for Ballast Water Treatment*. in *Ensus 2002*. 2002.
22. Sevaldsen, E.M. and P.H. Kvadsheim. *Active Sonar and the Marine Environement*. in *High Frequency Ocean Acoustics*. 2004. La Jolla, California: American Institute of Physics.
23. Tjallingii, F.J., *Global Market Analysis Released*, in *Ballast Water News 6*. 2001: London. p. 6 - 8.
24. Mountfort, D., T. Dodgshun, and M. Taylor. *Ballast Water Treatment by Heat - New Zealand Laboratory & Shipboard Trials*. in *1st Ballast Water Treatment R&D Symposium*. 2003: IMO London.
25. Greenman, D., K. Mullen, and S. Parmar, *Ballast Water Treatment Systems: A Feasibility Study*. 1997, Worcester Polytechnic Institute. p. 1 - 61.
26. Rigby, G., G. Hallegraeff, and C. Sutton, *Ballast Water Heating and Sampling Trials on the BHP Ship M.V. Iron Whyalla in Port Kembla and en-route to Port Hedland.* Ballast Water Research Series, 1997. **Report 11**.
27. Wright, D.A. and R. Dawson. *SeaKleen® - A Potential Natural Biocide for Ballast Water Treatment*. in *1st Ballast Water Treatment R&D Symposium*. 2003: IMO London.
28. McCracken, W.E. *Ballast Water Treatment with Currently Available Biocides*. in *1st Ballast Water Treatment R&D Symposium*. 2003: IMO London.
29. Dragsund, E., A.B. Andersen, and B.O. Johannessen. *Ballast Water Treatment by Ozonation*. in *1st Ballast Water Treatment R&D Symposium*. 2003: IMO London.
30. Browning Jr and Browning III. *Ballast Water Treatment by De-oxygenation - The AquaHabiStat™ System*. in *1st Ballast Water Treatment R&D Symposium*. 2003: IMO London.
31. Josefsen, K.D. and S. Markussen. *Biological De-Oxygenation of Ballast Water*. in *Ensus 2002*. 2002.
32. Tamburri, M.N., K. Wasson, and M. Matsuda. *Ballast Water Deoxygenation Can Prevent Species Introductions while Reducing Ship Corrosion*. in *Second International Conference on Marine Bioinvasions*. 2001. Orleans, La.
33. Jelmert, A. and A. Jelmert. *Gas Supersaturation, a Novel and Environmentally Friendly Method for Eliminating Unwanted Organisms in Ballast Water and Other Water Bodies*. in *Second International Conference on Marine Bioinvasions*. 2001. New Orleans, La.
34. Jelmert, A. *Ballast Water Treatment by Gas Supersaturation*. in *1st Ballast Water Treatment R&D Symposium*. 2003: IMO London.
35. Ronald Young, F., *Cavitation*. 2 ed. 1999: Imperial College Press.

36. Marine Engineers Review, *Which Ballast Water Treatment Option?*, in *Marine Engineers Review*. 2001. p. 14 - 15.
37. Endresen, O., et al. *Implications of Open Ocean Ballast Water Exchange*. in *Ensus 2002*. 2002.
38. PETROBRAS, *Ballast Water full scale trial on board M/V Lavras, a Brazillian product carrier, to evaluate the performance of the "Dilution Method", developed in Brazil - Final Technical Report*. 1998, Petroleo Brasileiro S.A. Petrobras.
39. Hay, C.H. and D. Tanis, *Mid-Ocean Ballast Water Exchange: Procedures, Effectiveness, and Verificationm*, in *Cawthron Report*. 1998, Ministry of Fisheries.
40. Forsberg, R., et al. *Fine Particle Persistence in Ballast Water Sediments and Ballast Tank Biofilms.* in *28th Annual Meeting of The Adhesion Society, Inc.* 2005. Mobile, Alabama: The Adhesion Society.
41. Nilsen, B., H. Nilsen, and T. Mackey. *The OptiMar Ballast System*. in *1st Ballast Water Treatment R&D Symposium*. 2003: IMO London.
42. Castilho, L.R. and R.A. Medronho, *A Simple Procedure for Design and Performance Prediction of Bradley and Rietema Hydrocyclones.* Minerals Engineering, 2000. **13**(2): p. 183-191.
43. Svarovsky, L., *Hydrocyclones*. 1 ed. 1984: Holt, Rinehart and Wilson. 198.
44. International Maritime Organization, *Ballast Water Management Convention*. 2005, London: IMO. 138.
45. Cullivan, J.C., R.A. Williams, and C.R. Cross, *Understanding the Hydrocyclone Separator Through Computational Fluid Dynamics.* Chemical Engineering Research and Design, 2003. **81**(4): p. 455 - 466.
46. Rietema, K., *Performance and Design of Hydrocyclones--I : General Considerations.* Chemical Engineering Science, 1961. **15**(3-4): p. 298-302.
47. Rietema, K., *Performance and Design of Hydrocyclones--II : Pressure Drop in the Hydrocyclone.* Chemical Engineering Science, 1961. **15**(3-4): p. 303-309.
48. Rietema, K., *Performance and Design of Hydrocyclones--III : Separating Power of the Hydrocyclone.* Chemical Engineering Science, 1961. **15**(3-4): p. 310-319.
49. Rietema, K., *Performance and Design of Hydrocyclones--IV : Design of Hydrocyclones.* Chemical Engineering Science, 1961. **15**(3-4): p. 320-325.
50. Svarovsky, L., *Description of Hydrocyclone Perfomance and Scale-Up using Dimensionless Groups.* Industrie Minerale, Les Techniques, 1983. **9**(84): p. 691 - 696.
51. Hoffman, A.C. and L.E. Stein, *Gas Cyclones and Swirl Tubes: Principles Design and operation*. 2 ed. 2008, New York: Springer.
52. Smithsonian Environmental Research Centre. *Containership Cross section - Photo by Monaca Noble*. 2008 [cited; Available from: http://www.serc.sl.edu/labs/marine_inmvasions/vector_ecology/bw_verification.aspx.
53. Launder, B.E. and D.B. Spalding, *Lectures in mathematical models of turbulence* 1972, London, New York: Academic Press.
54. Kolmogorov, A.N., *The Local Structure of Turbulence in Incompressible Viscous Fluid for Very Large Reynolds Number*. 1941: Dokl. Akad. Nauk SSSR. p. 301-305.

55. Wilcox, D.C., *Turbulence Modelling for CFD*. 2 ed. 2004, California: DCW Industries.
56. FLUENT, *FLUENT 6.3 User's Guide: 12.17 Setting up the Detached Eddy Simulation Model*. Vol. 2. 2006, Lebanon, NH: Fluent Inc.
57. Launder, B.E. and D.B. Spalding, *Mathematical Models of Turbulence*. 1972, London: Academic Press Inc.
58. Launder, B.E. and D.B. Spalding, *The Numerical Computation of Turbulent Flows.* Computer Methods in Applied Mechanics and Engineering, 1974. **3**: p. 269-289.
59. Davidson, L. *Turbulence Modelling - Reynolds Stress Models*. 2005 [cited; Available from: http://www.tfd.chalmers.se/doct/comp_turb_model.
60. FLUENT, *FLUENT 6.1 User's Guide*. Vol. 2. 2003, Lebanon, NH: Fluent Inc.
61. Spalart, P.R. and S.R. Allmaras, *A One-Equation Turbulence Model for Aerodynamic Flows*, in *American Institute of Aeronautics and Astronautics* 1992.
62. Shur, M., et al., *Detached-Eddy Simulation of an Airfoil at High Angle of Attack.*, in *4th International Symposium on Engineering Turbulence Modeling and Experiments*. 1999: Corsica, France.
63. Hinze, J.O., *Turbulence: An introduction to its mechanisms and theory*. Mechanical Engineering. 1959, New York: McGraw-Hill.
64. Abbott, M.B. and D.R. Basco, *Computational fluid Dynamics: An Introduction for Engineers*. Scientific and Technical. 1989: Longman Publishing Group.
65. Shalaby, H., et al., *Comparative Study of the Continuous Phase Flow in a Cyclone Separator Using Different Turbulence Models.* International Journal for Numerical Methods in Fluids, 2005. **48**(11): p. 1175 - 1197.
66. Ko, J. and S. Zahrai, *Simulating Single-Phase Swirling flows in Hydrocyclones.* Journal of Pulp and Paper Science, 2007. **33**(3): p. 133 - 137.
67. Travin, A., et al., *Detached-Eddy Simulations Past a Circular Cylinder.* Flow, Turbulence and Combustion, 1999. **63**: p. 293 - 313.
68. Squires, K.D. *Detached-Eddy Simulation: Current Status and Perspectives*. in *Mechanical and Materials Engineering Symposium and ME 598 Graduate Seminar*. 2005. Arizona State University.
69. Patankar, S.V., *Numerical Heat Transfer and Fluid Flow*. 1 ed. Hemisphere Series on Computational Methods in Mechanics and Thermal Science. 1980: Taylor & Francis.
70. The Open University, *Seawater: its composition, properties and behaviour*. 2 ed. 1995: Butterworth-Heinemann.
71. Bluhm, B. and R. Hopcroft. *Arctic Ocean Diversity - Benthic Larvae*. 2009 [cited; Available from: http://www.arcodiv.org.
72. National Oceanic & Atmospheric Administration. *Ocean Explorer - Copepod*. 2007 [cited; Available from: http://www.glerl.noaa.gov/.
73. USGS nonindigenous Aquatic Species Database. *NAS - Nonindigenous Aquatic Species: Calanoid copepod*. 2007 [cited; Available from: http://nas.er.usgs.gov.
74. University of Wisconsin. *Grouped Diatoms*. 2006 [cited; Available from: http://botit.botany.wisc.edu.
75. University of Tsukuba. *Biology - Dinoflagellates*. 2007 [cited; Available from: http://biol.tsukuba.ac.jp.

76. Mesbahi, E. *A European Community Funded Project for On-board Treatment of Ballast Water and Low Sulphur Fuels*. in *IMO Marine Environment Protection Commitee 47*. 2002. London: IMO.
77. Stairmand, C.J., *The Design and Performance of Cyclone Separators.* Transactions of the Institute of Chemical Engineeriing, 1951. **29**: p. 356 - 383.
78. Stairmand, C.J., *Pressure Drop in Cyclone Separators.* Industrial and Engineering Chemistry, 1949. **16**(B): p. 409 - 417.
79. Ioza, D.L. and D. Leith, *Effect of Cyclone Dimensions on Gas Flow Pattern and Collection Efficiency.* Aerosol Science and Technology, 1989. **10**: p. 491 - 500.
80. Barth, W., *Berechnung und Ausiegung von Zyklonabscheiden auf Grund neuerer Untersuchungen. [Design and Layout of the cyclone separator on the basis of new investigations].* Brennstoff-Warme-Kraft, 1956. **8**: p. 1 - 9.
81. Shepherd, C.B. and C.E. Lapple, *Calculation of Particle Trajectories.* Industrial and Engineering Chemistry, 1939. **32**(5): p. 605-617.
82. Shepherd, C.B. and C.E. Lapple, *Flow Pattern and Pressure Drop in Cyclone Dust Collectors.* Industrial and Engineering Chemistry, 1940. **32**(9).
83. Casal, J. and J.M. Martinez-Benet, *A Better Way to Calculate Cyclone Pressure Drop.* Chemical Engineering, 1983. **90**(3): p. 99 - 108.
84. Muschelknautz, E. and V. Grief, *Cyclones and other gas-solid separators*, in *Circulating Fluidized Beds*, J.R. Grace, A.A. Avidan, and T.M. Knowlton, Editors. 1996, Blackie Academic & Professional.
85. ERCOFTAC. *European Research Community On Flow, Turbulence And Combustion*. [cited; Available from: http://www.ercoftac.org.
86. Choi, Y.D., H. Iacovides, and B.E. Launder, *Numerical computation of Turbulent Flow in a Square Sectioned 180 Deg Bend.* Journal of Fluids Engineering, 1989. **111**: p. 59 - 68.
87. Choi, Y.D., C. Moon, and S.H. Yang. *Measurement of Turbulent Flow Characteristics of Square Duct with a 180° Bend by Hot Wire Anemometer*. in *International Symposium on Engineering*. 1990.
88. Suzuki, Y. and N. Kasagi, *Turbulent Air Flow Measurement with the Aid of 3-D Particle Tracking Velocimetry in a Curved Square Duct.* Flow, Turbulence and Combustion, 2004. **63**(1-4): p. 415 - 442.
89. Chang, M., J.A. Humphrey, and A. Modavi, *Turbulent flow in a strongly curved U-bend and downstream tangent of square cross-sections.* Physico Hydrodynamics, 1983. **4**: p. 243-269.
90. Tennekes, H. and J.L. Lumley, *A First Course in Turbulence*. 1 ed. 1972: The Massachusetts Institute of Technology. 300.
91. Moll, R., et al., *Dean flow and production of drinking water by ultrafiltration*, in *5th International Membrane Science and Technology Conference*, UNESCO, Editor. 2003: New South Wales, Australia.
92. Wenten, I.G., *Ultrafiltration in water Treatment and its Evaluation as Pre-Treatment for Reverse Osmosis*, Ultra-Flo Pte Ltd, Editor. 2009, Dept. of Chemical Engineering - Institut Teknologi Bandung.

APPENDIX A: PUBLICATIONS

CONTENTS

Journal Publications

Conference Proceedings

(papers removed for copyright reasons)

APPENDIX B: ANALYSIS DATA

CONTENTS

Test Case: Square Profile Duct with 180° Bend

CFD Reference Co-ordinates

Reference Rakes on 90° Plane

2Y/D Values for Y Where:

Line Pa = [2F/D = 0]	F = (0.04495 + 0)	= 0.04495
Line Pb = [2F/D = 0.25]	F = (0.04495 + 0.0112375)	= 0.0561875
Line Pc = [2F/D = 0.5]	F = (0.04495 + 0.022475)	= 0.067425
Line Pd = [2F/D = 0.75]	F = (0.04495 + 0.0337125)	= 0.0786625
Line Pe = [2F/D = 0.875]	F = (0.04495 + 0.03933125)	= 0.08428125

for simulations all x,y,z co-ordinates are as follows

X0 (m):	[0]	x1 (m):	[0.6]
y0 (m):	[-0.256845]	y1 (m):	[-0.256845]
z0 (m):	[F]	z1 (m):	[F]

Note: as the Choi et al data assumes the half model 2F/D = 0 actually starts at

F=0.04495

therefore all values have this figure added.

Test Case: Mesh Sensitivity study

Reference points

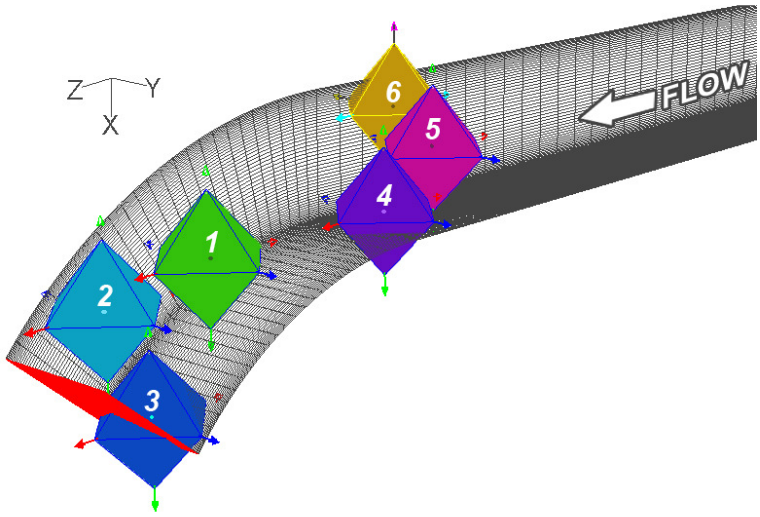

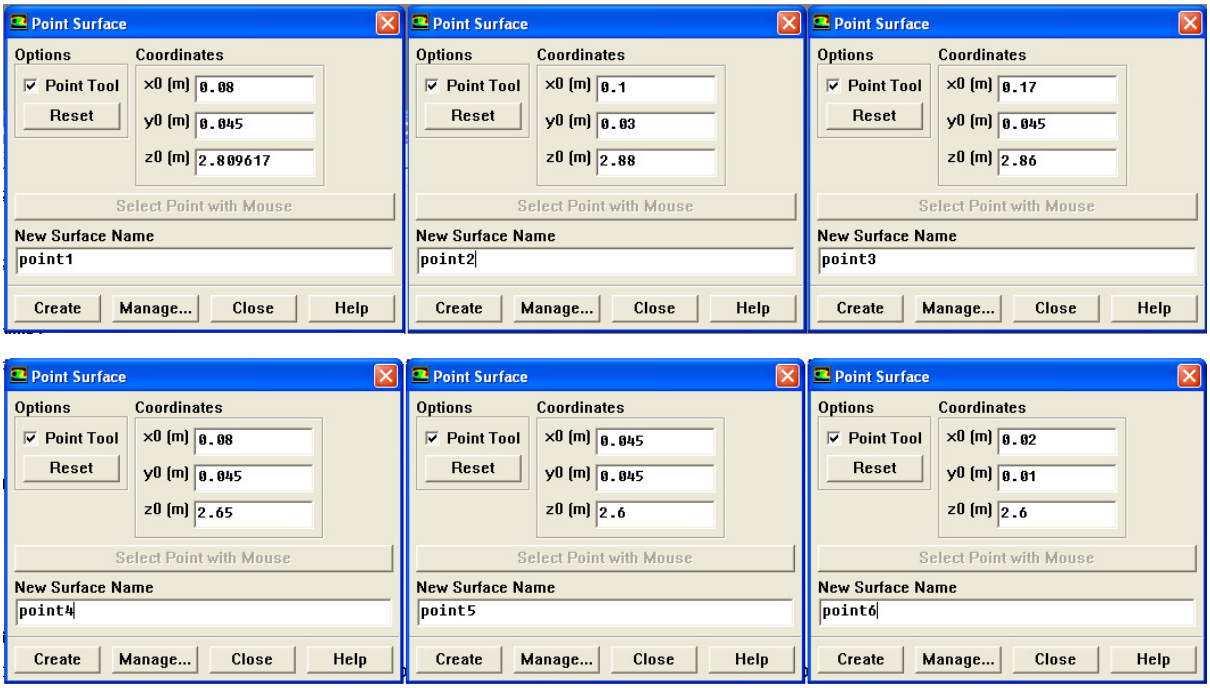

Turbulence modelling

All CFD simulations have been conducted using the commercially available software package FLUENT [Version 6.3.26]. The simulation has been run using default settings where applicable. The specific setup of each of tested turbulence models is as follows:

K Epsilon [Standard]

- Solver is pressure based using an implicit steady formulation and the gradient option selected is Green-Gauss Cell based.

- The K Epsilon model [Standard] version is selected. User Defined Functions are not included. The optional "Full Buoyancy effects" were not selected.

Model Constants				
Cmu	C1-Epsilon	C2-Epsilon	TKE Prandtl Number	TDR Prandtl Number
0.09	1.44	1.92	1	1.3

- The Inlet velocity is set at a Velocity magnitude of 11m/s. The turbulence specification method is 'K' and 'Epsilon'. Turbulent Kinetic Energy (m^2/s^2) is set at 1. Similarly Turbulent Dissipation Rate (m^2/s^3) is also set at 1.

- Solution controls include under-relaxation factors for Pressure- 0.2, Density- 0.9, Body Forces-0.9, Momentum-0.7, Turbulent Kinetic Energy- 0.8, Turbulent Dissipation Rate- 0.8, and Turbulent Viscosity- 0.9.

- Discretization for Pressure is standard. Momentum, Turbulent Kinetic Energy and Turbulent Dissipation Rate all utilise first order upwinding. This also incorporates the SIMPLE pressure-Velocity Coupling.
- The analysis was steady state and thus no time step was assigned.

K Epsilon Renormalized Group [KE-RNG]

- Solver is pressure based using an implicit steady formulation and the gradient option selected is Green-Gauss Cell based.

- The K Epsilon model [RNG] version is selected. User Defined Functions are not included. Neither RNG option has been selected [Differential Viscosity model, Swirl Dominated Flow].

Model Constants				
Cmu	C1-Epsilon	C2-Epsilon	TKE Prandtl Number	TDR Prandtl Number
0.09	1.44	1.92	1	1.3

- The Inlet velocity is set at a Velocity magnitude of 11m/s. The turbulence specification method is 'K' and 'Epsilon'. Turbulent Kinetic Energy (m^2/s^2) is set at 1. Similarly Turbulent Dissipation Rate (m^2/s^3) is also set at 1.

- Solution controls include under-relaxation factors for Pressure- 0.3, Density-1, Body Forces-1, Momentum-0.7, Turbulent Kinetic Energy- 0.8, Turbulent Dissipation Rate- 0.8 and Turbulent Viscosity- 1.

- Discretization for Pressure is standard. Momentum, Turbulent Kinetic Energy and Turbulent Dissipation Rate all utilise first order upwinding. This also incorporates the SIMPLE pressure-Velocity Coupling.

- The analysis was steady state and thus no time step was assigned.

Reynolds Stress Model [RSM]

- Solver is pressure based using an implicit steady formulation and the gradient option selected is Green-Gauss Cell based.

- The reynolds stress [7 Equation], Linear Pressure-Strain model is selected. User Defined Functions are not included. Reynolds Stress options for Wall BC from K Equation and Wall Reflection Effects have been selected.

Model Constants								
Cmu	C1-Epsilon	C2-Epsilon	C1-PS	C2-PS	C1'-PS	C2'-PS	TKE Prandtl Number	TDR Prandtl Number
0.09	1.44	1.92	1.8	0.6	0.5	0.3	1	1.3

- The Inlet velocity is set at a Velocity magnitude of 11m/s. The turbulence specification method is 'K' and 'Epsilon'. Turbulent Kinetic Energy (m^2/s^2) is set at 1. Similarly Turbulent Dissipation Rate (m^2/s^3) is also set at 1. Reynolds Stress Specification Method is 'K' or 'Turbulent Intensity'.

- Solution controls include under-relaxation factors for Pressure- 0.2, Density- 0.9, Body Forces-0.9, Momentum-0.7, Turbulent Kinetic Energy- 0.8, Turbulent Dissipation Rate- 0.8, Turbulent Viscosity- 0.9 and Reynolds Stresses- 0.5.

- Discretization for Pressure is standard. Momentum, Turbulent Kinetic Energy, Turbulent Dissipation Rate and Reynolds Stresses all utilise first order upwinding. This also incorporates the SIMPLE pressure-Velocity Coupling.
- The analysis was steady state and thus no time step was assigned.

Detached Eddy Simulation

- Solver is pressure based using 2nd order implicit unsteady formulation and the gradient option selected is Green-Gauss Cell based. Neither Transient control mode has been selected.

- The associated RANS model is the Spalart-Allmaras option with Vorticity-Based production selected. User Defined Functions are not included.

Model Constants						
Cdes	Cb1	Cb2	Cv1	Cw1	Cw3	Prandtl Number
0.65	0.1355	0.622	7.1	0.3	2	0.667

- The Inlet velocity is set at a Velocity magnitude of 11m/s. The turbulence specification method is the Modified Turbulent Viscosity set at a constant 0.001 m^2/s.

- Solution controls include under-relaxation factors for Pressure- 0.2, Density-0.9, Body Forces-0.9, Momentum-0.7, Modified Turbulent Viscosity- 0.8 and Turbulent Viscosity-0.9.

- Discretization for Pressure is standard; Momentum is bounded central differencing and Modified Turbulent Viscosity is first order upwind. This also incorporates the SIMPLE pressure-Velocity Coupling.

- Time step size was fixed at 0.005s for time dependent analysis once the simulations were shown to have stabilised.

Simulation Reference Files

File Ref.	Turbulence Model	Cell Count (No.)	Termination Time (s)	Notes
1.1	DES	2,836,800	4.8015s	-
1.2	DES	2,836,800	4.8025s	Verification of 1.1
1.3	Ke-RNG	2,836,800	Steady State	-
1.4	RSM	2,836,800	Steady State	-
1.5	DES	2,836,800		Incomplete
1.6	RSM	-	-	Corrupt save file
1.7	Ke-RNG	518175	Steady State	No Gravity
1.8	KE Standard	518175	Steady State	Not analysed
1.9	Ke-RNG	518175	Steady State	+ Gravity
1.10	RSM	518175	Steady State	-
1.11	RSM	518175	Steady State	+ Gravity
1.12	DES	518175	6.0s	No Gravity

APPENDIX C: BIOLOGICAL ORGANISM DATA

CONTENTS

UV Dosage required to induce mortality

Organisms:	Energy dosage of Ultraviolet radiation in μW/cm^2 needed for kill factor at 1 Foot distance	
Bacteria	**90%**	**100%**
Bacillus anthracis - Anthrax	4,520	8,700
Bacillus anthracis spores - Anthrax spores	24,320	46,200
Bacillus magaterium sp. (spores)	2,730	5,200
Bacillus magaterium sp. (veg.)	1,300	2,500
Bacillus paratyphusus	3,200	6,100
Bacillus subtilis spores	11,600	22,000
Bacillus subtilis	5,800	11,000
Clostridium tetani	13,000	22,000
Corynebacterium diphtheriae	3,370	6,510
Ebertelia typhosa	2,140	4,100
Escherichia coli	3,000	6,600
Leptospiracanicola - infectious Jaundice	3,150	6,000
Microccocus candidus	6,050	12,300
Microccocus sphaeroides	1,000	15,400
Mycobacterium tuberculosis	6,200	10,000
Neisseria catarrhalis	4,400	8,500
Phytomonas tumefaciens	4,400	8,000
Proteus vulgaris	3,000	6,600
Pseudomonas aeruginosa	5,500	10,500
Pseudomonas fluorescens	3,500	6,600
Salmonella enteritidis	4,000	7,600
Salmonela paratyphi - Enteric fever	3,200	6,100
Salmonella typhosa - Typhoid fever	2,150	4,100
Salmonella typhimurium	8,000	15,200
Sarcina lutea	19,700	26,400
Serratia marcescens	2,420	6,160
Shigella dyseteriae - Dysentery	2,200	4,200
Shigella flexneri - Dysentery	1,700	3,400
Shigella paradysenteriae	1,680	3,400
Spirillum rubrum	4,400	6,160
Staphylococcus albus	1,840	5,720
Staphylococcus aerius	2,600	6,600
Staphylococcus hemolyticus	2,160	5,500
Staphylococcus lactis	6,150	8,800
Streptococcus viridans	2,000	3,800
Vibrio comma - Cholera	3,375	6,500
Molds	**90%**	**100%**
Aspergillius flavus	60,000	99,000
Aspergillius glaucus	44,000	88,000
Aspergillius niger	132,000	330,000
Mucor racemosus A	17,000	35,200
Mucor racemosus B	17,000	35,200
Oospora lactis	5,000	11,000

Organisms:	Energy dosage of Ultraviolet radiation in µW/cm^2 needed for kill factor at 1 Foot distance	
Molds continued.	**90%**	**100%**
Penicillium expansum	13,000	22,000
Penicillium roqueforti	13,000	26,400
Penicillium digitatum	44,000	88,000
Rhisopus nigricans	111,000	220,000
Protozoa	**90%**	**100%**
Chlorella Vulgaris	13,000	22,000
Nematode Eggs	4,000	92,000
Paramecium	11,000	20,000
Virus	**90%**	**100%**
Bacteriopfage - E. Coli	2,600	6,600
Infectious Hepatitis	5,800	8,000
Influenza	3,400	6,600
Poliovirus - Poliomyelitis	3,150	6,600
Tobacco mosaic	240,000	440,000
Yeast	**90%**	**100%**
Brewers yeast	3,300	6,600
Common yeast cake	6,000	13,200
Saccharomyces carevisiae	6,000	13,200
Saccharomyces ellipsoideus	6,000	13,200
Saccharomyces spores	8,000	17,600

APPENDIX D: HYDROCYCLONE ANALYTICAL MODEL

CONTENTS

Additional Information for operation of the Muschelknautz Cyclone model.

The primary benefits of the Muschelknautz model (hereby referred to as the MK model) is in its complex features compared to other analytical models. In particular the MK model is able to account for the effects of wall roughness, and in particular to accommodate the potential increase in wall roughness due to the deposition of collected solids. For the purpose of the PIBBDT cyclone the saltation/mass loading effects are negligible, however were the initial boundary conditions to change the MK model is capable of adjusting to account for Mass loading effects. Finally the model is also capable of incorporating changes in particle size distributions within the inlet flow.

A brief breakdown of a number of key parameters utilised by the model follows:

Q – The volumetric inlet flow rate. However it is worth noting that the MK model assumes 10% of Q is lost via vortex finder short circuiting. This accounts for the 0.9Q (90% Q) parameter in the equation for wall axial velocity (v_{zw}). Typical ranges of VF short circuiting can vary from 4-16% according to the literature.

This is a fundamental detail in the evaluation of the x50 cut point as the model assumes that the inner vortex flow has a major influence on the calculated x50.

The MK model invests a large proportion of its calculation in determining the appropriate wall friction factors in order to determine a more comprehensive value for the associated velocity and pressure losses. This is evident in the calculations for fair and f respectively.

The values shown in the example analytical model have been determined for a cyclone constructed from acrylic block and assumes minimal-zero solids build up on the wall.

The Cyclone Reynolds number (Re_R) is based on fluid properties in conjunction with a number of velocity components including geometrical mean rotational velocity (VthetaM) which is based on the spin near the wall (Vthetaw). and the inner vortex itself (VthetaCS) where CS is the previously identified control surface which is in

effect an invisible surface extending from the end of the vortex finder to the wall of the cyclone.

Unfortunately the function VthetaCS is a function of Re_R itself. In most cases the value calculated can be neglected which helps to close the equation. However this is predominantly true I cases whereby Re_R is greater than 2000. This is true for the X3 Conical cyclone but does not apply to the X1 and X2 variant cyclones.

The calculated values for Fair and F are based on a number of charts provided by Hoffman and Stein (2008).

Finally the model incorporates a number of more common fluidic parameters such as density and viscosity differences, dimensionless terms such as Froude number and fluid/particle interaction aspects such as drag coefficients.

In all cases the model is relatively well explained and the primary input variables are geometry based with the relevant assumptions incorporated into the model already.

Analytical Model for Rietema Optimum Hydrocyclone Design

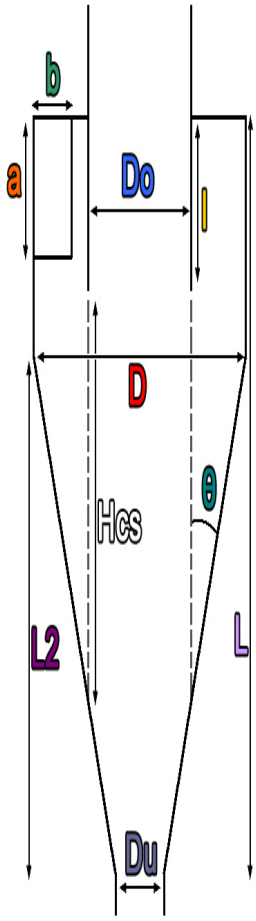

Component	Description	Dimension	Units
D	Cyclone Diameter	0.026	m
Do	VF Internal Diameter	0.0088	m
Du	Underflow Diameter	0.0017	m
L	Cyclone Length	0.13	m
l	VF Length	0.064	m
L2	Conical Length	0.0689	m
a	Slot Width	0.041	m
b	Slot Length	0.008	m
θ		10	°
Hcs		0.063698319	m

Vin		13.07	m/s
Vx		70.48465404	m/s
Solids density		0.001	kg m^-3
Fluid Density		1.2041	kg m^-3
Flow rate	Q	0.00428696	m^3/s
Concentration [s Kg/ g Kg]		1.00E-07	

Particle Diameter	x	0.0005	m
Particle Density	ρ_p	1365	kg m^-3
Particle Viscosity	μ_p	0.01	Ns m^{-2}
Fluid Density	ρ	1.2	kg m^-3
Viscosity	μ	0.000018	Ns m^{-2}

Particle Revolutions	Ns	3.525465422	-
Wall Roughness		4.60E-02	mm

Geometry Coefficient		ξ	0.615384615	
Constriction Coefficient		α	0.577571125	
Cyclone Radius		R=(D/2)	0.013	m
Radius Inlet path		R_{in}	0.009	m
Wall Velocity		$V_{\theta w}$	15.6664022	m/s
Geometric Mean Radius		R_m	0.007563068	m
Wall Axial Velocity		V_{zw}	10.98501442	m/s
Geometric Mean Spin Velocity		$V_{\theta m}$		m/s
Cyclone Reynolds No.		Re_R	723.4869039	
Wall Roughness		Ks/R	3.538461538	
Friction (Smooth Wall)		f_{sm}	0.005342902	
Friction (Wall Roughness)		f_r	0.040295173	
Wall Friction Factor		f_{air}	0.045638075	
Wall Strand Layer Density		ρ_{str}	0.4	kg m^-3
Froude No.		Fr_x	239.8936392	
Overall Collection efficiency		η	0.9	

Total Friction Drag		f	0.045638955	
Total Internal Surface		A_R	0.46	m^2
Tangential Velocity (inner core)		$V_{\theta cs}$	0.691503163	m/s
Correction Factor		x_{fact}	1	
Cut Point Diameter (Rep<0.5)		x50	6.79888E-05	m
Terminal Settling Velocity x50		U'_{t50} *(= Vrcs)*	2.434385101	
Particle Reynolds No.		Re_p	11.03405807	
Cut Point Diameter (Rep>0.5)		x50	**0.000115117**	m
Cyclone Wall Pressure Loss		Δp_{body}	116.4120669	Pa
Cyclone Core Pressure Loss		Δp_x	5980.772045	Pa
Cyclone Low Velocity (Point 1)		v1	9.94	m/s
Cyclone High Velocity (Point 2)		v2	12.97	m/s
Cyc. Acceleration Presure Loss		Δp_{acc}	41.65038417	Pa
Total Cyclone Pressure Loss		ΔP	6138.834496	Pa
Additional Useful Calculations				
Natural Vortex Length (Alexander)		Ln	0.025757367	m